The University of Alberta

The Development of A Macroscopic Model of Solids-Stabilized Emulsion Droplets in Reduced Gravity

By
Raymond Chiang

A Thesis Submitted to the Faculty of Graduate Studies and Research in Partial Fulfillment of the Requirements for the Degree of Master of Science

In
Chemical Engineering

Department of Chemical & Materials Engineering

Edmonton, Alberta
Fall, 2003

National Library
of Canada

Acquisitions and
Bibliographic Services

395 Wellington Street
Ottawa ON K1A 0N4
Canada

Bibliothèque nationale
du Canada

Acquisisitons et
services bibliographiques

395, rue Wellington
Ottawa ON K1A 0N4
Canada

Your file Votre référence
ISBN: 0-612-87739-6
Our file Notre référence
ISBN: 0-612-87739-6

The author has granted a non-exclusive licence allowing the National Library of Canada to reproduce, loan, distribute or sell copies of this thesis in microform, paper or electronic formats.

The author retains ownership of the copyright in this thesis. Neither the thesis nor substantial extracts from it may be printed or otherwise reproduced without the author's permission.

L'auteur a accordé une licence non exclusive permettant à la Bibliothèque nationale du Canada de reproduire, prêter, distribuer ou vendre des copies de cette thèse sous la forme de microfiche/film, de reproduction sur papier ou sur format électronique.

L'auteur conserve la propriété du droit d'auteur qui protège cette thèse. Ni la thèse ni des extraits substantiels de celle-ci ne doivent être imprimés ou aturement reproduits sans son autorisation.

Canada

University of Alberta

Library Release Form

Name of Author: *Raymond S. Chiang*

Title of Thesis: *The Development of A Macroscopic Model of Solids-Stabilized Emulsion Droplets in Reduced Gravity*

Degree: *Master of Science*

Year this Degree Granted: *2003*

Permission is hereby granted to the University of Alberta Library to reproduce single copies of this thesis and to lend or sell such copies for private, scholarly or scientific research purposes only.

The author reserves all other publication and other rights in association with the copyright in the thesis, and except as herein before provided, neither the thesis nor any substantial portion thereof may be printed or otherwise reproduced in any material form whatever without the author's prior written permission.

lam

July 10, 2003

Date Submitted

University of Alberta

Faculty of Graduate Studies and Research

The undersigned certify that they have read, and recommend to the Faculty of Graduate Studies and Research for acceptance, a thesis entitled 'The Development of A Macroscopic Model of Solids-Stabilized Emulsion Droplets in Reduced Gravity' submitted by Raymond Chiang in partial fulfillment of the requirements for the degree of Master of Science in Chemical Engineering.

August 7, 2003

ABSTRACT

Nano-scale solid particles have an affect on the stability of emulsion droplets but direct optical observation is impossible due to the particles' diminutive dimensions. In this study, silicon oil, water and glass beads were used to construct a solids-stabilized emulsion droplet model. Ground-based and reduced-gravity experiments with the model were performed and the model confirmed that particles that protrude from the droplets could form a physical barrier between the drops and prevent coalescence between two droplets. The model also showed that when hydrophobic beads were introduced from the water phase, additional energy is required to force the beads on to the interface. The beads' behaviour near the interface is consistent with fluid drainage (causes beads to stop on the interface before 'popping' to position), van der Waals forces (hold hydrophobic beads on water side of the interface) and line tension (prevents hydrophobic beads from crossing the interface), although surface heterogeneity cannot be completely ruled out.

To my parents, Peter and Judy Chiang, and to my fiancée, Liezl Lazaro.

ACKNOWLEDGEMENT

The completion of this thesis is simply not possible without the assistance of many people. Throughout my graduate studies, my supervisor, Dr. J. A. W. Elliott gave me inmeasurable amount of help and encouragement. I also received a great deal of help and advice from Tony Yeung, Walter Boddez, Andree Koenig, Bob Scott and James Mckinnon especially during the design and the construction of the apparatus. I am extremely grateful for the opportunity given by National Research Council of Canada and Canadian Space Agency. I also would like to thank Colleen Chan for introducing me to Dr. Elliott and all her help. Last but not least, I thank my parents and my fiancée for being extremely understanding especially during the difficult times.

And… thank you, God!

TABLE OF CONTENTS

CHAPTER 1 INTRODUCTION 1

1.1 Emulsion 1

1.2 Microgravity Flight 3

1.3 Thin Film Drainage 4

1.4 van der Waals Forces 6

1.5 Electrical Double Layer Forces 7

1.6 Line Tension Theory 8

1.7 Scope of this Thesis 12

CHAPTER 2 THEORETICAL EFFECTS OF LINE TENSION 14

2.1 Effect of Line Tension on Equilibrium Contact Angle 14

2.2 Stability of the Equilibrium Positions 18

CHAPTER 3 MATERIALS AND METHODS 23

3.1 Materials Used 23

3.1.1 Silicone Oil 23

3.1.1A Interfacial Tension Measurement 24

3.1.2 Water 24

3.1.3 Glass Beads 25

3.2 Cleaning and Treatment Procedure for the Glass Beads 27

3.2.1 Cleaning Procedure for the Glass Beads 27

3.2.2 Treatment Procedure for the Beads 28

3.3 Cleaning Procedure for Glassware, Test Cells, and Stainless Steel Tubes 28

3.3.1 Cleaning Procedure for the Glass Beakers and Glass Pipettes 29

3.3.2 Cleaning Procedure for the Test Cells 29

3.3.3 Cleaning Procedure for Stainless Steel Tubes 30

CHAPTER 4 EXPERIMENTS 31

4.1 Motivation 31

4.2 Ground-Based Oil Droplet Experiments 31

4.2.1 Set-up of the Apparatus 32

4.2.2 Coalescence Experiments 33

4.2.3 Area Contraction Experiments 35

4.3 The Development of the Microgravity Apparatus 37

4.3.1 Microgravity Experimental Set Up 38

4.3.2 Design of the Microgravity Experimental Apparatus 38

4.3.2A Camera and Data Acquisition 39

4.3.2B Frame 40

4.3.2C Test Cells 43

4.3.2D Lighting 47

4.3.2E Stage/Jack Stand 47

4.3.3 Design of the Microgravity Experimental Procedures 49

4.3.4 Procedure Used in Flight 5 51

4.3.5 Microgravity Experimental Observations 53

4.3.5A Flight 1 – Water Droplet in Oil with Hydrophobic Beads in Water 53

4.3.5B Flight 2 – Water Droplet in Oil with Hydrophobic Beads in Water 58

4.3.5C Flight 3 – Water Droplet in Oil with Hydrophilic Beads in Water 60

4.3.5D Flight 4 – Water Droplet in Oil with Hydrophilic Beads in Water 65

4.3.5E Flight 5 – Water Droplet in Oil with Hydrophobic Beads in Oil 69

4.4 Ground-Based Capillary Experiment 74

4.4.1 Set-up of the Apparatus and Procedures 74

4.4.2 Experimental Observations 75

CHAPTER 5 DISCUSSION 85

5.1 Thin Film Drainage 87

5.2 Electrical Double Layer Force 88

5.3 Line Tension 89

5.4 van der Waals Forces 91

5.5 Surface Heterogeneities 92

5.6 Summary 93

CHAPTER 6 CONCLUSIONS AND RECOMMENDATIONS 95

6.1 Experimental Conclusions 95

6.2 Recommendations 96

REFERENCES 98

APPENDIX 1 TEST EQUIPMENT DATA PACKAGE 104

APPENDIX 2 UNSUCCESSFUL MICROGRAVITY EXPERIMENTS 131

LIST OF TABLES

4-1 Microgravity Experiment Summary. 73

4-2 Capillary Experiment Summary (Set 1). 78

4-3 Capillary Experiment Summary (Set 2). 84

LIST OF FIGURES

1-1 Schematic diagram of solids-stabilized emulsion droplets 1

1-2 Force balance of a sphere sitting on an interface 5

1-3 Schematic of charges on an interface (Adapted from Heimenz and Rajagopalan) 8

1-4 A sessile drop on a flat plate. 9

1-5 A small sphere on an interface. 11

2-1 θ_∞ vs. particle θ_{eq}. Calculated from equation (2-3) for various values of positive τ^*. 16

2-2 θ_∞ vs. particle θ_{eq}. Calculated from equation (2-3) for various values of negative τ^*. 17

2-3 ΔF^* vs. Contact Angle for particles with θ_∞ equals 90° and dimensionless line tension of 0.0 and 0.2. Note: the value is large to emphasize the energy barrier. 19

2-4 ΔF^* vs. Contact Angle for particles with θ_∞ equals 45° and dimensionless line tension of 0.0 and 0.2. Note: the value is large to emphasize the energy barrier .20

2-5 First derivative of Equation (2-3) and Eqn (2-7). 22

3-1 Bead diameter distribution for size #8 beads. 26

3-2 Bead diameter distribution for size #7 beads. 26

4-1 Hydrophobic (treated) glass beads on a water-oil interface. 32

4-2 Hydrophilic (untreated) glass beads on a water-oil interface. 32

4-3 Schematic of the ground-based experimental apparatus. 33

4-4, 4-5 Coalescence experiment with oil drops coated with hydrophilic glass beads... 34

4-6, 4-7 Coalescence experiment with oil drops coated with hydrophobic glass beads. 34

4-8 to 4-10 An area contraction experiment with oil drop coated with hydrophilic beads. 36

4-11 to 4-16 An area contraction experiment with oil drop coated with hydrophobic glass beads. 37

4-17 The steel frame with aluminum rails for the spare test cells....42

4-18 The frame with the aluminum shelves in place. The light, the focusing rail and the light controller were mounted to the shelves. 42

4-19 Picture of a test cell. 44

4-20 The final design of the injection needle tip....46

4-21 The light and the focus rail mounted on the top shelf....47

4-22 An empty test cell on the jack stand, secured in place by brackets and a pin....48

4-23 A schematic diagram of beads-in-oil injection method. 50

4-24 A schematic of beads-in-water injection method....51

4-25 to 4-27 Two water drops coalesced and forced several beads onto the interface..54

4-28 The hydrophobic glass beads remain in the water drop....55

4-29 The pumping motion pushed some of the beads to the oil-side of the interface but it also mixed oil with the water droplet. 56

4-30 to 4-33 Area contraction experiment, Flight 1, Parabola 3. 57

4-34, 4-35 Two water drops coalesced during Flight 2, Parabola 3. 59

4-36, 4-37 A close up view of the interface and the beads after the two water drop coalesced. 59

4-38 to 4-40 Two water drops coalesced during Flight 2, Parabola 4. 60

4-41 to 4-44 Area contraction experiment conducted during Flight 3, Parabola 1....62

4-45 to 4-49 Area contraction experiment conducted during Flight 3, Parabola 3....62

4-50 to 4-53 Area contraction experiment conducted during Flight 3, Parabola 3....63

4-54 to 4-58 Area contraction experiment conducted during Flgiht 3, Parabola 4....64

4-59 to 4-62 Area contraction experiment conducted during Flight 4, Parabola 2....66

4-63 to 4-65 Area contraction experiment conducted during Flight 4, Parabola 3.....67

4-66 to 4-70 Area contraction experiment conducted during Flight 4, Parabola 4.....68

4-71 to 4-73 Area contraction experiment conducted during Flight 5, Parabola 1.....69

4-74 to 4-79 Area contraction experiment conducted during Flight 5, Parabola 2.....70

4-80, 4-81 Area contraction experiment conducted during Flight 5, Parabola 3.....71

4-82 Schematic of the capillary tube.....74

4-83 to 4-88 Hydrophilic glass beads were observed to 'pop' on to the interface.....76

4-89, 4-90 Hydrophilic glass beads on the water-oil interface. 79

4-91 Hydrophilic beads on the interface after the capillary tube had been turned over.. 80

4-92 Hydrophobic glass beads on the interface. The beads were first released into the water phase.....81

4-93 Hydrophilic glass beads after being released from the oil phase.....82

4-94 After the capillary tube was turned over, a hydrophobic glass bead can be seen falling away from the interface. 82

5-1 Free energy curve for beads entering the interface from the water phase. Various line tension values are used, which affect the energy barrier size. θ_∞=165°. When θ=0° the particle is completely submerged in the water phase... 90

5-2 Free energy curve for beads entering the interface from the oil phase. Various line tension values are used, which affect the energy barrier and well sizes. θ_∞=165°. When θ = 180° the particle is completely in the oil phase.....90

LIST OF NOMENCLATURE

A = Hamaker constant

F = Applied force

Fg = Force of gravity

F_S = Total force exerted on the interface

F_{sys} = Free energy of a system

$F_{sys}(\theta)$ = Free energy of a system at given θ

ΔF^* = Change in dimensionless free energy

ΔF_{sys} = Change in free energy

F_{vdw} = van der Waals' forces.

g = Gravitational force per unit mass=9.81 m/s^2

h = Final liquid film thickness

h_o = Starting liquid film thickness

m = Mass of a given particle

R = Radius of a given particle

r = Contact radius of the sessile drop

t = Time

z = Distance between the particle and the interface

γ_{ws} = Water-solid interfacial tension

γ_{wo} = Water-oil interfacial tension

γ_{os} = Oil-solid interfacial tension

μ = Viscosity of a given liquid

θ = Contact angle measured through the aqueous phase

θ_{ref} = Reference contact angle, set to 0° in this thesis

θ_{eq} = Equilibrium contact angle on a flat plate

ρ_D = Radius of the disc

$\Delta\rho$= Density difference between an object and the surrounding fluid

τ = Line tension of the three phase contact line

τ^* = Dimensionless line tension = $\tau / (\gamma R)$.

1.0 INTRODUCTION

1.1 Emulsion

Emulsions are often encountered in food, cosmetics, oil and gas, and many other industries. There are many mechanisms that are responsible for the stabilization of emulsion droplets and one of these mechanisms is stabilization by fine particles. Such emulsions are referred to as solids-stabilized emulsions. A schematic diagram of solids-stabilized emulsion droplets is shown in Figure 1-1. Solids-stabilized emulsions were first studied by Pickering in the early 1900s (Pickering, 1907). Since then, much research has been done on these emulsions.

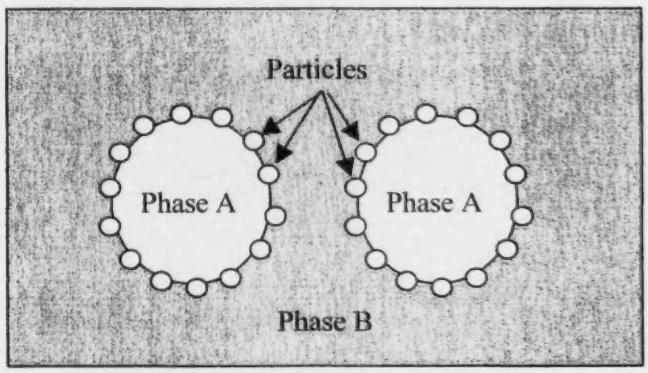

Figure 1-1 Schematic diagram of solids-stabilized emulsion droplets.

Since the diameters of these emulsion droplets are typically on the order of microns and the diameters of the fine solids on the order of nanometers, the behaviour of the solids on the interface is impossible to observe with an optical microscope. Researchers have extracted information about these fine particles from the macroscopic behaviour of the bulk phases. From the observed behaviour, it was concluded that hydrophobic particles stabilize water-in-oil emulsions and hydrophilic particles stabilize oil-in-water emulsions (Pickering, 1907). In a recent study, it was discovered that the

phase in which the particles reside before emulsification can have an impact on emulsion stability (Yan and Masliyah, 1994). In their study, hydrophobic particles were introduced into the bulk aqueous phase of an aqueous/oil system. The aqueous/oil system was then shaken to mix the two bulk phases. It was found that only stable oil-in-water emulsion, which is normally associated with hydrophilic particles, had been formed. They repeated the experiments by releasing the hydrophobic particles into the oil phase and found stable water-in-oil emulsion. The result suggests that when the hydrophobic particles started in the aqueous phase, they did not cross the interface into their thermodynamically favourable position. Although the macroscopic effect of these nano-scale particles can be observed, it is desirable to understand the cause. Electron microscopes (Levine, Bowen and Partridge, 1989) and x-ray spectromicroscopes (Neuhausler, Jacobsen and Lagaly, 1999) have been used to better understand the partitioning of particles between the bulk phases and the interface, as well as to map the mineral concentration in the bulk phases. These methods have their limitations and they have not yet been used to observe the formation of emulsion droplets.

The formation of emulsion droplets from the contraction of a larger droplet has recently been observed (Dabros et al., 1999). This experiment was conducted using diluted bitumen and water. A micro-syringe was used to form a water droplet in the oil phase and the drop was retracted into the syringe. In solution of low bitumen concentration, the interface of the water droplet would crumple like a paper bag and in solutions with higher concentration of bitumen, small emulsion droplets would form from the original droplet. Although the phenomenon was observed, the mechanism for this emulsification is not understood.

1.2 Microgravity Flight

Nano-scale solid particles are known to have an affect on the stability of the emulsion droplets but direct optical observation is impossible due to the particles' diminutive dimensions. In this thesis an enlarged model of a solids-stabilized emulsion drop will be described. However, under the effect of gravity, an enlarged model would be extremely unstable; the three phases would separate in a relatively short period of time, and therefore be difficult to study. By reducing the gravitational force exerted on the droplets and particles, it is possible to obtain a stable system such that the particles and their behaviour on the interface can be studied. Furthermore, by enlarging the system some of the effects of the colloidal forces will be minimized and the study can focus on the effects of geometry and interfacial forces.

The microgravity experiments took place inside a modified Falcon 20 business jet, provided by the National Research Council of Canada (NRC). The aircraft produced the near-zero gravity environment by flying on a parabolic path. The aircraft began the parabolic flight path by initiating a shallow dive, then pulling-up into a nose high attitude. The aircraft then travelled in a parabolic path, which was the same path as a projectile travelling through air. During this time (approximately 20 seconds) the aircraft and the objects inside the cabin experienced near weightlessness (on the order of 0.02-*g*). The near weightless condition terminated when the aircraft pulled-out of the parabolic path. During the entry and exit of such a manoeuvre the aircraft experienced an increased g-load (approximately 2.0 to 2.5-*g*'s) for approximately 10 seconds.

Due to the nature of this flight, the design and the construction of the experimental apparatus complied with NRC's safety standards and was inspected by Transport Canada (TC) prior to the flight. The apparatus is designed for various unusual

acceleration loads, which include positive 6-*g*'s, negative 3-*g*'s, and forward 9-*g*'s. The liquid carried onboard the Falcon 20 must not pose any danger to the operators and the aircraft, and must be approved by NRC. The complete safety standards can be found in the *Falcon 20 User's Guide* (National Research Council of Canada). In order to understand the observations made from the microgravity and ground-based studies using the enlarged solids-stabilized emulsion drop model, it is important to understand the different effects that may play a role in the behaviour of small particles interacting with an interface.

1.3 Thin Film Drainage

Solids-stabilized emulsions have particles on the interface that prevent the emulsion droplets from coalescing. In order to understand how the particles come to be adsorbed on the interface, consider particles originally existing in the bulk liquid phases. As these solids move towards the interface, a thin film of fluid, which can be approximated to be in the shape of a disc, will be trapped between the solids and the interface. The liquid in this film then needs to be drained until the film becomes thin enough to rupture. Although the film rupturing process is a statistical process, the time for the film to drain down to a given thickness can be estimated. As a first approximation, the Stefan-Reynolds equation, Equation 1-1 is used. This equation is a mathematical model of liquid drainage from a thin disc (Taylor, 2002).

$$\frac{1}{h^2} - \frac{1}{h_0^2} = \frac{16Ft}{3\pi\rho_D{}^4\mu} \qquad \textbf{(1-1)}$$

where

h = final film thickness
h_o = starting film thickness

F = net force on the disc
t = time
ρ_D = radius of the disc
μ = viscosity

A force balance for a sphere sitting on an interface is first used to approximate the radius of the disc, ρ_D, (Figure 1-2).

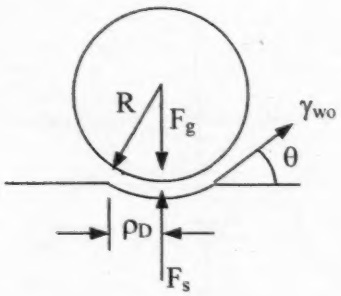

Figure 1-2 Force balance of a sphere sitting on an interface.

The force due to gravity on a bead is given by:

$$F_g = mg = \frac{4}{3}\pi R^3 \Delta\rho g \qquad \textbf{(1-2)}$$

where

R = radius of the object, *m*.
g = gravitational force per unit mass = 9.81 m/s^2.
$\Delta\rho$ = density difference between the fluid and the solid, kg/m^3.

The particle is assumed to be very close to the interface and moving very slowly such that the hydrodynamic force (drag force) on the particle is negligible. The particle is also assumed to be moving at a constant rate such that the force exerted on the interface equals to the weight of the particle. This force balance in the vertical direction is then

used to find the approximate radius of the indent made on the interface by the weight of the particle (Mingins and Scheludko, 1975).

$$F_S = 2\gamma_{wo}\pi\rho_D \sin(\theta) = 2\gamma_{wo}\pi R \sin^2(\theta) \quad \textbf{(1-3)}$$

where

F_S = Total force exerted on the interface

As an example, a spherical particle with a radius of 65 μm and a density difference of 1500 kg/m^3, is used. It is assumed that the system has an interfacial tension of 35 x 10^{-3} N/m. The calculated radius of the disc for such a system is approximately 2 μm. From this calculation it is shown that the radius of the disc is indeed small relative to the radius of the bead. Therefore the curvature of the disc can be neglected and the approximation of the thin disc is valid for the system discussed.

Using Equation 1-1, it can be shown that a finite amount of time is required before the thin film drains and eventually ruptures. If the fluid is viscous, then this process may take a significant amount of time.

1.4 van der Waals Forces

When the particles are near the interface, intermolecular forces may affect the particles' behaviour. One of the intermolecular forces is the van der Waals force between the particles and the fluid on the opposite side of the interface. van der Waals forces may either generate a net attractive or repulsive force. The magnitude and the direction of this force for a given system can be estimated using mathematical models. For a spherical particle near a flat interface, the van der Waals force is given by (Cooper et al., 2000):

$$F_{vdW} = \frac{AR}{6z^2} \quad \textbf{(1-4)}$$

where

A = Hamaker Constant
R = radius of the particle
z = distance between the particle and the interface

One could compare the magnitude of the van der Waals force with the gravitational force. The force of gravity is given by:

$$F_g = mg = \frac{4}{3}\pi R^3 \Delta\rho g \qquad (1\text{-}5)$$

By comparing these two forces, the significance of the two can be found for a given system. Generally, van der Waals forces are weak when the distance between the particle and the interface is large, but they play an important role when distance is reduced to the order of molecular diameters.

1.5 Electrical Double Layer Forces

Close to the interface, another intermolecular force that could affect the behaviour of the particles is the electrostatic force. If an interface is charged there will be a region near the interface where the concentration of the opposing charges is higher than in the bulk phase. This layer is usually referred to as the diffuse part of the electrical double layer (Figure 1-3) (Hiemenz and Rajagopalan, 1997). The magnitude of the electrostatic potential in the charged layer decreases with distance and thus, this layer is usually discussed in terms of a characteristic length, more commonly called the Debye length. The Debye length is the distance where the strength of the electrostatic potential is 1/e (where e is the universal constant) of that at the interface and is typically on the order of several nanometers. The existence of double layer repulsion could prevent the particles from coming into contact with the interface.

According to the theory, by adding various types and concentrations of salt, the electrical double layer thickness can be reduced. If this electrical double layer could prevent particles from reaching the interface, the addition of salt would allow the particles to get closer to the interface. Once the particles are closer to the interface, it is more probable that the particles will enter the interface.

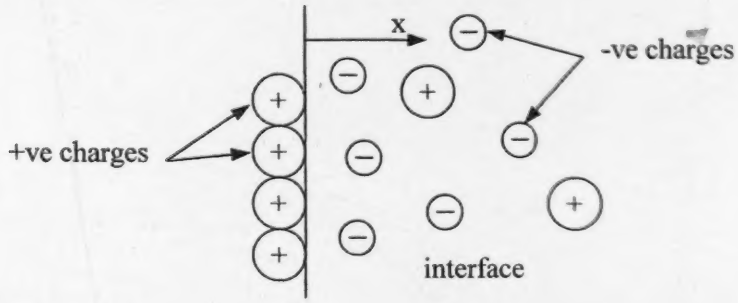

Figure 1-3 Schematic of charges on an interface (Adapted from Heimenz and Rajagopalan).

1.6 Line Tension Theory

Line tension can best be described as the one-dimensional analogue of surface tension that exists on a three-phase contact line. Gibbs first theorised the existence of line tension in a footnote in 1906 but it is still not fully understood (Gibbs, 1906). Numerous studies, both theoretical and experimental, have been done in this area. The magnitude of line tension is expected to be small, and because of this, determining the sign and the value of line tension is not trivial. Theoretical models and computer simulations have predicted line tension to be on the order of 10^{-12} to 10^{-10} *N*. Numerous methods have been employed to measure the value of line tension. In general either directly observing the drop geometry or measuring the energy required to displace a particle from an interface have been used to study line tension. The line tension results in

published literature vary by six orders of magnitude (10^{-12} to 10^{-6} *N*) and the signs also vary.

The sessile drop method is a popular method in which the geometry of the drop is directly observed and the value of line tension is extrapolated from the geometry. For a small sessile drop on a flat, solid surface, the effect of line tension is described by the modified Young equation. The modified Young equation for a water sessile drop in oil (Figure 1-4) on a flat plate is (Jensen and Li, 1999):

$$\gamma_{WS} + \gamma_{WO}\cos\theta_{eq} + \frac{\tau}{r} = \gamma_{OS} \qquad \textbf{(1-6)}$$

where

γ_{ws} = Water-solid interfacial tension
γ_{wo} = Water-oil interfacial tension
γ_{os} = Oil-solid interfacial tension
θ_{eq} = Equilibrium contact angle on a flat plate
τ = line tension of the three phase contact line
r = contact radius of the sessile drop

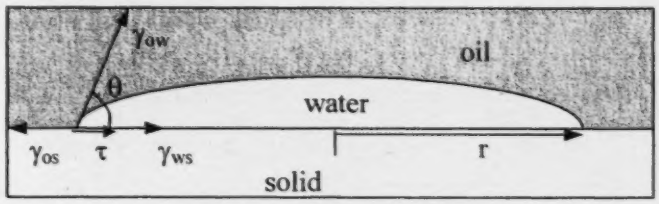

Figure 1-4 A sessile drop on a flat plate.

Rearranging equation 1-6

$$\cos\theta_{eq} + \frac{\tau}{r\gamma_{WO}} = \frac{\gamma_{OS} - \gamma_{WS}}{\gamma_{WO}} \qquad \textbf{(1-7)}$$

If the drop is large then the line tension term becomes negligible and equation 1-7 becomes:

$$\gamma_{WS} + \gamma_{WO} \cos\theta_{\infty} = \gamma_{OS} \quad \textbf{(1-8)}$$

or

$$\cos\theta_{\infty} = \frac{\gamma_{OS} - \gamma_{WS}}{\gamma_{WO}} \quad \textbf{(1-9)}$$

where θ_{∞} is the contact angle when the sessile drop radius is large.

Substituting the above into equation 1-7

$$\cos\theta_{eq} + \frac{\tau}{r\gamma_{WO}} = \cos\theta_{\infty} \quad \textbf{(1-10)}$$

By measuring the contact angle and the radius of various sessile drops, the value of line tension can be determined. Although this method is simple, the results can be greatly affected by contact angle hysteresis. To minimise the problems associated with contact angle hysteresis, researchers have conducted experiments using liquid drops on a vapour-liquid interface (Aveyard and Clint 1995). This removed the possibility of contact angle hysteresis caused by molecularly rough surfaces but also added an additional geometric variable, the contact angle formed between the drop and the continuous liquid phase, which is beyond the scope of this thesis.

The magnitude and direction of line tension can also be found using more sophisticated methods that measure the energy required to remove small spherical particles from the interface. Researchers have conducted experiments where small spheres were floating on an interface in Langmuir troughs. The interface area was then reduced until the spheres were forced to depart the interface. The surface pressure was measured and the energy required was then calculated. Others researchers measured the required force to remove an individual sphere and calculated the energy required. Once

the energy required to remove spheres from the surface is found, the value of line tension can then be calculated because line tension has an effect on the energy required to remove spheres from the interface (Aveyard and Clint, 1996). Consider a bead with radius R on an interface (Figure 1-5). The modified Young's equation for this case is (Aveyard and Clint, 1996):

$$\gamma_{WS} + \gamma_{WO}\cos\theta_{eq} - \frac{\tau\cos\theta_{eq}}{R\sin\theta_{eq}} = \gamma_{OS} \qquad \textbf{(1-11)}$$

where R is the bead radius and θ_{eq} is the equilibrium contact angle on a bead.

Rearranging equation 1-10 and substituting in equation 1-11 results in

$$\tau = \gamma_{WO} R\sin\theta_{eq}\left(1 - \frac{\cos\theta_{\infty}}{\cos\theta_{eq}}\right) \qquad \textbf{(1-12)}$$

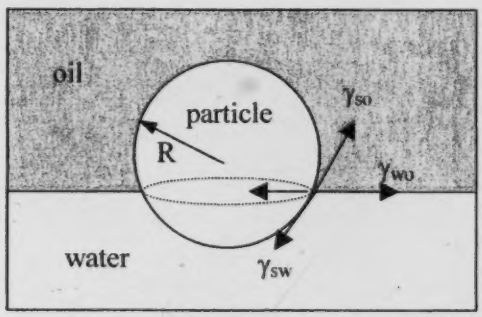

Figure 1-5 A small sphere on an interface.

If all phases are immiscible, no adsorption is considered, and none of the volumes can change, then the free energy associated with a spherical particle on the interface can be described by:

$$F_{sys} = \gamma_{WO}A_{WO} + \gamma_{WS}A_{WS} + \gamma_{OS}A_{OS} + \tau L \qquad \textbf{(1-13)}$$

By replacing the variables with geometric variables, the above equation can be shown to be (Aveyard and Clint, 1996):

$$F_{sys}(\theta) = \pi R^2 \gamma_{wo}\left(2\cos\theta_\infty(1-\cos\theta) - \sin^2\theta + 2\frac{\tau}{\gamma R}\sin\theta\right) \qquad \textbf{(1-14)}$$

Using the above equation, Aveyard and Clint have shown that if the magnitude of line tension increases to a critical threshold then the interface would be an unstable location for the particles to reside. Since the particle is located at an unstable location, it should leave the interface spontaneously.

1.7 Scope of this Thesis

Research on emulsions thus far has focused much of the attention on colloidal sized systems for obvious reasons. This means that emulsion droplets are micron sized while stabilizing particles have dimensions of the order of nanometers. Unfortunately the particles' diminutive size has made direct observations of their behaviour on the interface extremely difficult and therefore limited. Scientists have been learning the behaviour of these particles by interpreting the macroscopic properties observed. The intention of this study is to develop an enlarged model of a solids-stabilized emulsion droplet such that the behaviour of the particles can be observed. This thesis will cover the work done in the development of this enlarged emulsion model. In Chapter 2, the theoretical effect that line tension could have on a small spherical particle attempting to enter an interface is examined by using energy curves and the particle's stability on the interface is discussed. Also in the Chapter 2, the relationship between interface-particle contact angle and line tension is examined. In Chapter 3, the materials used in the model are listed and the preparation procedures followed are given. The experimental apparatus and the experiments conducted both on the ground and in the reduced gravity environment are

presented in Chapter 4. The results of these experiments are then discussed in Chapter 5. Lastly, Chapter 6 outlines the conclusions made from these experiments and the recommendations to further improve this model.

2.0 THEORETICAL EFFECTS OF LINE TENSION

Line tension can be best described as the one-dimensional analogue of surface tension that exists on a three-phase contact line. As discussed in the previous chapter, the direction and the magnitude of line tension are still topics for debate. Therefore, the effects of both negative and positive line tension will be discussed in this chapter.

2.1 Effect of Line Tension on Equilibrium Contact Angle

Consider a small, somewhat hydrophobic spherical particle on an interface as shown in Figure 1-5. If line tension does not exist at the three-phase contact line then the oil-water interface should have the same contact angle on the surface of the particle as it would have for a large drop on a flat plate. However, if line tension exists then it would have an effect on the contact angle. If line tension is positive then it would tend to minimize the length of the contact line. Since the length of the contact line is a maximum when the contact angle is 90° and minimum when the angle is either 0° or 180°, a positive line tension will force the particle away from 90°. If line tension is negative (tendency to expand), then it would bring the contact angle closer to 90°. These effects can be shown mathematically by combining the Young equation for a large sessile drop on a flat plate (Equation 1-6), and the Young equation for a particle on an interface (Equation 1-11) which gives (Aveyard and Clint, 1996):

$$\cos\theta_{\infty} = \cos\theta_{eq} - \frac{\tau \cos\theta_{eq}}{R\gamma_{WO} \sin\theta_{eq}} \qquad \textbf{(2-1)}$$

or

$$\cos\theta_{\infty} = \cos\theta_{eq} - \frac{\tau^{*} \cos\theta_{eq}}{\sin\theta_{eq}} \qquad \textbf{(2-2)}$$

where

$$\tau^* = \frac{\tau}{R\gamma_{WO}}$$

τ^* is known as the dimensionless line tension.

Note: Equation (2-2) assumes that the surface of the flat plate has the same surface properties as the particle.

Rearranging equation (2-2) yields

$$\theta_\infty = \cos^{-1}\left(\cos\theta_{eq} - \frac{\tau^* \cos\theta_{eq}}{\sin\theta_{eq}}\right) \qquad \textbf{(2-3)}$$

Equation (2-3) relates the contact angle of a large sessile drop on a flat plate (which is not affected by line tension) to that of a small sphere on an interface. First, let us consider the effects of a positive line tension. Figure 2-1 shows the relationship between θ_∞ and the particle θ_{eq} if the dimensionless line tension is greater than or equal to zero. If line tension does not exist then θ_∞ and particle θ_{eq} would always be identical. If line tension exists and has a positive value, then particle θ_{eq} would take on a different value than θ_∞ everywhere except when θ_∞ equals 90°. For example, consider a plate and a spherical particle with identical surface properties except for their geometry. If a large sessile drop on the plate has a contact angle of 40°, then the contact angle on the sphere could be found for a given value of line tension. To predict the contact angle on the sphere, a horizontal line can be drawn on Figure 2-1 for a given value of θ_∞. For any given positive line tension, the horizontal line will intercept the equilibrium curve at one, two or three locations. For example when θ_∞ equals 40°, there are three intercepts for all the dimensionless line tension values showing. From left to right, the first intercept will have a very small particle θ_{eq} (close to 0°). The second intercept of the horizontal line

and the equilibrium curve is similar to that of the flat plate equilibrium contact angle but it is less then 40°. Finally, a third intercept can be found at a very large contact angle (close to 180°). This suggests that if line tension is positive, then for every flat plate equilibrium contact angle, there could be up to three equilibrium contact angles for a particle. As the dimensionless line tension increases (i.e. for either a larger line tension or a smaller sphere) the first and the third equilibrium contact angles move towards 90°

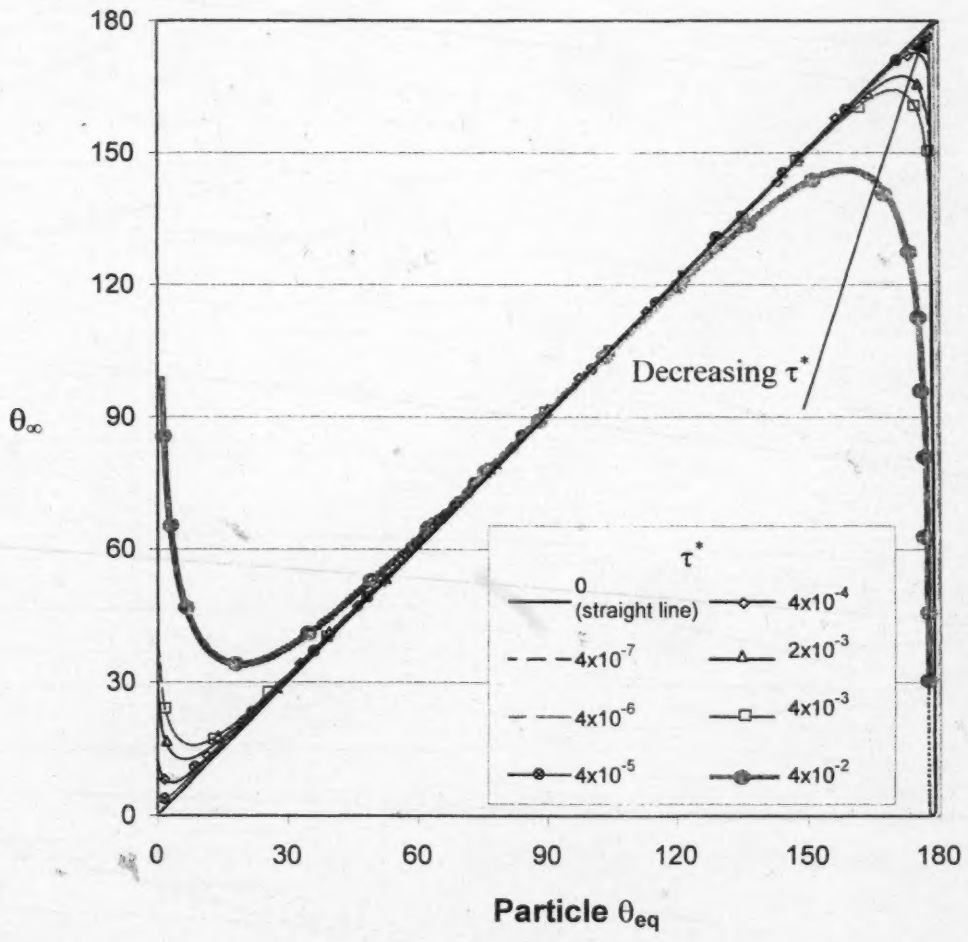

Figure 2-1 θ_∞ vs. particle θ_{eq}. Calculated from equation (2-3) for various values of positive τ^*.

Figure 2-2 shows the effects of a negative line tension. If the previous example is used again, θ_∞ =40°, for negative line tension values then one would find that for a given θ_∞ only one equilibrium particle θ_{eq} exists. Since a negative line tension would increase the length of the three-phase contact line, the particle θ_{eq} will be closer to 90° than θ_∞.

Whether line tension is positive or negative in value, if it exists it will have an effect on the positions of small spherical particles on an interface.

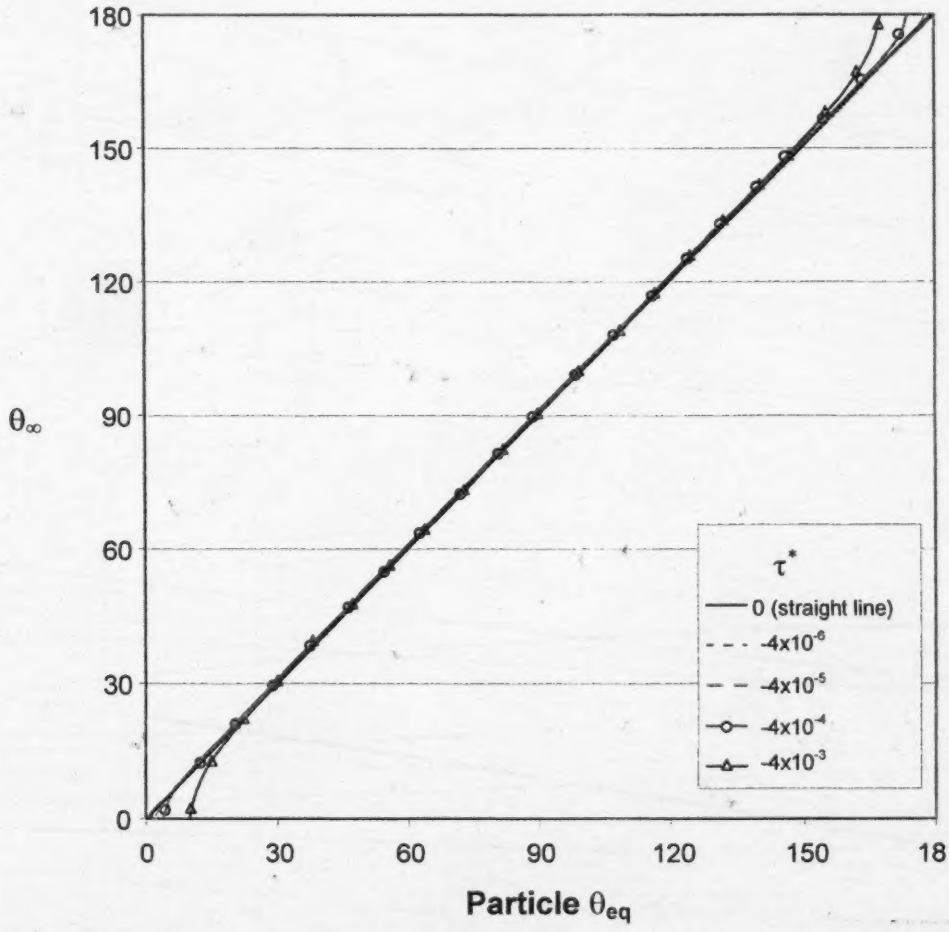

Figure 2-2 θ_∞ vs. particle θ_{eq}. Calculated from equation (2-3) for various values of negative τ^*.

2.2 Stability of the Equilibrium Positions

If line tension does not exist, then the flat plate contact angle would be identical to the contact angle on a particle. If line tension has a positive value, then for a given flat plate contact angle there could be up to three possible equilibrium positions for a particle on the interface. If line tension is negative then there would only be one possible equilibrium position for a particle on the interface. The stability of these equilibrium positions can be determined by examining the free energy of a particle on the interface. The change in free energy (relative to $\theta_{ref} = 0$) of a system consisting of the particle plus two bulk phases is given by (Aveyard and Clint, 1996):

$$\Delta F^* = \frac{\Delta F_{sys}}{\pi R^2 \gamma_{wo}} = \frac{F_{sys}(\theta) - F_{sys}(\theta_{ref})}{\pi R^2 \gamma_{wo}} = 2\cos\theta_\infty (1 - \cos\theta) - \sin^2\theta + 2\tau^* \sin\theta \qquad \textbf{(2-4)}$$

Where
ΔF^* = change in dimensionless free energy
ΔF_{sys} = change in free energy
θ = contact angle measured through the aqueous phase
$F_{sys}(\theta)$ = free energy at θ
θ_{ref} = reference contact angle = 0°
R = radius of the sphere
γ_{wo} = water-oil interfacial tension
τ^* = dimensionless line tension= τ / (γR)
Note: Equation (2-4) assumes that the surface of the flat plate has the same surface properties as the particle and that the phases are immiscible, and incompressible and no adsorption is considered.

Figures 2-3 and 2-4 show the dimensionless free energy of a particle with θ_∞ equals 90° and 45° for dimensionless line tension values of 0.0 and 0.2. On the free energy curve, a minimum corresponds to a stable equilibrium state and a maximum corresponds to an unstable equilibrium state. If the value of line tension is zero, then there is only one stable equilibrium position and it has the same contact angle as the flat

plate contact angle. As discussed earlier, for the case where line tension is positive, there are two additional equilibrium points on the curve. These two points are located near 0° and 180° and they are maximums as shown in Figure 2-3. This not only means that they are unstable equilibrium points but it also indicates that an activation energy is required for particles to enter the interface from the bulk phase. If the activation energy is large enough, it might delay or even prevent the particles from reaching their stable equilibrium positions on the interface.

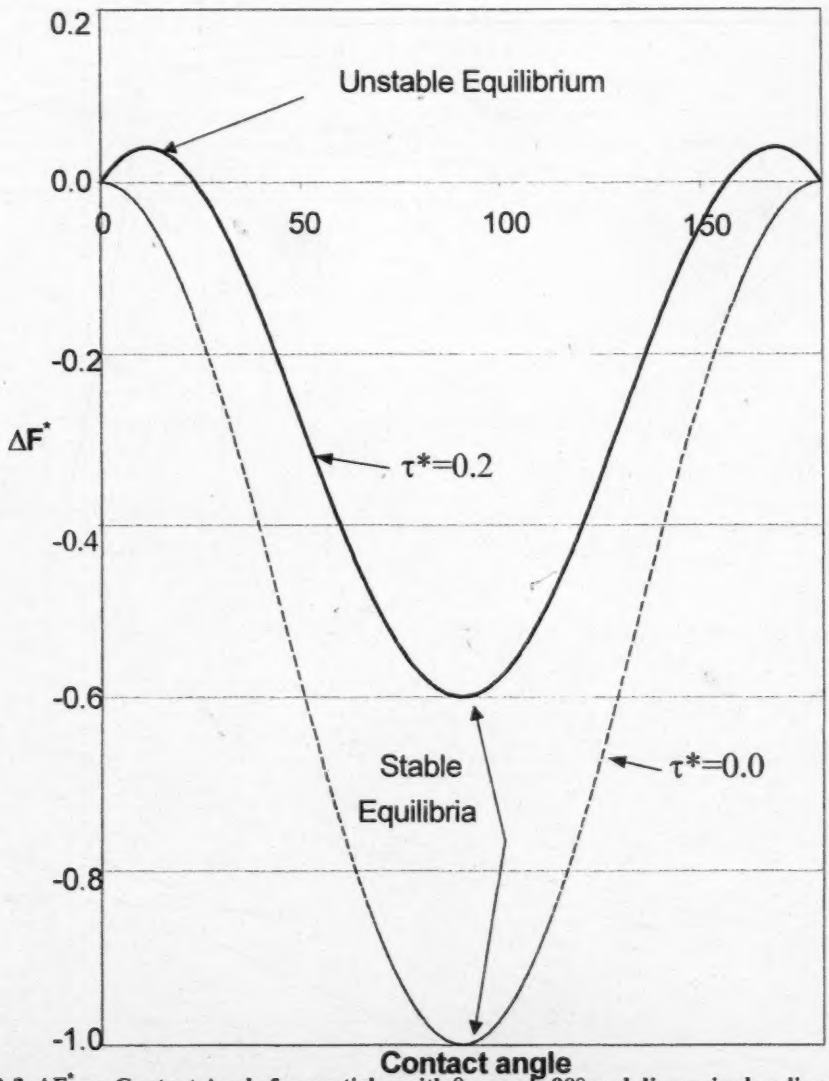

Figure 2-3 ΔF^* vs. Contact Angle for particles with θ_∞ equals 90° and dimensionless line tension of 0.0 and 0.2. Note: the value is large to emphasize the energy barrier.

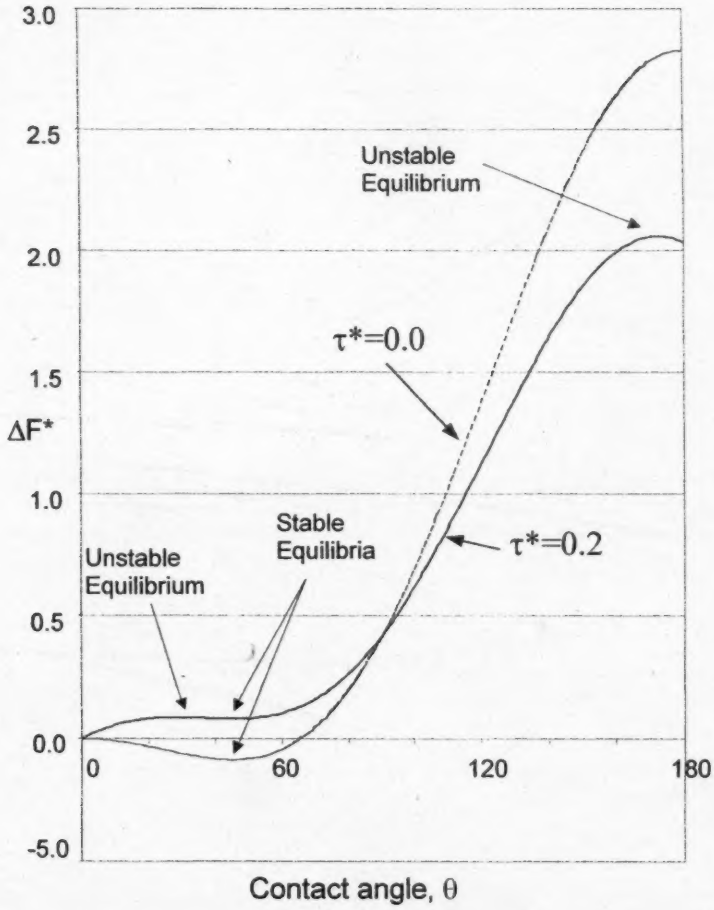

Figure 2-4 ΔF^* vs. Contact Angle for particles with θ_∞ equals 45° and dimensionless line tension of 0.0 and 0.2. Note: the value is large to emphasize the energy barrier.

Equation (2-4) shows the free energy for a particle with a particular θ_∞. The second derivative of equation (2-4) is used to find the stability of the equilibrium state of the particle on the interface for various flat plate equilibrium contact angles.

$$\frac{d(\Delta F^*)}{d\theta_{eq}} = 2 * \cos\theta_\infty \sin\theta_{eq} - 2\sin\theta_{eq}\cos\theta_{eq} + 2\tau^* \cos\theta_{eq} \qquad \textbf{(2-5)}$$

and

$$\frac{d^2(\Delta F^*)}{d\theta_{eq}{}^2} = 2*\left(\cos\theta_\infty \cos\theta_{eq} + 2\sin^2\theta_{eq} - 1 - \tau^* \sin\theta_{eq}\right) \quad \textbf{(2-6)}$$

Where θ_{eq} is the equilibrium contact angle on the particle.

Substituting equation (2-3) into (2-6) yields

$$\frac{d^2(\Delta F^*)}{d\theta_{eq}{}^2} = 2*\left(\cos^2\theta_{eq}\left(1 - \frac{\tau^*}{\sin\theta_{eq}}\right) + 2\sin^2\theta_{eq} - 1 - \tau^* \sin\theta_{eq}\right) \quad \textbf{(2-7)}$$

For a given particle θ_{eq}, equation (2-7) yields either a positive or a negative value. A positive value means that the given particle θ_{eq} corresponds to a minimum in free energy, which indicates a stable equilibrium point, and if equation (2-7) has a negative value then the equilibrium point is unstable. To show that the slope of equation (2-3) is also related to the stability of the equilibrium position of the particle, the first derivative of equation (2-3), which was obtained numerically, and equation (2-7) are plotted on the same graph (Figure 2-5). This graph shows that for a given dimensionless line tension the first derivative of equation (2-3) always has the same sign as equation (2-7). When equation (2-7) is positive, the first derivative of equation (2-3) is also positive and vise-versa when the equations become negative. This means that for a stable equilibrium contact angle on a particle, the slope of equation (2-3) is positive.

From Figures 2-1 and 2-5, it can be seen that if positive line tension exists then a stable equilibrium position cannot be found at contact angles of 0° and 180° because the slopes of the curves, on Figures 2-1, become negative infinity at those locations. The same graph also shows that if line tension is positive and if a stable contact angle exists near 0° or 180° then the value of line tension must be sufficiently small. If line tension is

less than or equal to zero then all particle θ_{eq} will be stable because the slope of equation (2-3) will always be positive (See Figure 2-2). However, Figure 2-2 shows that if a particle θ_{eq} exists near 0° or 180° then the magnitude of line tension must be small and this would be useful to narrow down the upper limit of the line tension value.

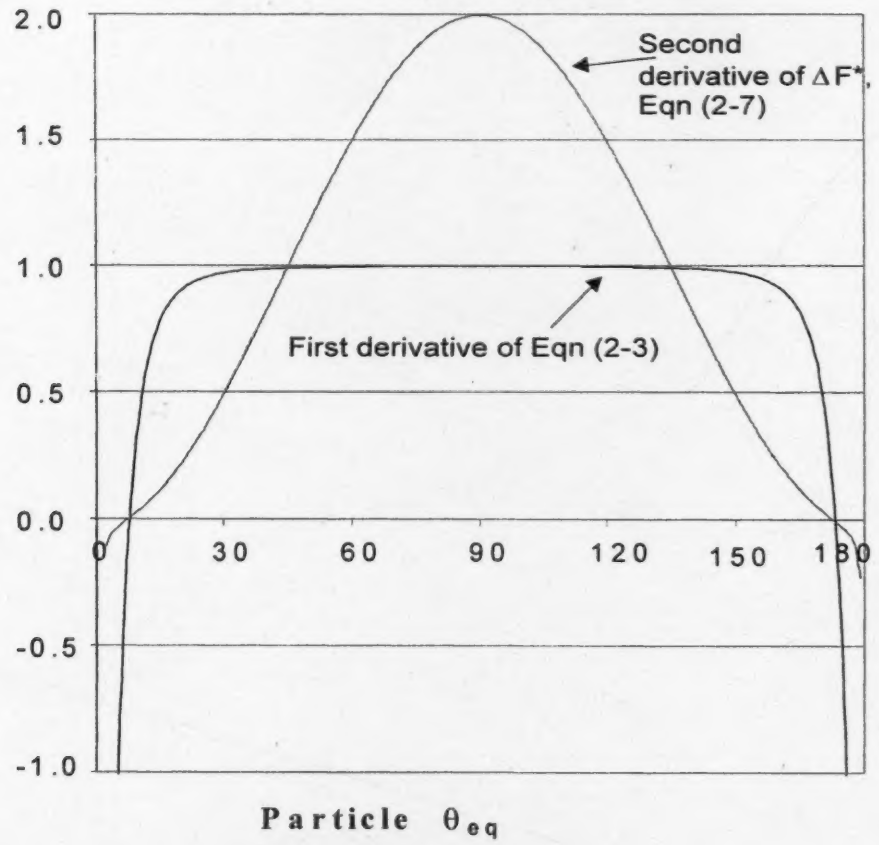

Figure 2-5 First derivative of Equation (2-3) and Eqn (2-7).

3.0 MATERIALS AND METHODS

3.1 Materials Used

The macroscopic solids-stabilized emulsion model was made from silicone oil, distilled water and glass beads. The silicone oil and distilled water were used to model the oil and aqueous phases of an industrially relevant system. Silicone oil was chosen because its density is similar to that of the water and this is important for two reasons. First the small density difference allows a relatively large spherical droplet to be formed in the ground-based experiments. Second, the microgravity flight profile includes a series of positive-*g* accelerations and having fluids of similar densities minimizes the possibility that the droplet will fall off the needle from which the droplet was formed and attached to. Glass beads were used to model the solid particles on the interface because the surface hydrophobicity of glass can be modified.

Test cells, which were made from plexiglass and glass panels, were used to contain the liquids for the microgravity experiments. The droplets were formed inside the test cells via two stainless steel tubes. Cleaning procedures for the test cells and the stainless steel tubes are given in this chapter and a detailed description of the test cells is given in the next chapters.

3.1.1 Silicone Oil

In the initial ground-based experiments, Dow Corning 710 (DC 710) silicone oil was used. The specifications of DC 710 as supplied by the manufacturer, Dow Corning, claim the specific gravity at 25°C is 1.11 and this was independently confirmed in the reference published by Chan (2001). The interfacial tension between water and silicone

oil measured using the Wilhelmy plate method in a Kruss K-12 tensiometer, was found to be 17.86 mNm^{-1} at room temperature.

Dow Corning 200 Fluid 500 (DC 200-500) was used in the microgravity experiments and the subsequent ground-based experiments to accommodate for the changes in the procedures, which will be discussed in a later section. According to the manufacture, DC 200-500 has a specific gravity of 0.975 and this was confirmed using an Anton Paar DMA45 density meter.

3.1.1A Interfacial Tension Measurement

The small density difference between the water and oil presented a challenge in obtaining the interfacial tension value. Three methods, which include the Du Nuoy ring, pendant drop, and spinning drop, were tried before obtaining a useful result.

The interfacial tension between oil and water was measured with a spinning drop tensiometer from SDT Ltd. (University of Minnesota, Minneapolis). A small drop of silicone oil was injected into a water-filled glass tube. The tube was then rotated about its long axis at a high rate. At a high enough rotation rate, the lighter fluid, silicone oil, migrated to the center of the tube and elongated along the axis of the tube. By measuring the diameter of the drop, the oil-water interfacial tension value was calculated using the SDT software. The result was 36.5 ± 1.5 mNm^{-1} at 21°C. This data was obtained with rotation rates between 10,000 and 15,000 *RPM*.

3.1.2 Water

In all the experiments the water used was ultra-filtered, deionized and double-distilled using a Millipore Elix water purification system within 24 hours prior to the experiments, with the exception of the microgravity experiments in which the water was

stored for over four days. For the ground-based experiments, the water used was transported and stored in a 10 liter Nalgene container that had only been used to store distilled water. The microgravity experiments took place in Ottawa; therefore, a new Rubbermaid 2-quart container was used to store the distilled water. The Rubbermaid container was first cleaned using Palmolive dish soap and then rinsed with distilled water by filling the container and pouring it out three times. The container was filled just prior to departing the University of Alberta campus and was sealed once the container was filled.

3.1.3 Glass Beads

In industrially relevant emulsion systems, the droplet size is on the order of microns and the surface-active solids are sub-micron in size. Since our droplets are millimeters in size, the surface-active solids chosen can be larger. The solids used in our experiments are glass beads supplied by Manus Abrasive System Inc. Beads of size #7 (average radius of 100 μm) and #8 (average radius of 65 μm) were used in the experiments. The size number refers to the mesh that the manufacturer used to sort the glass beads. Although the manufactures have sorted the beads using different meshes, there was a variation in the size of the beads within the same bag.

Samples of the beads were collected from the bags using strips of clear-tape. These strips of tapes were then placed on a microscope slide. Each slide was then placed in front of a Hitachi KP-161 CCD camera, which was first calibrated with a rod of known diameter, and pictures were taken. A circle template was then used to approximate the size of each bead. The number of beads that fell into each diameter size range was then

recorded. The beads size distributions for size #7 and #8 Glass Beads are shown in Figures 3-1 and 3-2.

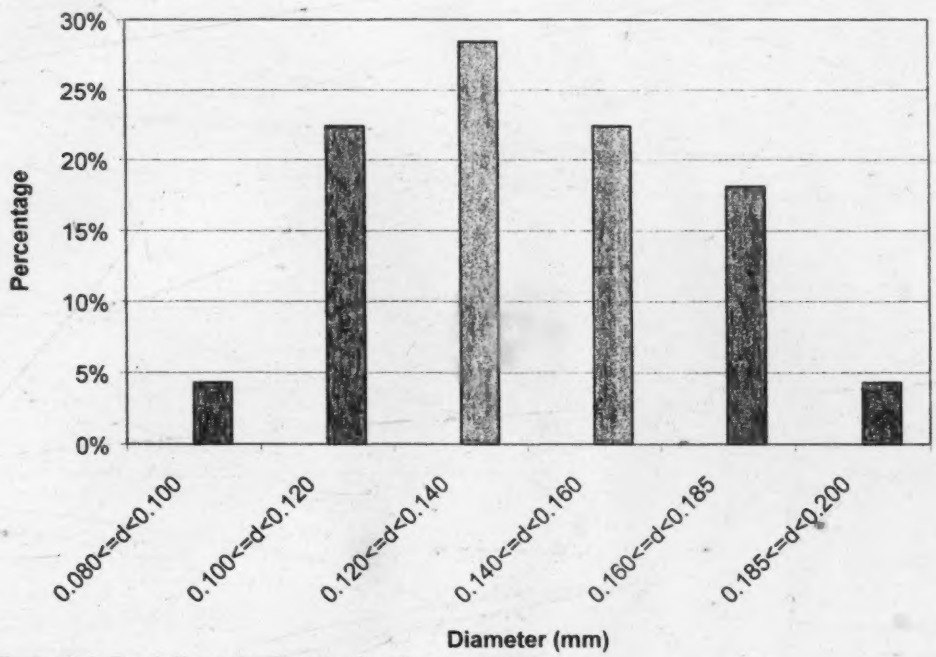

Figure 3-1 Bead diameter distribution for size #8 beads.

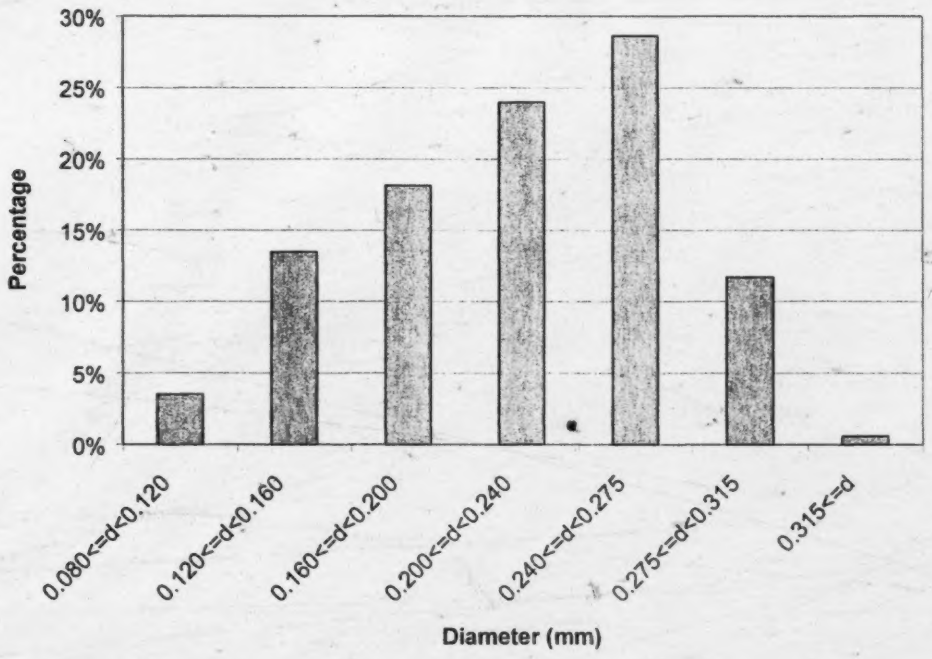

Figure 3-2 Bead diameter distribution for size #7 beads.

3.2 Cleaning and Treatment Procedure for the Glass Beads

The glass beads used in the experiments were divided into two groups. The first group was cleaned but untreated. These beads retained their hydrophilic property. The second group of beads was treated to change the surface properties such that they become hydrophobic. A piece of flat glass plate (cut from Fisherbrand Precleaned Plain Microscope Slide) was placed in the jar with the beads so that the contact angle on a flat plate could be determined.

3.2.1 Cleaning Procedure for the Glass Beads

All the glass beads used were cleaned following the procedure below. Starting in July 2002, Chromic Acid was replaced by Sulfuric Acid with No Chromix for health and safety reasons (as recommended by Andree Koenig).

1. Poured 20 *mL* of glass beads, measured with a 50 *mL* Pyrex beaker, into a 125 *mL* wide mouth glass jar with a Teflon-coated cap.
2. Poured 10% Chromic Acid (replaced by Sulfuric Acid with No Chromix as of July 2002) into the jar until the acid covered all the beads.
3. Shook the jar vigorously by hand for approximately 15 to 20 seconds.
4. The jar was left in the fume hood over night.
5. The acid was then poured out of the jar.
6. Filled the jar with distilled water and shook by hand for approximately 5 to 10 seconds and the acid-water solution was then poured out. Repeated this step 6 times or until all visible traces of acid (orange colouring of Chromic Acid) disappeared.

7. Place the jar, with its cap on but not tightened, in a vacuum oven (90 to 110 °C and –10" to –15" *Hg* gauge) for 24 hours.

3.2.2 Treatment Procedure for the Beads

After cleaning the glass beads, approximately half of the glass beads were treated with trimethylchlorosilane (TMCS). Step five was added in as of July 2002 to improve safety in the procedures used.

1. 80 *mL* of Toluene and 10 *mL* of trimethylchlorosilane (TMCS) were poured into the jar of cleaned glass beads.
2. The jar was shaken vigorously by hand for approximately 15 to 20 seconds.
3. The jar was allowed to sit in the fume hood for over 24 hours.
4. The solution was then poured out of the jar.
5. As of July 2002, this procedure was added in. The jar was filled with Toluene and shaken by hand. Toluene was then poured out and this process was repeated 6-times to remove any excess TMCS that might still be in the jar.
6. Placed the jar, with its cap on but not tightened, in a vacuum oven (90 to 110 °C and –10" to –15" *Hg* gauge) for 24 hours.

Additional details and the explanations of the glass treating procedure can be found in reference published by Blake and Ralston (1985).

3.3 Cleaning Procedure for Glassware, Test Cells, and Stainless Steel Tubes

All items that came in contact with the fluids were cleaned to minimize contamination. The following sections outline the procedures used.

3.3.1 Cleaning Procedure for the Glass Beakers and Glass Pipettes

1. Glassware was first rinsed thoroughly with distilled water for approximately 30 seconds to 1 minute, depended on the size and shape.
2. The glassware was soaked in 10% Chromic Acid (replaced by Sulfuric Acid with No Chromix as of July 2002) in the fume hood overnight.
3. Poured out the acid and rinsed the glassware with distilled water (at room temperature) for approximately 1 to 3 minutes.
4. The glass beakers were placed upside down on the counter to dry.
5. The glass pipettes were placed in a clean beaker and a sheet of Parafilm was placed over the beaker to minimize contamination from dust. The pipettes were then left on the counter to dry.

3.3.2 Cleaning Procedure for the Test Cells

The test cells can not be cleaned with solvents or acids for two reasons. First, the test cells were made of plexiglass and glass panels and the plexiglass manufacturer warned that most solvents and acids could damage the plexiglass. Second, solvents or acids would dissolve the glues that held the panels together. The following describes the cleaning procedure used in preparation for the microgravity flights.

1. Held the test cell upside down and rinsed it with hot tap water for approximately 2 minutes.
2. Scrubbed the cell in Palmolive dish washing detergent solution with a flask brush for approximately 3 minutes.
3. Held the cell upside down and rinsed it with hot tap water for approximately 5 minutes.

4. Cleaned the cell in an ultrasonic cleaner (Fisherbrand FS20) with Fisherbrand Ultrasonic Cleaning Solution for approximately 10 minutes.
5. Rinsed the cell with distilled water for 2 minutes.
6. Placed the cell upside down on the counter to dry over night.

3.3.3 Cleaning Procedure for the Stainless Steel Tubes

The following describes the procedure used to prepare the stainless steel tubes used in the microgravity experiment.

1. Submerged the tubes in toluene for approximately 10 minutes.
2. Scrubbed the outer wall with a flask brush for approximately 1 minute.
3. Allowed the tube to dry in the fume hood for approximately 2 hours.
4. A syringe was used to force 30 to 40 *mL* of distilled water through the tube.
5. Allowed the tubes to dry on the counter.

4.0 EXPERIMENTS

4.1 Motivation

As discussed in Chapter 1, several mechanisms have been observed to be responsible for the formation of emulsion droplets. In some cases, nano-scale solid particles that exist on the surface of these emulsion droplets have an effect on emulsion behaviour. These nano-scale particles are difficult to observe because of their dimensions. The goal of this research was to study solids-stabilized emulsion droplet systems using macroscopic models based on ground-based (1-g), and reduced-gravity parabolic-flight experiments. Ground-based capillary experiments were also conducted in an effort to understand the behaviour of beads near interfaces.

4.2 Ground-Based Oil Droplet Experiments

Ground-based experiments were set up to test whether a macroscopic model of an emulsion droplet would have similar behaviour to a real emulsion system. Experiments were also done analogous to the colloidal-scale work by Dabros et al. (1999) but with an enlarged model. In a real emulsion system, the droplets are small such that the surface tension dominates and the effect of gravity can be neglected. This is evident as small emulsion droplets are always spherical. However, with an enlarged model, the effect of gravity can be significant and this might alter the results of the experiment. With large droplets, the force of gravity would deform the droplets, which alters the surface geometry, and might change the emulsion droplets' behaviour. To minimise this possibility, the diameters of the droplets were kept bellow a critical diameter such that the Bond number would be less than 0.10. Prior to conducting the experiments, the hydrophibicities of the glass beads were first confirmed by placing the beads on a water-

silicone oil interface. A water filled syringe was used to create a small water droplet in a beaker of oil. The water droplet was then pressed on to a layer of glass beads resting on the bottom of the beaker. The droplet was then brought up and more water was squeezed out to form a bigger droplet. Figures 4-1 and 4-2 show the contact angle difference between the treated and the untreated beads.

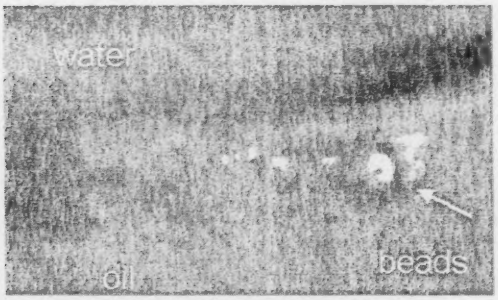

Figure 4-1 Hydrophobic (treated) glass beads on a water-oil interface.

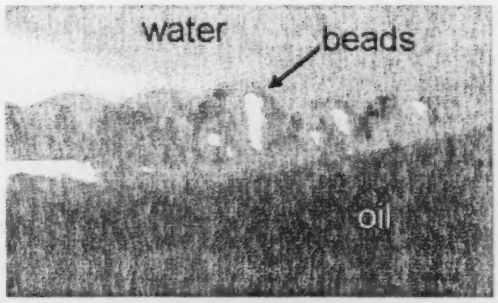

Figure 4-2 Hydrophilic (untreated) glass beads on a water-oil interface.

4.2.1 Set-up of the Apparatus

The selected fluids used for the ground experiments were ultra-filtered, deionized, doubly-distilled water and Dow Corning 710 silicone oil. The small difference in density between the two fluids allowed a relatively large spherical droplet to be formed under the effect of gravity.

A beaker of distilled water was used as the continuous phase, and a layer of glass beads covered the bottom of the beaker (Figure 4-3). A 10 *mL* silicon oil filled syringe was used to create oil droplets in the water. The oil droplets were rolled on the glass beads to collect the beads onto the droplet's surface. The oil droplets were then manipulated for individual experiments. A Hitachi CCD digital camera, model KP-M1U with Navitar lenses, and a computer were used to capture and record the behaviour of the droplets and the beads. The following figure shows a schematic diagram of the system.

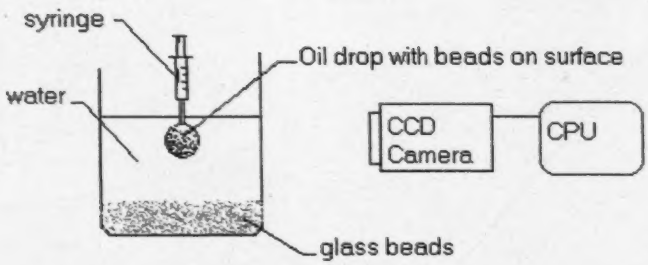

Figure 4-3 Schematic of the ground-based experimental apparatus.

4.2.2 Coalescence Experiments

The first set of experiments involved comparing the model with the known behaviour of solids-stabilized emulsion systems. It is understood that hydrophilic particles stabilize oil-in-water emulsions, and hydrophobic particles stabilize water-in-oil emulsions. This is because hydrophilic particles prevent the coalescence of oil droplets and hydrophobic particles prevent the coalescence of water droplets. To test whether the enlarged model would also exhibit this known behaviour, two droplets were formed and covered in beads. They were then pushed together with glass rods.

Hydrophilic glass beads were first used to cover the oil droplets. Consistent with their hydrophilic surface properties, the beads were mostly in the water phase and only partially submerged in the oil droplets. When oil droplets coated with hydrophilic glass beads were forced together, the droplets did not coalesce (Figures 4-4 and 4-5). It appeared that the beads came in contact with each other and formed a physical barrier that prevented the two oil droplets from coalescing.

Next hydrophobic glass beads were used to cover the oil droplets. Only small portions of the beads were visible in the water phase. When the droplets coated with hydrophobic beads were pushed together, the droplets coalesced almost at the moment

they came to contact with each other and formed a large droplet (Figures 4-6 and 4-7). This behaviour is consistent with colloidal solids-stabilized emulsion studies.

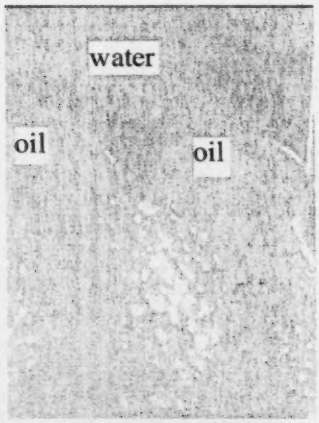

Figure 4-4 Two oil drops coated with hydrophilic glass beads being pushed together.

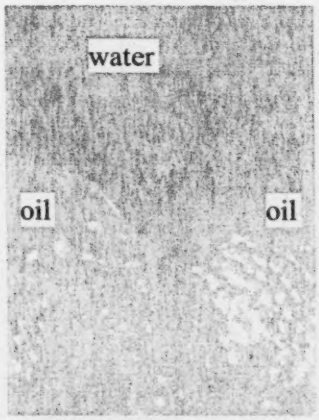

Figure 4-5 The two oil drops after the coalescence attempt.

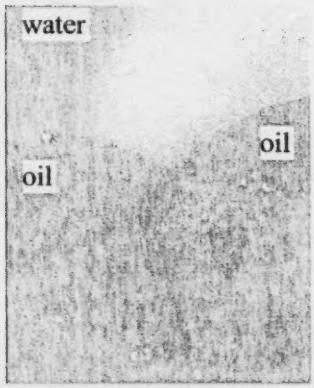

Figure 4-6 Two oil drops coated with hydrophobic glass beads being pushed together.

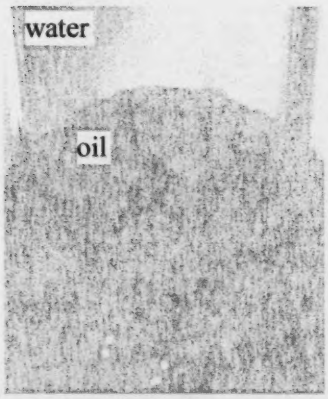

Figure 4-7 One large oil drop was formed after the coalescence attempt.

4.2.3 Area Contraction Experiments

Dabros et al. (1999) recently reported a mechanism of emulsification. They found that by reducing the volume of a large drop, smaller emulsion droplets could be formed. The observations were made for a water/bitumen system using the micropipet technique. A water droplet was first formed in a heptol*-diluted bitumen solution. Negative pressure was then applied to the droplet to rapidly reduce its volume. At low concentrations of bitumen in heptol (< 1% by volume), the droplet surface crumpled. At higher concentrations (> 10% by volume), the drop remained spherical but exhibited small protrusions, which were referred to as dimples, on the surface. When the drop was subjected to further volume reduction, the dimples on the surface would then bud off and form separate emulsion droplets. Dabros et al. suspected the observed phenomena were directly linked to the interfacial properties between the two fluids. It is known that various particles exist at the interface, but it is difficult to observe the behaviour of these particles because of their dimensions.

Experiments with the macroscopic model were set up to mimic the above study so that the beads' behaviour on the interface could be observed as the volume of the droplet was reduced. A droplet, approximately 3 *mm*, was first formed on the tip of the needle. The droplet was then coated with glass beads. The syringe was then used to draw in the droplet and thus reduced the interfacial surface area.

Untreated, hydrophilic beads were first used to coat a 3 *mm* oil droplet. The oil droplet was then drawn back into the syringe. Figures 4-8 through 4-10 show the droplet shrinking with untreated glass beads (size #7) on the surface. From the video, some

* A 1:1 mixture, by volume, of n-heptane and toluene.

beads can be seen to have left the interface and entered the water phase, but the majority of the beads remain on the droplet. As the suction continued, the droplet deformed and eventually the entire droplet fell off the needle (Figures 4-8 through 4-10). It can be seen from the video that a layer of beads had accumulated at the opening of the needle. Which eventually blocked off the connection between the oil droplet and the needle.

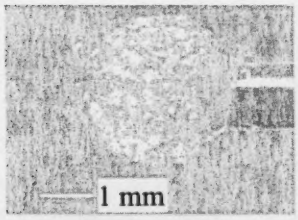

Figure 4-8 An oil drop coated with hydrophilic beads at the start of an area contraction experiment.

Figure 4-9 As suction was applied, the drop deformed.

Figure 4-10 The drop began to detach itself from the needle.

Treated, hydrophobic, glass beads were then used to coat oil droplets. The surface of these droplets first appeared smoother than the droplets coated with hydrophilic beads (Figure 4-11). Suction was again applied to the oil droplet to retract the droplet (Figures 4-11 through 4-16). Similar to the droplets coated with hydrophilic beads, the droplets coated with hydrophobic beads also deformed and became non-spherical. From the video, no beads can be seen to have entered the water phase. In order to account for the reduction in the interfacial area available for the beads during contraction, the beads must have left the interface and entered the oil phase. As the syringe continued to pull the oil into the needle, the surface of the droplet appeared to be rough and 'bumpy' (Figure 4-14). These bumps on the interface were likely to be the glass beads. By applying further suction, the entire oil droplet was pulled into the needle (Figure 4-16).

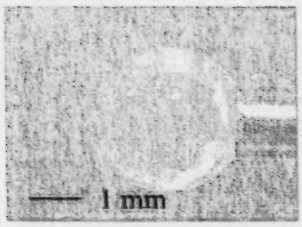

Figure 4-11 An oil drop coated with hydrophobic glass beads.

Figure 4-12 As suction was applied, the oil drop began to deform.

Figure 4-13 The drop continued to deform.

Figure 4-14 The surface of the drop became rough.

Figure 4-15 The drop continued to move into the needle.

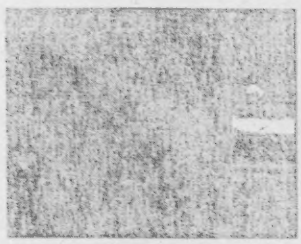

Figure 4-16 The entire drop moved into the needle.

4.3 The Development of the Microgravity Apparatus

The ground-based experiments showed that the macroscopic model behaved similarly to industrially relevant solids-stabilized emulsion systems in several ways. Hydrophilic glass beads prevented the coalescence of oil droplets in water and hydrophobic glass beads allowed the oil droplets to coalesce. Under the effect of gravity, the enlarged emulsion model had several weaknesses. First, the beads on the interface accumulate at the bottom of the droplet. Second, in recent published studies, theoretical as well as experimental investigation had concluded that even in a weak gravity field, the three-phase contact angle will vary with height in a closed system (Ward and Sasges, 1998). It was observed that the three-phase contact angle might have varied with the vertical position of the beads on the droplets. For these reasons, it would be desirable to carry out similar experiments under the reduced gravity conditions that the Falcon 20

could provide. An apparatus was designed to conduct similar experiments under reduced gravity conditions.

4.3.1 Microgravity Experimental Set Up

The basic set up of the microgravity experiment was similar to the ground-based experiments discussed in section 4.2. A steel frame was designed and built to house the components. Closed test cells replaced the open containers that were used to store the liquids. A digital video camera was used instead of the digital camera and computer set up. All the components were either secured to the frame or secured to each other. The total weight of the equipment was approximately 66 pounds (including all the test-cells). The normal electrical power consumption from the aircraft's on board 60 *Hz* power source would be less then 30 *W* and the maximum power usage from the 60 *Hz* power source would be 53 *W*.

4.3.2 Design of the Microgravity Experimental Apparatus

The microgravity experimental apparatus had to meet the following design criteria. First, the apparatus must contain all the equipment and allow convenient access to all the controls that were necessary to perform the experiment. Second, a data recording device must be installed to record the experiments. Third, the entire apparatus must fit within the dimensions given by the *Falcon 20 User's Guide* because the available space inside the aircraft was limited. Finally, the apparatus must satisfy Canadian National Research Council's safety criteria as stated in the *Falcon 20 User's Guide*. The Test Equipment Data Package (TEDP) prepared according to the specifications in the *Falcon 20 User's Guide* is included as Appendix 1.

4.3.2A Camera and Data Acquisition

It was necessary to record the behaviour and the conditions that the experiments were performed in. The primary data collection system for the ground-based experiments included the camera and the computer. The same system that was used for the ground-based experiments would have been too large and heavy to carry on board the aircraft. Alternatives had to be used to successfully capture and record the behaviour of the droplet. Also, the acceleration of the aircraft and the cabin temperature may be important to data analysis. A video camera with a LCD display replaces the CCD camera, the computer and the monitor.

A Sony digital video camera (DCR-TRV530) with a special Raynox lens attachment, which converts a video camera into a video microscope, was used in the microgravity experiments. A digital camera was chosen for its ability to capture imagines with extreme clarity, which will be critical when analysing the data. The Sony digital video camera also offered the largest LCD screen available at the time. Since this screen serves as the primary monitor during the experiment, it was desirable to obtain the largest LCD screen available. The primary power source for the video camera was a lithium battery (Model NP-FM91), which when fully charged had an expected battery life of over 7 hours. A second battery (Model NP-FM31), which had an expected battery life of 70 minutes, was brought on board the aircraft as a back up battery. The video camera could also be powered from a standard 115 VAC power source via an AC-adapter. This AC-adapter was also brought on board the aircraft as a second back up power source.

The temperature data was recorded on the videotape and on a temperature log sheet just before the aircraft entered the microgravity parabola. The operator read the

temperature data while the video camera was recording and at the same time, the operator would write down the temperature data as a back up.

The acceleration data of the flight was recorded by NRC's onboard data acquisition system. Prior to each flight, the video camera was brought to the onboard computer to capture the system clock. By doing so, the difference between the video camera's clock and the system clock can be obtained and the acceleration data can then be traced for each video frame.

4.3.2B Frame

The frame was designed to support and protect all the equipment that was required for the experiment. The frame must also allow the experiments to be set-up in a position such that one operator could perform the experiment comfortably. Since the operator was not restricted to a seat during the microgravity period, there were at least two configurations in which the experiment could be set up in the aircraft. The first choice was to have the operator sit in a seat either in front of, or behind, the apparatus such that the operator would face the experiment throughout the flight. The second option was to have the apparatus open towards the aisle with the operator conducting the experiment while seated on the aisle floor.

By analysing the two available options, the latter of the two appeared to offer several advantages over the first choice. If the operator was to remain in a seat, the apparatus would need to be elevated by a significant amount, while if the operator was to sit on the floor, the apparatus could be situated at a much lower level. A smaller frame would be lighter and therefore easier to set up in a small aircraft cabin. By having the apparatus facing the aisle, the platform could also be significantly wider and thus allow a

much larger working area. The drawback of this option was that there would be no seat belts or any types of restraining devices to hold the operator in position. However based on previous experience of others, lack of restraint would not affect the experiment.

The frame was made out of 1010 square steel tubing and the construction of the frame was contracted out to Stamco Specialty Tool and Mfg. Co. Ltd. Although a number of materials, which offered better strength to weight ratio, could be used, 1010 square steel tubing was the most common and therefore had the fastest turn around time and the lowest cost. Further more, the weight of the frame was not a critical factor in this project and timely completion of the frame was crucial to the experiment; thus it was decided to build the frame out of 1010, square steel tubing.

The frame was designed to fit on the 'Single Mounting' rack as shown in the *Falcon 20 User's Guide*. As discussed above, the frame was used to raise the apparatus so the operator could conduct the experiment comfortably. The basic frame was in the shape of a box and was design to support two shelves (Figure 4-17). The top shelf was used for the primary experimental apparatus which included a video camera, focusing rail, light, stage, and the test cells. The bottom shelf was used to contain any experimental support system, which included lighting control, electrical power bar, thermometer, and AC-adapter for the video camera. The sides of the frame were extended above the rest of the frame. The purpose of these extensions was to protect the equipment on the top shelf and also to act as handles during set up in the cabin. The frame's front, top and side views are included in Appendix 1. The frame was designed without any diagonal members because access to the equipment on the top and bottom

shelves was important. Furthermore the stress calculation in Appendix 1 shows that with the given tubing size diagonal members were not necessary to provide adequate support.

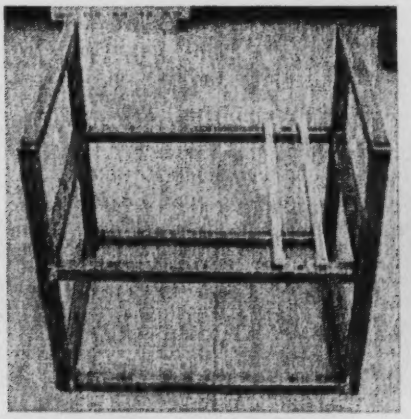

Figure 4-17 The steel frame with aluminum rails for the spare test cells.

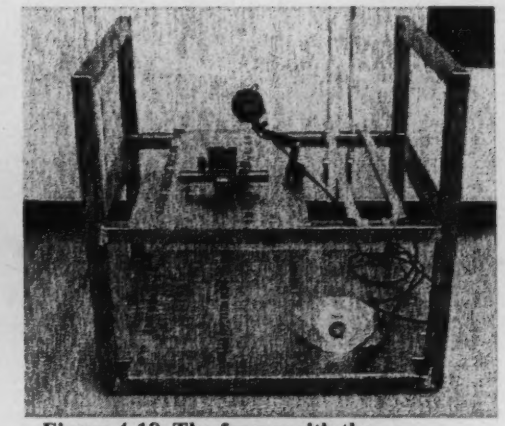

Figure 4-18 The frame with the aluminum shelves in place. The light, the focusing rail and the light controller were mounted to the shelves.

Two shelves made from ¼ inch aluminium plates were also used to support the equipment (Appendix 1). The top shelf was only large enough to support the primary equipment (Figures 4-17 and 4-18). The remaining space on the top shelf was used to store spare test cells, which will be discussed in the ensuing section. Two aluminium rails were bolted to the right hand side of the top shelf. These rails had the same width and thickness as the stage and the test cells could slide on to these rails in the same manner that the test cells slid on to the stage. The brackets that secure the test cells will be discussed in the following section. A safety lock pin was used to prevent the spare test cells from sliding off the rail while allowing the operator to remove the cells with out the use of any tools. Limited by the size of the frame, the rail could hold a maximum of six spare test cells. Various mounting holes were drilled in the bottom shelf and all the necessary instruments can be bolted and strapped directly to the shelves. Additional holes can be drilled in place to provide mounting points for other equipment.

Appendix 1 shows the expected loading on the frame and the formulae used to set up an Excel spreadsheet, which was used to calculate the maximum stress on the frame under the conditions described in the *Falcon 20 User's Guide*. The maximum load that could be exerted on the frame is also shown in Appendix 1. Also in the same appendix, is included an estimate of maximum deflection which the top shelf could experience during the 2.5 g pull up as well as stress calculations for various components.

4.3.2C Test Cells

The test cells were originally designed so that the reduced gravity experimental procedures would be similar to previous ground-based experimental procedures. Each test cell was formed by gluing four acrylic panels and one glass panel together into a box with an open top (Figure 4-19). The glass panel was used as the front panel to minimize optical distortion when viewing through the front. To seal each test cell, a rubber gasket and an acrylic panel were then clamped down with six three quarter inch 4-40 machine screws.

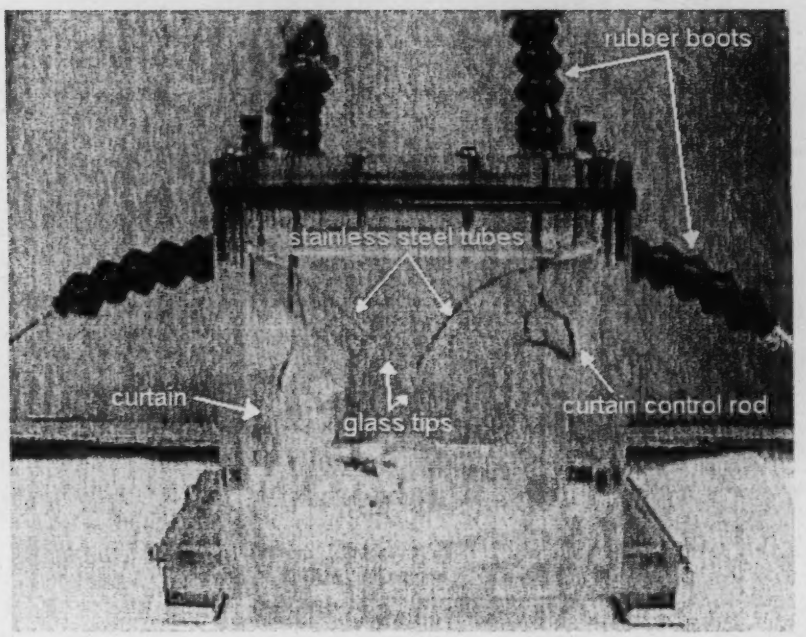

Figure 4-19 Picture of a test cell.

Two stainless tubes protruded into each cell's side panels (Figure 4-19). The holes for these tubes were oversized so that the tubes could be moved around. Rubber boots, normally used for mountain bike brakes, were used to seal the entrances and still allow the tubes to move. Each tube could then be locked in place with a 4-40 by 1 ¾ inch cap screw.

The base of each test cell was extended out and a pair of aluminium brackets was screwed on to the sides. These brackets would latch on to the stage and the spare test cell rack. A hole was drilled on the right hand-side of the base. When the cell was mounted on the stage correctly, this hole would match up with another hole drilled in the stage. A safety pin would then be inserted through these holes to secure the test cell in place. This allowed the operator to switch test cells with out the use of any tools.

In previous ground-based experiments, the glass beads used were at the bottom of the container. If the same procedures were to be used, the beads might float up during reduced gravity and obstruct the camera's view. A two-layer-plastic curtain was used to contain the beads for each cell. The first layer had a square hole cut out of it and the second layer was just big enough to cover the square hole in the first layer. The first curtain with the square hole could be slid to the bottom to expose the beads. Prior to microgravity, the second curtain would then slide over the square hole and divide the cell into two compartments. Two control rods, made from stainless steel wires, could be slid up or down to control the curtain. The openings for the control rods were also sealed using rubber boots.

In the ground-based experiments described earlier, water was used as the continuous phase and oil was injected into the aqueous phase to create an oil droplet. The glass beads rested at the bottom of the container. The oil droplet was then pressed into the glass beads to collect the beads onto the interface. During the practice runs it was realised that the oil droplet had the tendency to wet the side of the needle tips because the needle was not positioned perfectly vertically. Once the oil wetted the side of the needle, the oil droplet would climb up the sides of the needle and the droplet would no longer be symmetrical. The asymmetrical droplet would have a much more complicated flow, be difficult to control and may change the outcome of the experiments. This problem would only worsen in a reduced gravity environment where the force pulling the droplet down on the needle is reduced.

Silicone oil was used as the continuous phase and water was injected into the oil. The water droplet was first injected into the oil bath via stainless steel needle tips, but the

water droplet wetted the stainless tips. Plastic tips were then tried because they are hydrophobic and thus the water will not wet the side of the tips. However, the plastic tips were extremely hydrophobic and water droplets did not always stay on the tips. Finally, a small glass tip was inserted into the plastic tube thus creating a hydrophilic tip with a hydrophobic side (Figure 4-20). This allowed the water droplet to stay on to the tip but prevented the water droplet from climbing the sides of the needles.

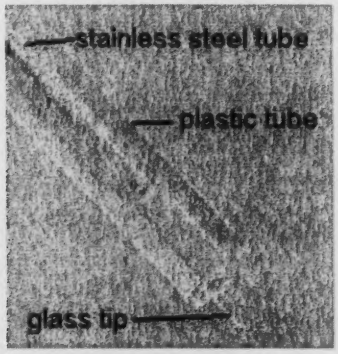

Figure 4-20 The final design of the injection needle tip.

The silicon oil used in the previous ground-based experiments was Dow Corning 700 but for the reduced gravity experiment the oil was changed to Dow Corning 200 Fluid 500 CST (DC 200-500). When the silicone oil became the continuous phase, it was obvious that the amount of silicone oil required for the experiment had increased greatly. The silicone oil used in the ground-based experiments was leftover from a previous research project. There simply was not enough oil for all the experiments. Furthermore, DC 700 oil was extremely expensive because of its stability at high temperature. Since the current experiment operates at room temperature, DC 200-500 was chosen. DC 200-500 was even better density matched to water and the risk of the droplet being pulled off the tip by the vibration or during high-g manoeuvres was reduced.

4.3.2D Lighting

To illumine the experiment, a halogen lamp (Leica Model 13410311) provided the lighting for the camera (Figure 4-21). The light requires a 120 *V* 60 *Hz* power source and the maximum power consumption is 30 *W*. The base of the lamp was removed due to its heavy weight and an aluminium post was used for the lamp to clamp on to. The light control box was mounted to the bottom shelf. Two assembly screws from the bottom of the control box were removed. Two longer screws with the same pitch were used to secure the control box to the shelf and to hold the box together.

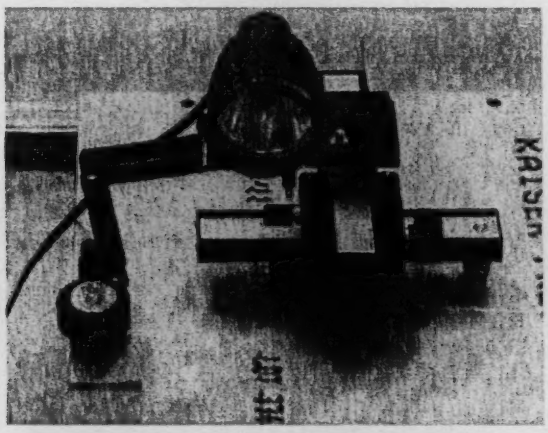

Figure 4-21 The light and the focusing rail mounted on the top shelf.

4.3.2E Stage/Jack Stand

A stand was needed to elevate the test cell such that the experiment would be directly in front of the video camera. Since all the droplets would not be at exactly the same height, it was desirable to use a stand with adjustable height. A Fisher Lab Jack (Figure 4-22), which consists of a top and a bottom plate separated by two scissor-jacks, was modified so that it could be used to elevate and secure a test cell. Four holes were drilled through the bottom plate so it could be mounted to the top shelf. The test cell was

designed to slide on to the stage and a pin that goes through the cell and the top plate would secure the cell into position. During ground testing, it was discovered that the Fisher lab jack had a significant amount of slack in the jacking mechanism. Under the effect of gravity, the weight of the test cell would push down and the slack would not cause any problems. However, when held upside down and excited by vibration, the test cell could bounce up and down as well as side to side. Three steel springs were added to the lab jack to tighten up the slack and increase the overall stiffness, which significantly reduced the vibration.

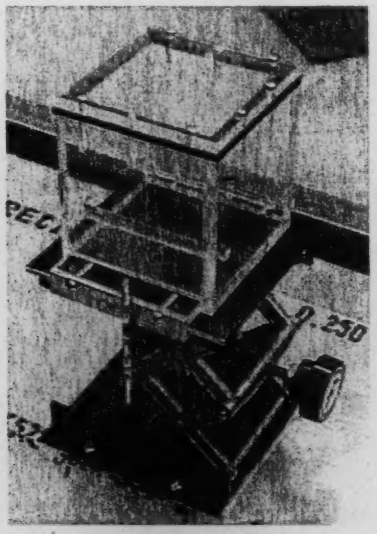

Figure 4-22 An empty test cell on the jack stand, secured in place by brackets and a pin.

4.3.3 Design of the Microgravity Experimental Procedures

After the fluids in the test cell had been changed so that silicone oil was the continuous phase, the procedure used in the ground-based experiments was tested. A water droplet was first formed on the needle and it was then moved down to collect the glass beads which were at the bottom of the cell. During this test, it was realised that because the silicone oil was much more viscous than water, the water droplet needed to be moved significantly slower than the previous oil drops; otherwise it would get pulled off the needle. Thus, the procedure needed to be modified to reduce the preparation time since it might cause delay during microgravity when only 20 seconds were available for an entire experiment.

For the first modified procedure, a needle sucked up the beads, which were submerged in the oil phase, from the bottom of a test cell. The second needle then injected water in and formed a water droplet. The first needle was then directed toward the droplet and the beads were then squeezed out (Figure 4-23). This was first done with hydrophilic beads and thus the beads were expected to attach to the water. This was not observed, and instead the beads stayed in the oil phase and slid past the water droplet.

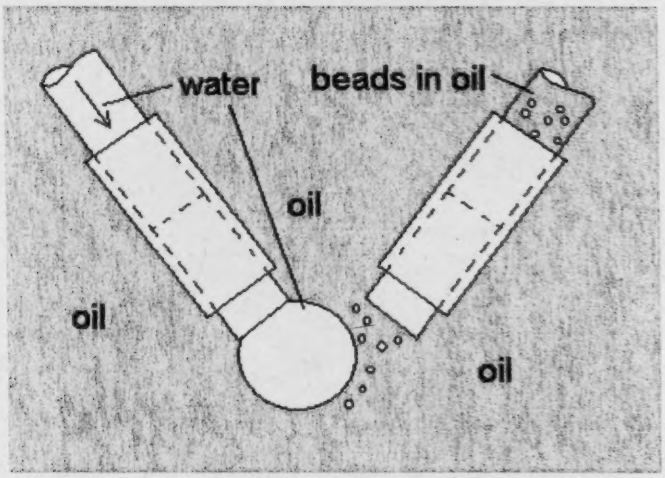

Figure 4-23. A schematic diagram of beads-in-oil injection method.

The next trial procedure was to have hydrophilic beads starting in the water phase and inject water and beads together. The second needle would then be used to adjust the size of the water droplet by injecting in or sucking out water from the droplet (Figure 4-24). During the practice trials, it was observed that the beads would collect inside the water droplet as if the interface of the droplet was a solid bag. The second needle was used to create a flow within the droplet by injecting and sucking in water repeatedly. The flow created through this pumping motion was enough to move some of the beads onto the surface. It was hoped that the vibration on the flight would shake the beads on to the interface and the pumping action may be used as an additional method to assist more beads to the interface. This procedure was adapted for experiments conducted in flights 1 through 4. A detailed check list format of the procedure can be found in Appendix 1.

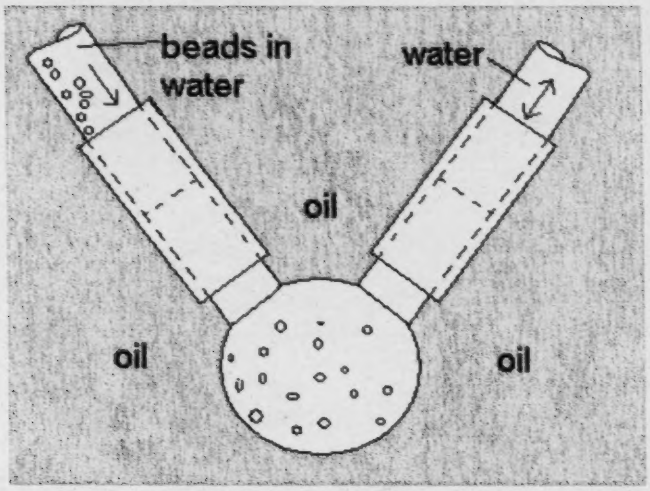

Figure 4-24. A schematic of beads-in-water injection method.

4.3.4 Procedure Used in Flight 5

The experimental procedure in flight 5 was modified due to the observations made from the flights 1 to 4. The observations will be further discussed in the following section. During the first few microgravity experiments, hydrophobic glass beads were used and it was observed that the glass beads did not obtain their thermodynamic equilibrium position. The procedure described in section 4.3.3 had the hydrophobic glass beads start in the water phase but despite their hydrophobic property, most of the beads stayed in the water phase. The procedure was then modified such that the hydrophobic beads would start in the oil phase for experiments conducted in flight 5.

In the ground-based experiment, the glass beads were placed in the continuous phase and the glass beads got on the interface by forcing the droplets against the beads. This procedure was abandoned for flights 1 through 4 because the set up time for this procedure was much too long. However, this was the only procedure that physically forced the glass beads to be on to the interface.

A jar of hydrophobic beads was placed inside an oven and baked overnight to remove any moisture. These glass beads were then soaked in silicone oil and injected into a test cell until the bottom of the test cell was completely covered by the beads.

The problem with using the ground-based procedure in an environment where oil is the continuous phase, was that the viscous oil would drag the water droplets off the needle tips. Various techniques, such as smaller droplets, slower speeds, injecting and retracting droplets, were tried to minimise this effect. The final procedure used was to dip the needle into the beads. This would collect some glass beads in and around the needle tip. Once the aircraft began the microgravity portion of the flight, the needle was then brought back up to the camera's field of view. A droplet of water would then be squeezed out and worked with. This new procedure was tried and practised prior to the take-off and during level flight. The major draw back of this procedure was that the droplet and the video camera had to be set up during microgravity. Since the time was limited, two operators were needed to perform the experiment and even with two operators there was still a risk of not getting the droplet or the camera ready before the microgravity portion of the flight ended.

4.3.5 Microgravity Experimental Observations

The section below describes the experiments that are significant to this thesis. Detail description of other microgravity experiments can be found in Appendix 2. The diameter of the needle tips, 2 *mm*, was used to estimate the size of the droplets, and the thickness of the beads collected at the bottom of the drop. For estimating the volume occupied by beads inside the drops, the drops were assumed to be spherical and the all glass beads were assumed to be perfect spheres with a radius of 65 μm (average radius for the size 8 beads). The packing efficiency coefficient used to estimate the number of beads was 0.6 (Torquato, Truskett, and Debenedetti, 2000).

Only one camera was used in this experiment, therefore, the observed position of the beads with respect to the interface is only valid when the beads are on the side of the droplets.

4.3.5A Flight 1 – Water Droplet in Oil With Hydrophobic Beads in Water

Hydrophobic beads were used for the first flight. A number of questions were to be answered with the first set of experiments. First, although calculations showed that a 5 *mm* droplet would easily stay on the needle during the 2-*g* pull up, the vibration in the cabin could shake the droplet off the needle. Second, during previous ground-based experiments a pumping action was required to push the beads from the water phase on to the interface. It was hoped that the vibration would cause the beads to move on to the interface.

Flight 1 Parabola 1

A droplet, approximately 7 *mm* in diameter was created at the tip of the needles prior to take off. As estimated by the volume occupied, there were approximately 2000

beads on and in the droplet. This droplet stayed on the needle through take-off and level flight, and also remained in position through the 2-*g* pull up. Although some vibration could be felt in the cabin, it was not strong enough to shake the droplet off the needle nor was it able to shake the hydrophobic beads onto the interface.

During the first parabola, it was observed that the hydrophobic beads remained together regardless of the direction of the acceleration. The vibration did not shake the beads apart as originally hoped. The beads also stayed on the water-side of the interface, which was unexpected because of their hydrophobicity.

Flight 1 Parabola 2

Between parabola 1 and 2, a droplet with diameter approximately 8 *mm* was formed. While forming this droplet, a smaller droplet was formed at the tip (Figure 4-25). The smaller droplet quickly coalesced with the main droplet and sprayed some glass beads onto the interface (figure 4-26). A similar event repeated itself a few seconds later and more glass beads got onto the interface. Figure 4-27 shows at least one bead was on the oil-side of the interface after the two droplets coalesced.

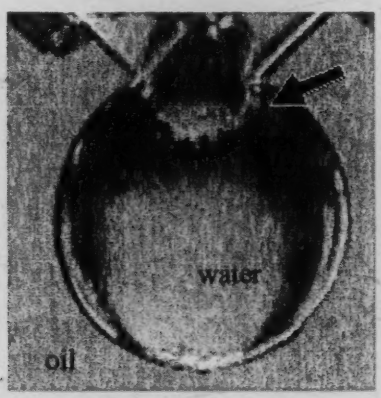

Figure 4-25 A second water droplet formed on top of the first water droplet.

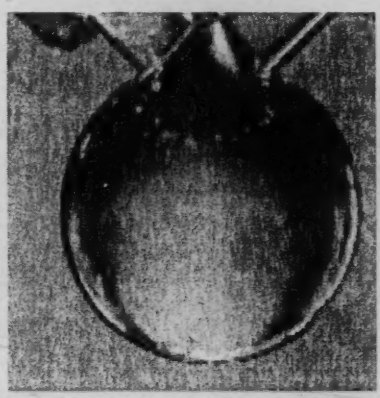

Figure 4-26 The second water droplet coalesced with the first water droplet and sprayed out several hydrophobic glass beads.

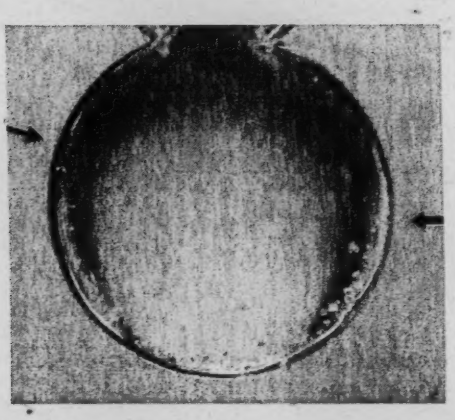

Figure 4-27 Several seconds after the two water droplets coalesced, hydrophobic glass beads can be seen on the oil-side of the interface.

Another droplet with a diameter of approximately 8 *mm* was created during level flight. Approximately 2000 beads were in the droplet. Once again, the vibration was not violent enough to shake the hydrophobic beads apart and they stayed on the water side of the interface (Figure 4-28).

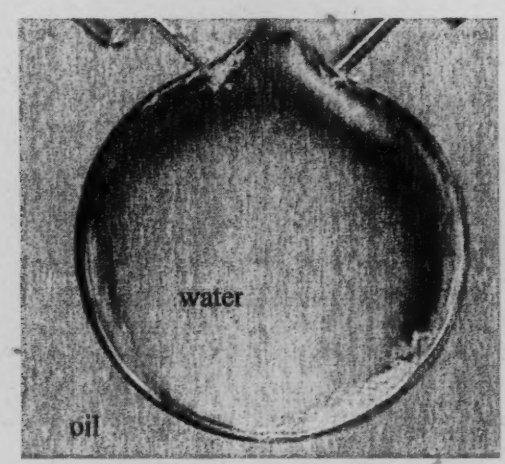

Figure 4-28 The hydrophobic glass beads remain in the water drop.

Flight 1 Parabola 3

The vibration from the aircraft does not appear to be able to shake the beads apart. Therefore, during the level flight between parabola 2 and 3, the pumping technique,

which was discussed earlier, was used to force the beads apart and through the interface but it had only limited success. Although this technique did manage to push some beads onto the oil-side of the interface it had a few drawbacks. Several droplets with promising numbers of beads on the interface were lost because the pumping motion made it difficult to keep the droplet on the needle. In addition to losing droplets, the rapid pumping motion mixed oil and water. Small oil droplets were observed in the water droplets and several beads can be seen on the interface (Figure 4-29).

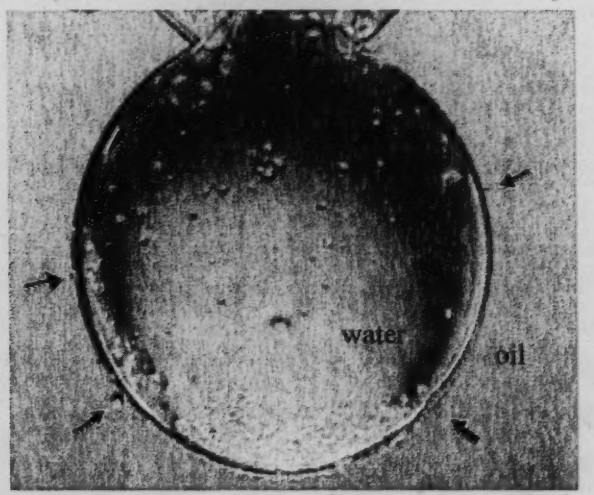

Figure 4-29 The pumping motion pushed some of the hydrophobic beads to the oil-side of the interface but it also mixed oil in with the water droplet.

After several droplets were lost, a droplet was created with few beads on the interface. The pumping motion was to be delayed until the reduced gravity condition began. The pumping action introduced more beads into the droplet but most of the beads remained inside the water droplet (Figure 4-30). The beads were not evenly distributed, as most of them rested on the bottom of the droplet. An attempt to contract the droplet was made just prior to the 2-*g* pull out. At the beginning of the area contraction, the

droplet diameter was approximately 12 *mm*. The number of beads cannot be estimated because it was difficult to estimate the volume that the beads had occupied during the reduced gravity portion of the flight. During the first portion of the contraction, the water retracted into the needle did not contain any glass beads (Figure 4-31 and 4-32). The droplet broke off almost as soon as the first bead entered the needle (Figure 4-33). When the droplet left the needle, the diameter of the droplet was 3.5 *mm* and the glass beads occupied almost the entire droplet.

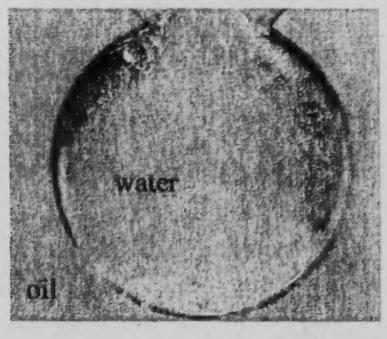

Figure 4-30 The water droplet just before it was retracted.

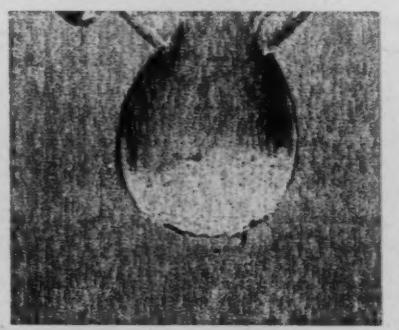

Figure 4-31 The water droplet deforms as the water moves into the needle. Note several glass beads have exited the water droplet.

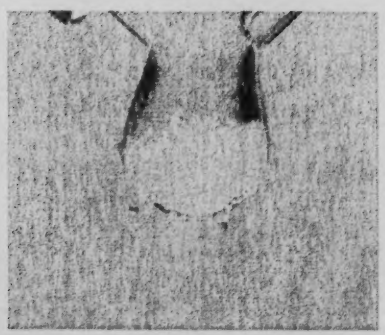

Figure 4-32 The water droplet continued to retract into the needle.

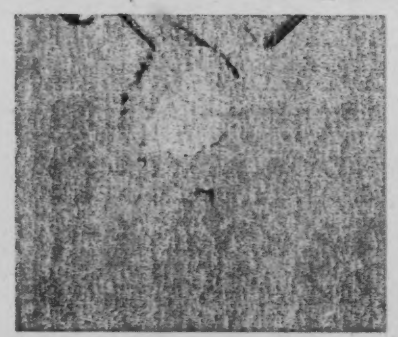

Figure 4-33 As the first few hydrophobic beads entered the needle, the rest of the water droplet broke away.

Flight 1 Parabola 4

In this parabola, no tangible results were produced. See Appendix 2 for detail.

4.3.5B Flight 2 – Water Droplet in Oil With Hydrophobic Beads in Water

Hydrophobic beads were used again for flight 2. The major problem encountered in flight 1 was that the beads were not able to get onto the oil side of the interface. During the 4th parabola of flight 1, a droplet was formed in the reduced gravity portion of the flight and a number of beads were observed to be on the oil-side of the interface of this droplet. Therefore, attempts were made to create the droplet during microgravity in flight 2.

Flight 2 Parabola 1

In this parabola, no tangible results were produced. See Appendix 2 for detail.

Flight 2 Parabola 2

In this parabola, no tangible results were produced. See Appendix 2 for detail.

Flight 2 Parabola 3

A droplet of 6.5 *mm* in diameter with approximately 8000 beads was created during level-flight between parabola 2 and 3. While the droplet was created, several smaller droplets were also formed and coalesced with the main droplet (Figures 4-34 and 4-35). As observed in other parabolas, a few glass beads seemed to get pushed onto the interface when the droplets coalesced (Figure 4-35). This time however, it was much more difficult to tell which side the beads were on (Figure 4-36). This droplet was pulled off the needle during the 2-*g* pull up. Another droplet was formed during the parabola and a few beads appeared to be on the interface. Despite their hydrophobicity, the beads were observed to be on the water-side of the interface (Figure 4-37). These beads did not continue to move to the oil-side of the interface before the 2-*g* pull out.

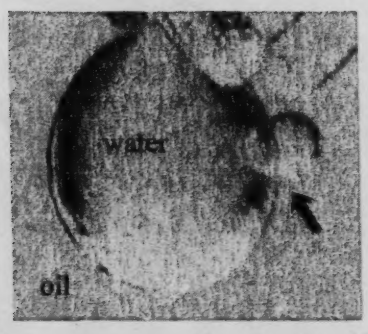

Figure 4-34 Two water droplets just before they coalesce.

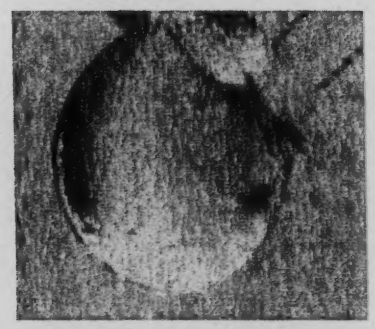

Figure 4-35 The small water droplet joins in with the first water droplet.

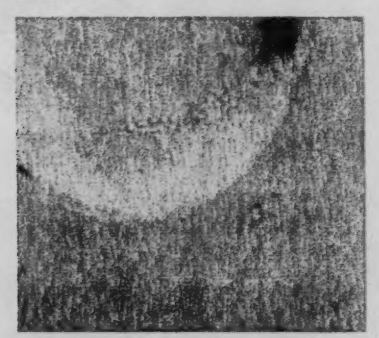

Figure 4-36 A close up view of the interface after the two water droplets have coalesced.

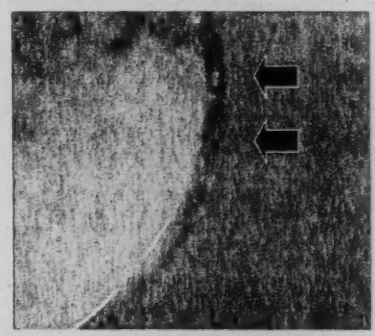

Figure 4-37 The hydrophobic beads are on the interface but they are mostly in the water droplet.

Flight 2 Parabola 4

A 3.5 *mm* diameter droplet with approximately 600 beads was formed during level flight but it was hanging onto the side of the left needle. A second droplet was formed during reduced gravity. Although the injection created significant fluid motion, no beads were observed to be on the oil side of the interface. When the second droplet began to squeeze the first droplet, the first droplet burst and the two droplets coalesced (Figure 4-38). After the two droplets coalesced, and the beads settled, a bead appeared to have moved to the oil-side of the interface (Figure 4-39). This bead then left the interface when the droplet was retracted (Figure 4-40).

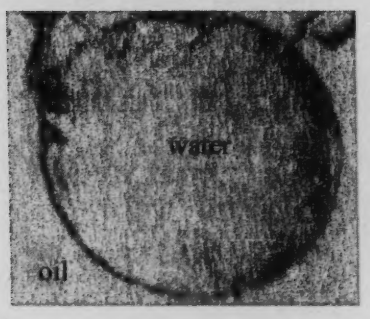

Figure 4-38 Two water droplets coalescing.

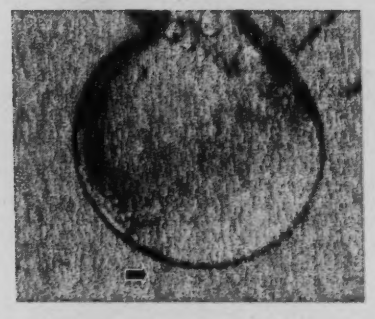

Figure 4-39 After the two water droplets coalesced, a hydrophobic bead was pushed out of the water droplet.

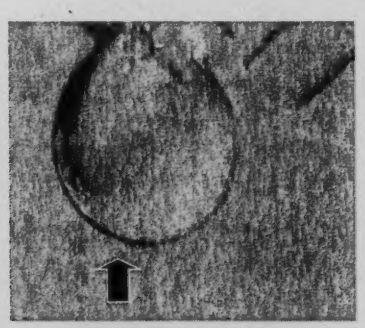

Figure 4-40 The hydrophobic bead left the interface immediately after the water droplet began to retract.

4.3.5C Flight 3 – Water Droplet in Oil With Hydrophilic Beads in Water

Hydrophilic beads were used for flight 3. Similar to the experiments of the previous two flights, the beads started in the water phase and were injected into the test cell via one of the needles. The second needle was used to either inject or remove water from the droplet.

Flight 3 Parabola 1

A droplet was prepared during level flight but it was lost during the 2-*g* pull up and a new droplet was formed under reduced gravity. The beads, however, collected in the direction of the acceleration. The syringe was pumped to force the beads onto the

interface. The syringe was pulled back to retract the droplet. The droplet size just before the droplet retracted was approximately 7 *mm* (Figure 4-41). The amount of beads in the droplet was not determined because the volume that the beads occupied was difficult to approximate. Water and the beads flowed smoothly into the needle while they retracted into it (Figures 4-42 and 4-43). The entire droplet was almost fully retracted into the needle before the 2-*g* pull-out pulled the droplet off the needle (Figure 4-44).

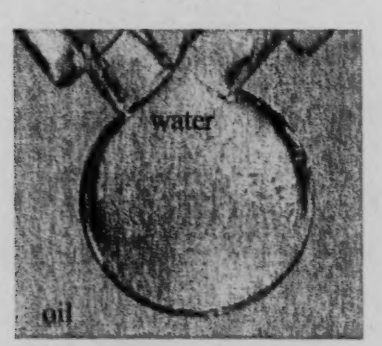

Figure 4-41 A water droplet full of hydrophilic beads.

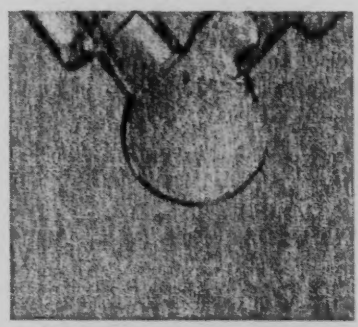

Figure 4-42 Hydrophilic beads flowed into the needle with the water.

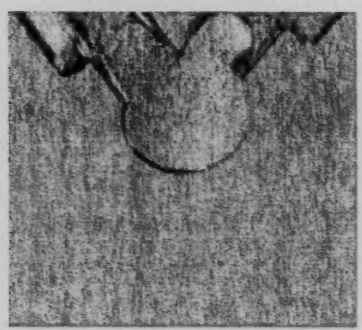

Figure 4-43 Hydrophilic beads continue to flow into the needle.

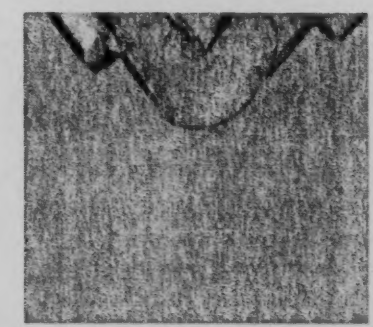

Figure 4-44 Hydrophilic beads filled the needle just prior to the 2-*g* pull-out.

Flight 3 Parabola 2

In this parabola, no tangible results were produced. See Appendix 2 for detail.

Flight 3 Parabola 3

A droplet was formed during level flight but more water and beads were injected to form a larger droplet and to stir the beads around. Similarly to the previous parabolas, the beads continued to settle down in the direction of the acceleration. The droplet was retracted into the needle and pushed out two times before the 2-*g* pull-out. The first droplet started at approximately 4.5 *mm* and was completely drawn into the needle within 0.57 seconds (Figures 4-45 through 4-48). Several small droplets were formed during this procedure (Figure 4-49).

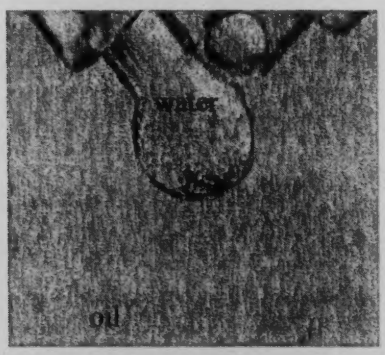

Figure 4-45 A water droplet partially coated with hydrophilic beads.

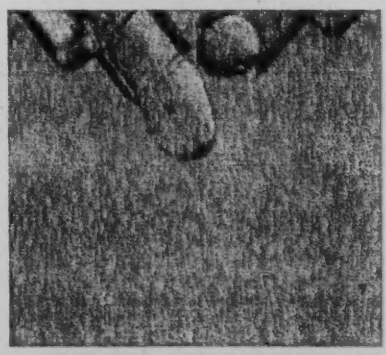

Figure 4-46 The syringe brought the droplet back into the needle.

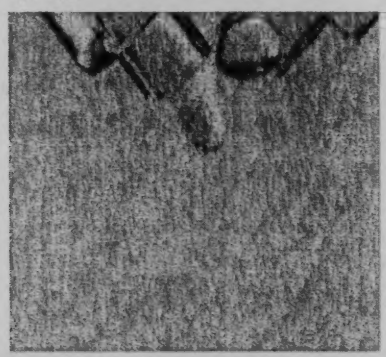

Figure 4-47 The water droplet deforms while being pulled into the needle.

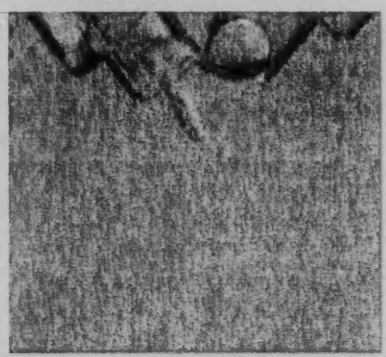

Figure 4-48 The water droplet narrows as it continues to be pulled into the syringe.

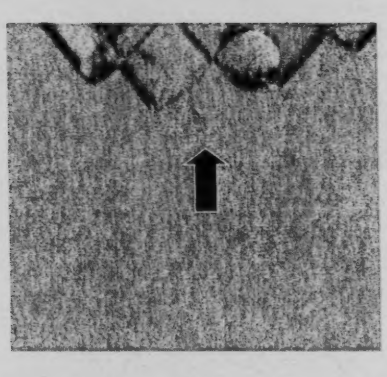

Figure 4-49. A small droplet of water has been left behind.

The droplet was then pushed out to about the same size (4.5 *mm*, Figure 4-50) and drawn into the needle within 1.03 seconds (Figures 4-51 through 4-53). This time, no small droplets detached from the main droplet. It was difficult to determine whether the small droplets formed during the first retraction contain any glass beads. The small droplets did not coalesce with each other nor with the second droplet.

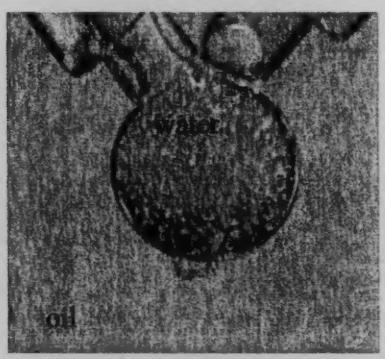

Figure 4-50 Another water droplet with hydrophilic beads was formed after the first one was retracted into the needle. The small droplets hanging under the main water droplet were part of the first water droplet.

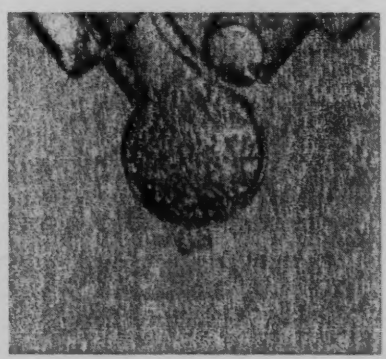

Figure 4-51 The second water droplet began to retract into the needle.

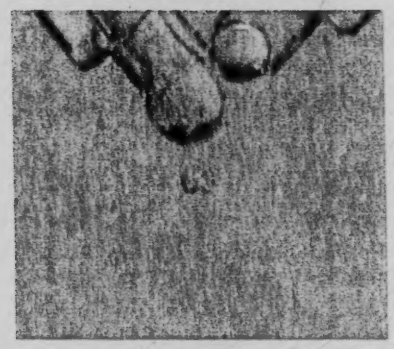

Figure 4-52 The two smaller water droplets were left behind as the second water droplet moved into the needle.

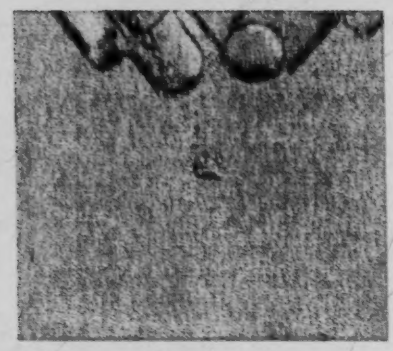

Figure 4-53 The second water droplet was retracted into the needle without breaking up into smaller droplets.

Flight 3 Parabola 4

A 9 *mm* droplet was formed under reduced gravity conditions (Figure 4-54). A number of beads were observed to be on the interface as well as in the water phase. This droplet was retracted into the needle in about 8 seconds (Figures 4-55 through 4-57). There were not any small droplets after the droplet was retracted (Figure 4-58).

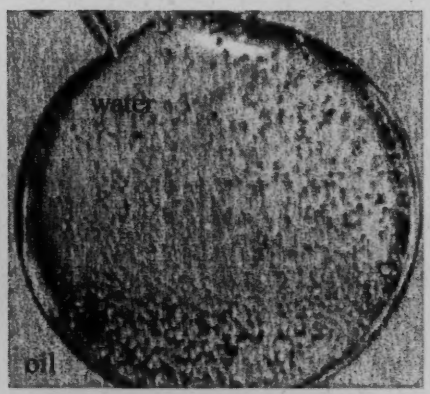

Figure 4-54 A 9 *mm* water droplet was formed in reduced gravity.

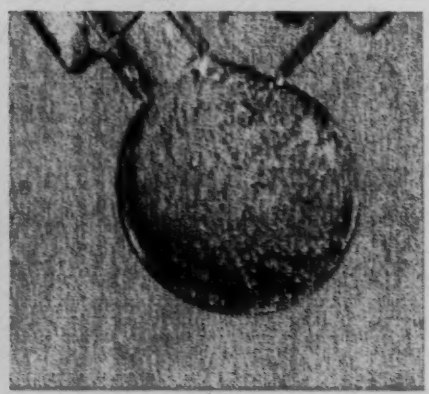

Figure 4-55 As it began to retract, part of the water droplet came in contact with the needle on the right.

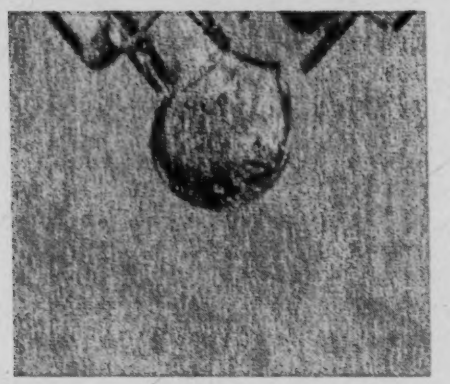

Figure 4-56 The water droplet continues to retract into the needle.

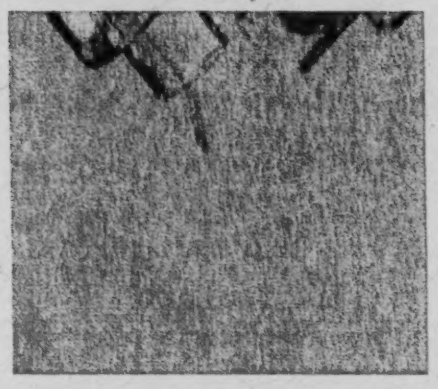

Figure 4-57 The water droplet deformed as it moved into the needle.

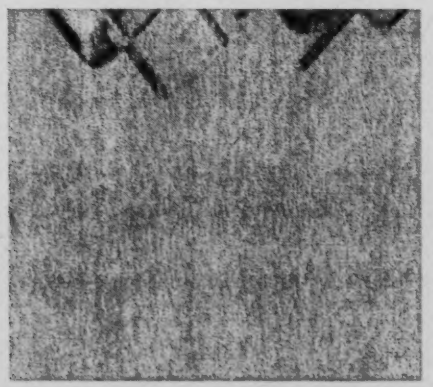

Figure 4-58 The entire water droplet was retracted into the needle.

4.3.5D Flight 4 – Water Droplet in Oil With Hydrophilic Beads

Hydrophilic beads were again used for flight 4. The procedure for the experiments was similar to the previous flights.

Flight 4 Parabola 1

In this parabola, no tangible results were produced. See Appendix 2 for detail.

Flight 4 Parabola 2

A large droplet, approximately 10.5 *mm*, was created with almost all of its volume and surface occupied by glass beads. The droplet was pumped twice before being

retracted (Figure 4-59). The droplet diameter just before it was retracted was approximately 5.5 *mm*. After about 3 seconds, the beads clogged the needle and the flow stopped (Figure 4-60). At this point the droplet that was fully occupied by the beads was no longer spherical. The droplet had the shape of a bowl (Figure 4-61). The largest diameter was 4.5 *mm* and its height was 3.5 *mm*. This droplet remained in place until the 2-*g* pull-out when it detached. As the droplet disappeared from the view of the camera, its shape remained irregular (Figure 4-62).

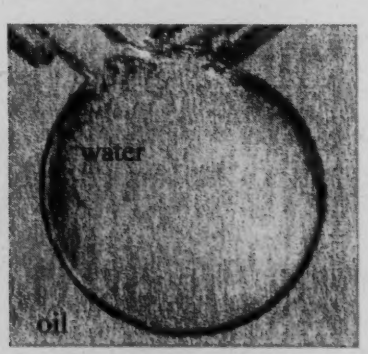

Figure 4-59 A water droplet being pumped.

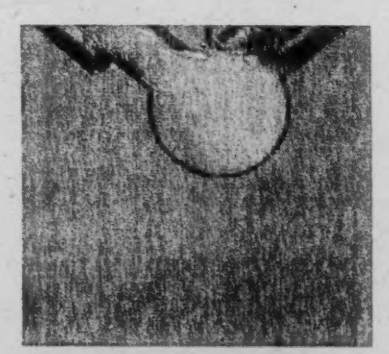

Figure 4-60 The hydrophilic beads flowed into the needle with the water droplet.

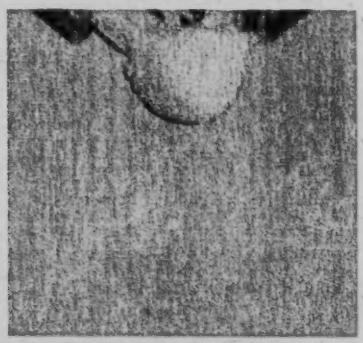

Figure 4-61 The flow stopped and the water droplet deforms.

Figure 4-62 The water droplet being pulled off during the 2-*g* pull out.

Flight 4 Parabola 3

A 10 *mm* diameter droplet was formed and retracted under reduced gravity (Figure 4-63). The droplet was retracted for less then 3 seconds when a portion of the

droplet became attached to the side of the other needle and formed a separate droplet (Figure 4-64). The new droplet contained most of the beads and had a diameter of 3 *mm* (Figure 4-65).

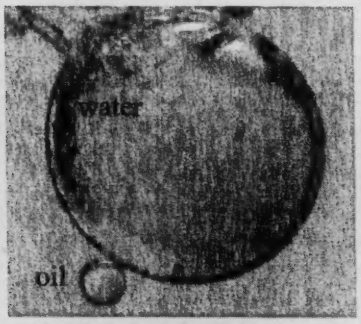

Figure 4-63 A 10 mm water droplet formed.

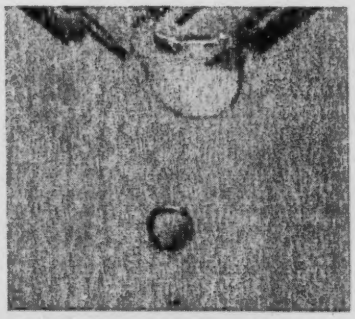

Figure 4-64 The droplet became attached to the needle on the right hand side.

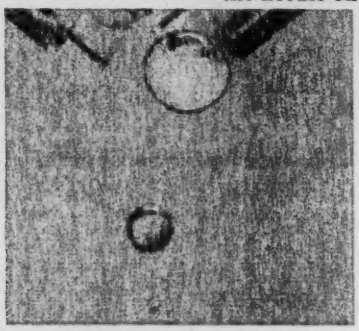

Figure 4-65 The water droplet left behind on the needle.

Flight 4 Parabola 4

A 10.5 *mm* droplet was formed with few beads on its interface and then retracted (Figure 4-66). Note that several small water droplets were left behind from previous attempts at forming a droplet and they will remain in the frame throughout the retraction. Although part of the droplet appeared to be in contact with the side of the needle, the droplet retracted without leaving behind any additional small droplets (Figures 4-67 through 4-70). The time taken to retract the droplet was approximately 4.5 seconds.

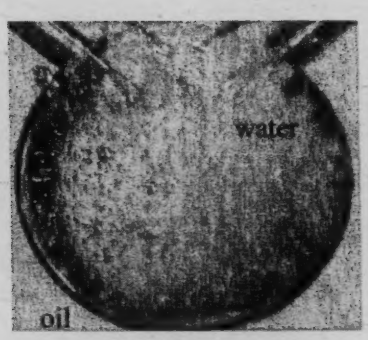

Figure 4-66 A 10.5 *mm* water droplet prior to retraction. Several small water droplets were in the foreground.

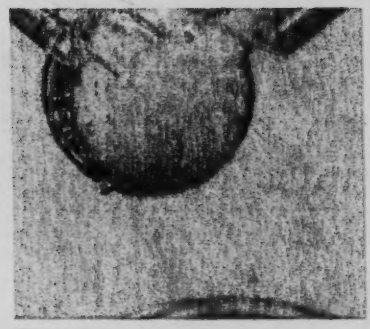

Figure 4-67 The water droplet began to retract.

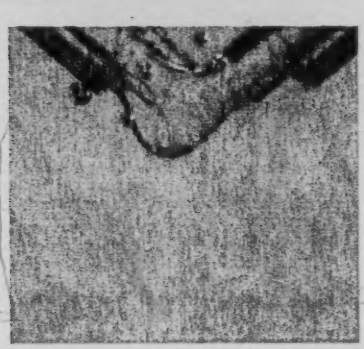

Figure 4-68 The water droplet retracts into the left needle while attached to the right needle.

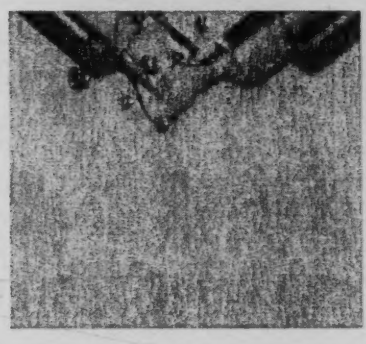

Figure 4-69 The water droplet began to split into two parts.

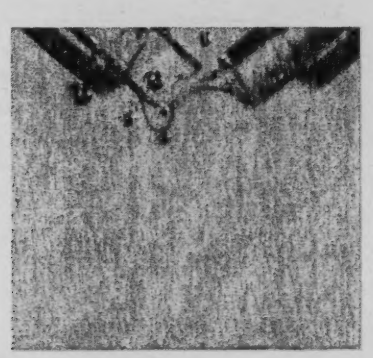

Figure 4-70 The water droplet retracts into the needle without leaving additional water droplets in the continuous phase.

4.3.5E Flight 5 – Water Droplet in Oil With Hydrophobic Beads in Oil

The experiments conducted during flights 1 and 2 showed that when hydrophobic beads start in the water phase, they will not spontaneously get onto the interface. A new procedure was developed to force the hydrophobic glass beads on to the interface. This was discussed in section 4.3.4.

Flight 5 Parabola 1

A 3 *mm* droplet was formed with several beads on the oil side of the interface (Figure 4-71). The droplet was then retracted back into the needle in 1.5 seconds. Although the droplet was slightly out of focus, at least one bead can be seen leaving the interface (Figures 4-72 and 4-73).

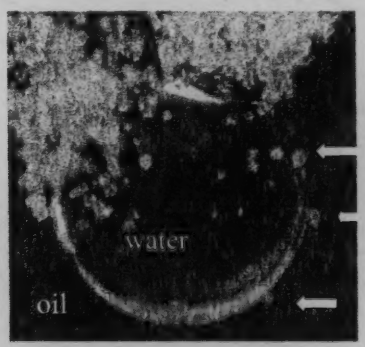

Figure 4-71 At least three hydrophobic beads can be seen to be on the interface.

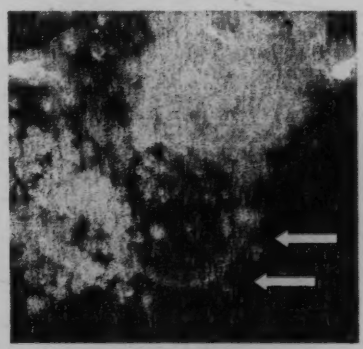

Figure 4-72 At least two beads left the interface.

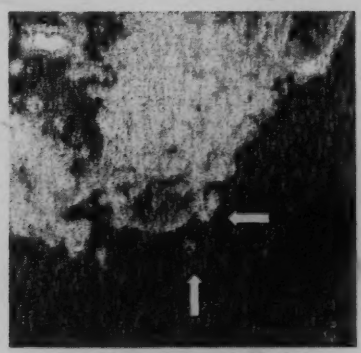

Figure 4-73 These beads were left in the continuous (oil) phase.

Flight 5 Parabola 2

Another 3 *mm* droplet with over 50 beads on the interface was formed in the second parabola (Figure 4-74). This droplet was retracted in about 2.5 seconds and at the same time the beads were observed to leave the interface (Figures 4-75 and 4-76). The 3 *mm* droplet was squeezed out again until the beads came in contact with the interface (Figure 4-77). Once the beads were on the interface of the droplet, the droplet was pulled into the needle once more. This time, the droplet was retracted in about 1.5 seconds. Similarly to the previous observation, the beads were observed to leave the interface during the retraction (Figure 4-78 and 4-79).

Figure 4-74 A 5 *mm* water droplet was formed with numerous hydrophobic beads on its interface.

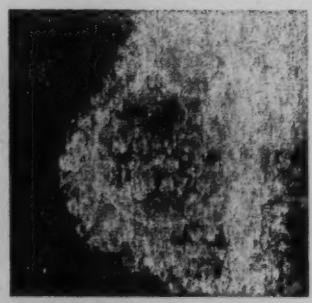

Figure 4-75 As the water droplet retracted, the hydrophobic beads detached and did not retract with the droplet.

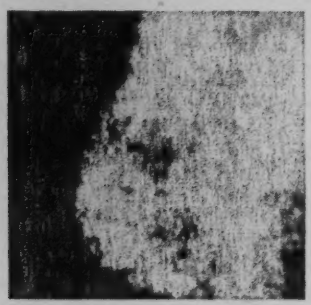

Figure 4-76 The water droplet was brought into the needle.

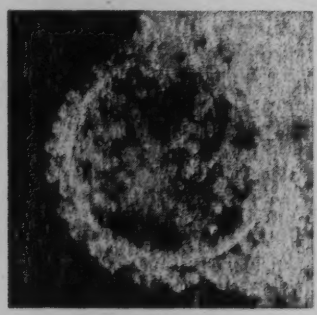

Figure 4-77 A second water droplet of similar size was formed during the same parabola.

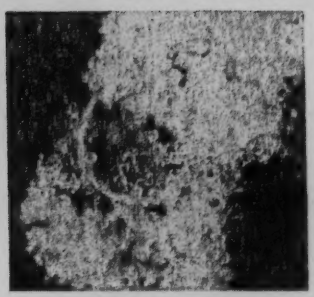

Figure 4-78 When the water droplet retracted, the hydrophobic beads detached themselves from the interface.

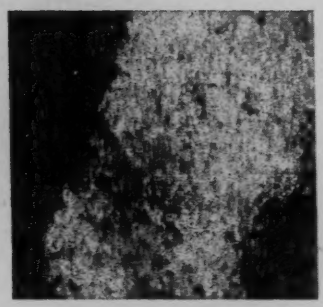

Figure 4-79 The water droplet just before it disappeared into the needle.

Flight 5 Parabola 3

A droplet was formed with a few beads on the interface but it was outside of the camera frame during the parabola.

Flight 5 Parabola 4

Another 3 *mm* droplet with about 10 beads on the interface was retracted (Figure 4-80). At least 2 beads can be seen to have left the interface halfway through the experiment (Figure 4-81).

Figure 4-80 A small water droplet with few beads on the interface. The arrow is pointing at a hydrophobic bead that can be seen to leave the interface.

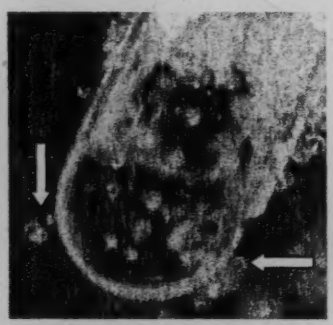

Figure 4-81 Arrows showing the beads that left the interface.

The following table provides a brief summary of the microgravity observations. The flight and the parabola number are indicated in columns 1 and 2. The type of beads used was either extremely hydrophobic or extremely hydrophilic and is recorded in the third column. The number of beads released into the system was approximated by volume which the beads occupied during level flight and it is shown in the fourth column. The number of beads released during microgravity could not be approximated because the volume occupied by the beads can not be estimated. In the fifth column, the approximated number of beads on the interface is recorded for the hydrophobic glass beads. For the hydrophilic glass beads, it was difficult to tell which of the beads were on the interface and which ones were floating inside the droplet because in either case, they were all inside the droplet. The next three columns show if droplet coalescence was observed, if the pumping method discussed earlier was applied and if the area retraction experiment was performed. Special notes and observations are included in the last column.

Table 4-1 Microgravity experiment summary. All experiments are consist of water droplets in oil.

Flight #	Parabola #	Bead type and starting phase	Approx. # of beads released	Approx. # of beads on interface	Coalesce of droplets?	Pumping ?	Retraction Exp.	Note
1	1	Hydrophobic	1500	0	No	No	No	
	between 1,2		>150	10	Yes	No	No	Coalescence moved beads to oil side.
	2	Started in water	1500	0	No	No	No	
	Between 2,3		>4000	7	No	Yes	No	
	3		Formed in microgravity	>5	No	Yes	Yes	Droplet deformed and broke away from the needle.
2	1	Hydrophobic	Formed in microgravity	0	No	Yes	No	
	2		Formed in microgravity	0	No	Yes	No	
	3	Started in water	>8000	Few, and difficult to tell	Yes	No	No	Coalescence moved beads to oil side.
	4		600	>1	Yes	Yes	Yes	Retraction did not complete. Coalescence moved beads to oil side.
3	1	Hydrophilic	Formed in microgravity	Difficult to tell	No	No	Yes	The entire droplet was almost inside the needle before microgravity ended.
	2		Formed in microgravity	Difficult to tell	No	No	Yes	Droplet retracted rapidly and broke into several smaller droplets.
	3	Started in water	Formed in microgravity	Difficult to tell	No	No	Yes	Droplet retracted rapidly and a smaller droplet was left behind.
							Yes	Droplet was retracted slower and the entire second droplet was retracted.
	4		Formed in microgravity	Difficult to tell	No	No	Yes	The entire droplet was retracted into the needle.
4	1	Hydrophilic	Formed in microgravity	Difficult to tell	No	No	Yes	Asymmetric droplets.
	2		Formed in microgravity	Difficult to tell	No	Yes	Yes	Beads clogged the needle during retraction.
	3	Started in water	Formed in microgravity	Difficult to tell	No	No	Yes	Asymmetric droplets.
	4		Formed in microgravity	Difficult to tell	No	No	Yes	The entire droplet was retracted into the needle.
5	1	Hydrophobic	>100	>10	No	No	Yes	Entire droplet was retracted. Beads left the interface.
	2	Started in oil	>200	>20	No	No	Yes	Entire droplet was retracted. Beads left the interface.
	4		>100	>10	No	No	Yes	Entire droplet was retracted. Beads left the interface.

4.4 Ground-Based Capillary Experiment

The experiments conducted in microgravity had shown that the hydrophobic glass beads did not enter the silicone oil-water interface spontaneously. A ground-based experiment was designed to study the behaviour of the glass beads near the interface.

4.4.1 Set-up of the Apparatus and Procedures

The basic equipment of this experiment consisted of a glass pipette, test cell, and a digital video camera. Disposable glass pipettes used in the experiments were approximately 2 *mm* in diameter at the narrowest section. Each pipette was filled with silicone oil and distilled water or silicone oil and an electrolyte solution to create an interface (Figure 4-82). In Figure 4-82 the top fluid is referred to as fluid A and the bottom fluid is fluid B. The pipette was immersed in a water filled test cell (the same as that used in the microgravity experiments) to reduce the distortion caused by the round pipette. The beads' behaviour on the interface was then recorded by the Sony digital video camera also used in the microgravity experiments.

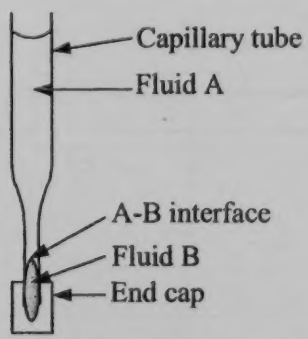

Figure 4-82 Schematic of the capillary tube.

The pipette was first dipped into a beaker filled with fluid A and the fluid was drawn in to the pipette. The pipette was then dipped into a beaker filled with fluid B and a small amount of fluid A was first squeezed out of the beaker before drawing fluid B into the pipette. Once both fluids were in place, a plastic end cap was placed on the bottom of the pipette to close the system. The interface was placed inside the water filled test cell and then brought in front of the camera and examined for air bubbles. If the interface was free of air bubbles, then fluid A was poured into the pipette through the top opening. If any air bubbles were visible at or near the interface then the capillary tube was discarded. Glass beads of different hydrophobicities were then released into the tube and moved toward the interface under gravity. The behaviour of the glass beads was recorded with the digital video camera.

4.4.2 Experimental Observations

Hydrophilic glass beads that started in the water phase remained on the aqueous side of the interface and hydrophobic glass beads that started in the oil phase remained in the oil phase. These results were expected given their hydrophobicities. However, from the capillary experiments, it was observed that hydrophilic beads that started in the oil phase and hydrophobic beads that started in the aqueous phase behaved differently at the interface.

The hydrophilic beads stopped on the oil-side of the interface for a finite amount of time before they rapidly crossed over the interface and settled into their thermodynamically stable position (Figures 4-83 through 4-88). This rapid motion is referred to as 'popping' (across the interface).

The hydrophobic beads that started in the aqueous phase stopped on the aqueous side of the interface and appeared to remain there. The hydrophobic beads did not appear to have moved to the oil side of the interface, which, in theory, is a more favourable position for the hydrophobic beads. Beads that were treated by summer student, R. Dowell, with 10 *mL* of TMCS for one hour, versus 24 hours as described in Chapter 3, were also used in some of the experiments. They were observed to have a contact angle around 90° at the water-silicone oil interface. Those beads started in the water phase and popped onto the interface soon after they came in contact with the interface.

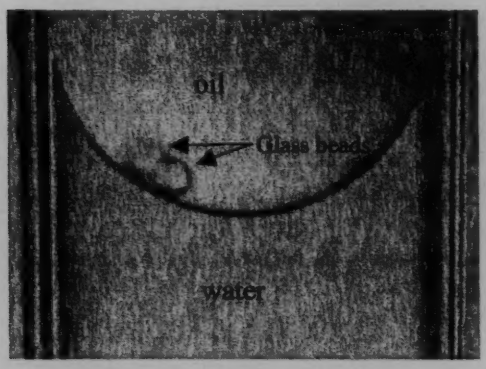

Figure 4-83 Hydrophilic glass beads first came in contact with the interface.

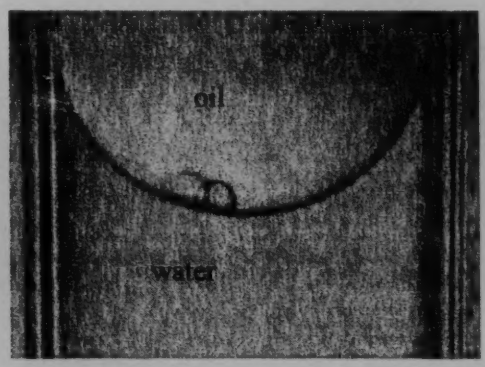

Figure 4-84 Hydrophilic glass beads stopped on the interface for approximately 4 seconds.

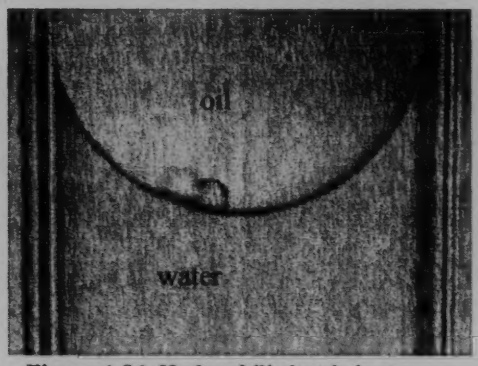

Figure 4-86 Hydrophilic beads just before crossing the interface. Frame 20:55:09.

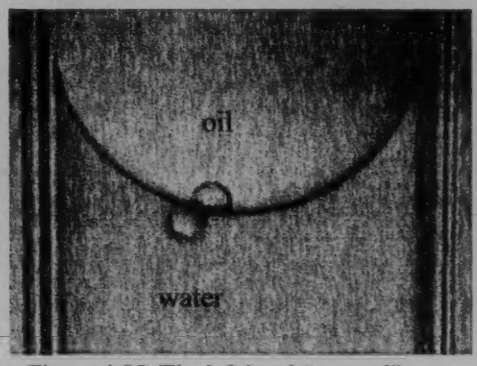

Figure 4-85 The left bead "popped" across the interface. Frame 20:55:10.

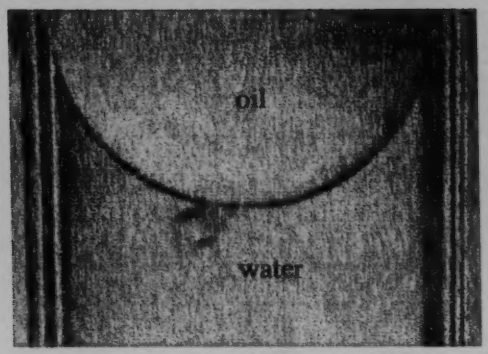

Figure 4-87 The second bead "popping" across the interface. Frame 20:55:21.

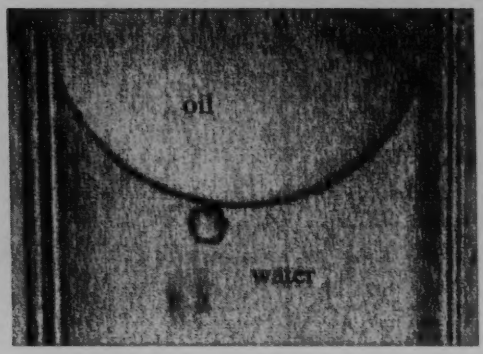

Figure 4-88 The second bead settled on the interface. Frame 20:55:22

A summary of the initial capillary experiments can be found in Table 4-2. The first three columns describe the controlled parameters such as the fluids and the type of beads used. The fourth column describes the approximate equilibrium bead contact angle. The methods in which these numbers are obtained are discussed below. The curvature of the interface was observed to be either concave up or down. This was noted in the fifth column with symbols that best describe the interface geometry. In the sixth and the seventh columns the number of beads that popped onto the interface and the approximate number of beads that came into contact with the interface were recorded. If the beads had attained their thermodynamic equilibrium contact angle then a 'Y' is placed in the eighth column, otherwise an 'N' is used. If the beads paused before popping onto the interface then the observed times were recorded in the ninth column.

Table 4-2 Capillary Experiment Summary (Set 1).

	Top Fluid	Bottom Fluid	Beads	Approx. Equilibrium Contact Angle	Curvature of Interface	# of Beads Popped On	# of Beads dropped	Attained Thermo eq contact angle	Drainage Time (s)
9-Apr	oil	water	hydrophilic	15	⌣	>20*	>50	Y	1.6
9-Apr	oil	water	hydrophilic	15	⌣	~30	~30	Y	0.5 - 5.5
9-Apr	oil	water	hydrophilic	15	⌣	6	6	Y	6.7 - 57.8
6-Jun	$CaCl_2$ Soln	oil	10 mL	90	⌣	~20	~20	Y	0.1 - 0.13
6-Jun	$CaCl_2$ Soln	oil	10 mL	90	⌣	~20	~20	Y	0.03 - 0.06
6-Jun	$CaCl_2$ Soln	oil	10 mL	90	⌢	~20	~20	Y	0.03 - 0.1
6-Jun	$CaCl_2$ Soln	oil	10 mL	90	⌣	~20	~20	Y	0.03 - 0.2
6-Jun	water	oil	10 mL	90	⌢	2*	>20	Y	0.03 - 0.06
6-Jun	water	oil	10 mL	90	⌢	1*	~20	Y	0.03
9-Apr	oil	water	hydrophobic	160	⌣	0	>50	Maybe	
9-Apr	oil	water	hydrophobic	160	⌣	0	>50	Maybe	
9-Apr	oil	water	hydrophobic	160	⌣	0	>50	Maybe	
9-Apr	water	oil	hydrophilic	15	⌢	0	>50	Maybe	
9-Apr	water	oil	hydrophilic	15	⌢	0	>50	Maybe	
10-Apr	water	oil	hydrophilic	15	⌢	0	>50	Maybe	
9-Apr	water	oil	hydrophobic	160	⌢	0	>50	N	
9-Apr	water	oil	hydrophobic	160	⌢	0	>50	N	
9-Apr	water	oil	hydrophobic	160	⌢	0	>50	N	
9-Apr	water	oil	hydrophobic	160	⌢	0	>50	N	
April 11to12	water	oil	hydrophobic	160	⌢	0	>50	N	
26-Apr	NaCl Soln	oil	hydrophobic	160	⌢	0	>50	N	
26-Apr	NaCl Soln	oil	hydrophobic	160	⌢	0	>50	N	
26-Apr	NaCl Soln	oil	hydrophobic	160	⌢	0	>50	N	
26-Apr	$CaCl_2$ Soln	oil	hydrophobic	160	⌢	0	>50	N	
9-May	$CaCl_2$ Soln	oil	hydrophobic	160	⌢	0	>50	N	
9-May	$CaCl_2$ Soln	oil	hydrophobic	160	⌣	0	>50	N	
9-May	$CaCl_2$ Soln	oil	hydrophobic	160	⌢	0	>50	N	
9-May	$CaCl_2$ Soln	oil	hydrophobic	160	⌣	0	>50	N	
9-May	$CaCl_2$ Soln	oil	hydrophobic	160	⌣	0	>50	N	
10-May	water	oil	hydrophobic	160	⌢	0	>50	N	

In the first set of capillary experiments, it was clear (when a sudden change in speed and direction occurred) that the hydrophilic glass beads entered the interface from the oil side. However, this 'popping' motion was not observed for every experiment. In the cases where the hydrophobic and hydrophilic beads started in the aqueous phase, the beads did not pop on to the interface (Figures 4-89 and 4-90). Also, when hydrophobic glass beads approached the interface from the oil phase, the popping motion was not observed. Without the popping motion, one can only guess whether the beads were on the interface or not. For the hydrophobic beads that started in the oil phase and the hydrophilic beads that started in the water phase, it was possible that they were on the interface because they appeared to have obtained their thermodynamic equilibrium position. For the hydrophobic beads that started in the water phase, one could assume that they were not on the interface because they remained on the water side of the interface.

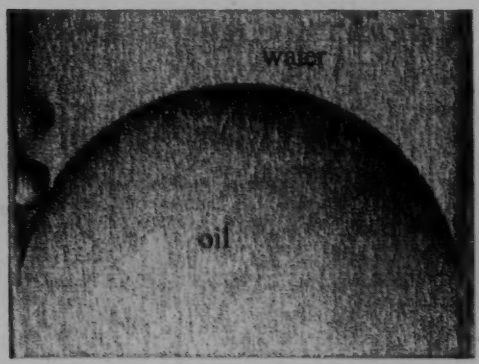

Figure 4-89 Hydrophilic glass beads on the interface.

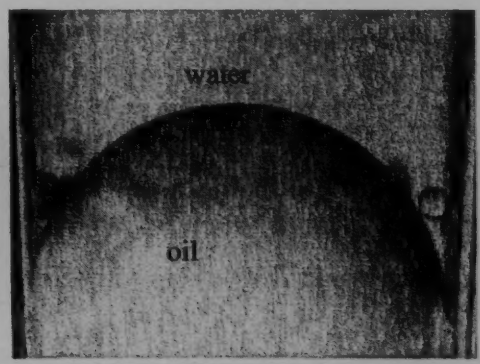

Figure 4-90 Hydrophobic glass beads on the interface.

In the second set of experiments, the procedure and the apparatus remained the same as the first set of the capillary experiments but the capillary was turned upside down after the beads settled on the interface. If the beads stayed on the interface then it may be

an indication that they were on the interface. If the beads fell off, then one could postulate that they did not get on the interface. In order to turn the capillary tube upside down, the tube needed to be removed from the test cell because the test cell was not deep enough to accommodate the top portion of the tube. Since the tube was observed without the use of the test cell, a significant amount of distortion was noted. These observations could only tell whether the beads were on the interface and the phase that they were in. The exact contact angle could not been obtained due to the severe distortion.

Hydrophilic glass beads were first released into the water phase. In the previous experiments, these glass beads stopped at the interface but were not observed to pop on to the interface. When the capillaries were turned over, the majority of the experiments (12 out of 13) showed that the hydrophilic glass beads were indeed on the interface (Figure 4-91). However, the first experiment conducted showed that no glass beads were on the interface. Also during the second experiment, the experimental apparatus was accidentally nudged and at least one bead was observed to pop onto the interface after the accident.

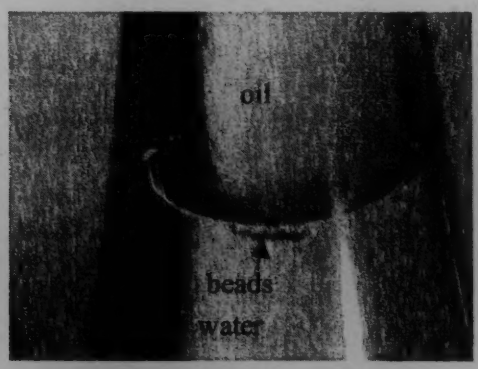

Figure 4-91 Hydrophilic beads on the interface after the capillary tube had been turned over.

In the previous experiments, when hydrophobic glass beads were released into the water phase, they did not pop across the interface. Since they did not reach their equilibrium position, it was assumed that they were not on the interface. The second set of experiments was first conducted by releasing a large number of hydrophobic beads into the capillary tube. When the tubes were turned over, glass beads were clearly visible on the interface; unfortunately it was difficult to tell which side the beads were on because of the number of beads on the interface. Fewer beads were then used and it appeared that the hydrophobic glass beads remained on the water-side of the interface (Figure 4-92).

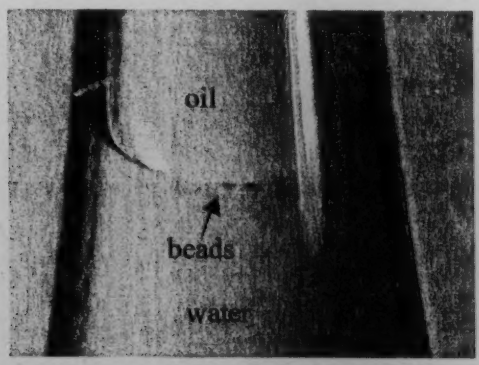

Figure 4-92 Hydrophobic glass beads on the interface. The beads were first released into the water phase.

Hydrophilic glass beads were also released through the oil phase. As in the previous experiments, the hydrophilic glass beads popped across the interface and settled on the water-side. When the capillary tube was turned over, the glass beads can still be seen on the water-side of the interface even though the curvature of the tube caused a significant distortion (Figure 4-93).

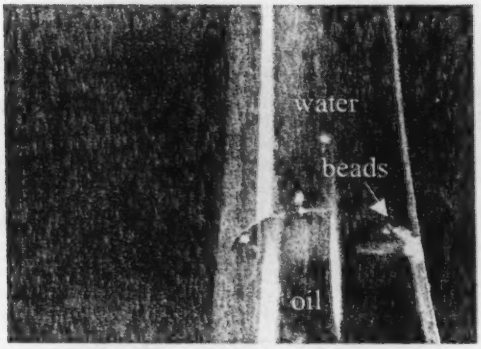

Figure 4-93 Hydrophilic glass beads after being released from the oil phase.

Finally, hydrophobic glass beads were released through the oil phase. Since they were hydrophobic, it was expected that they would to stay in the oil phase as in the previous experiments. When the beads came to the interface, they did stop in the oil phase but when the orientation of the tube were reversed, the beads did not stay on the interface (Figure 4-94).

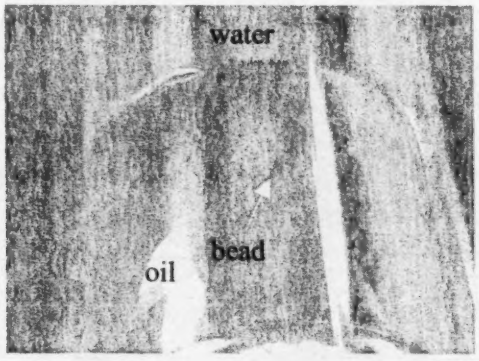

Figure 4-94 After the capillary tube was turned over, a hydrophobic glass bead can be seen falling away from the interface.

The following table is a summary of the capillary experiments conducted. In the second and third column, the top and bottom fluids used in each experiment prior to being turned upside down are identified. The fourth column records the designation of

the jar from which the beads were taken. In the second set of experiments, only the extremely hydrophobic and the extremely hydrophilic glass beads were used. The hydrophobicity of the beads was recorded in the fifth column. In the sixth column, the observed number of beads released into the capillary tube is noted. The symbols that best represent the shape of the interfaces before the capillary tubes were turned over are given in the seventh column. Finally, the eighth column is used to note the observations made after the capillary tubes were turned and any other observations made during the experiments.

Table 4-3 Capillary Experiment Summary (Set 2).

Date	Top Fluid	Bottom Fluid	Jar #	Type of Bead	# of Beads Released	Interface Shape	Stayed after flipped over?
17-Jul	water	oil	08R	Hydrophilic	9	⌣	NO
17-Jul	water	oil	08R	Hydrophilic	>100	⌣	Maybe, some looked like they were stuck on the wall.
17-Jul	water	oil	08R	Hydrophilic	~15	⌣	*3:05:19pm beads appeared to have been shaken on to the interface. * At least a few beads were on the interface.
17-Jul	water	oil	08R	Hydrophilic	>50	⌣	Some might be on the interface or on the wall.
17-Jul	water	oil	08R	Hydrophilic	>100	⌣	Some might be on the interface or on the wall.
30-Jul	water	oil	08R	Hydrophilic	>100	⌢	Yes
30-Jul	water	oil	08R	Hydrophilic	>50	⌢	Yes
30-Jul	water	oil	08R	Hydrophilic	>100	⌢	Yes
30-Jul	water	oil	08R	Hydrophilic	>100	⌢	Yes
9-Aug	water	oil	08R	Hydrophilic	12	⌢	Yes, water side
9-Aug	water	oil	08R	Hydrophilic	8	⌢	Yes, water side
9-Aug	water	oil	08R	Hydrophilic	2	⌢	Yes, water side
30-Jul	water	oil	08Z	Hydrophobic	>100	⌢	Yes
30-Jul	water	oil	08Z	Hydrophobic	>100	⌢	Yes
30-Jul	water	oil	08Z	Hydrophobic	>100	⌢	Yes
30-Jul	water	oil	08Z	Hydrophobic	>50	⌢	Yes
30-Jul	water	oil	08Z	Hydrophobic	>50	⌢	Yes
30-Jul	water	oil	08Z	Hydrophobic	>20	⌢	Yes
30-Jul	water	oil	08Z	Hydrophobic	>50	⌢	Yes
30-Jul	water	oil	7B	Hydrophobic	>100	⌢	Yes
30-Jul	water	oil	8B	Hydrophobic	>20	⌢	Yes
30-Jul	water	oil	8B	Hydrophobic	>100	⌢	Yes
30-Jul	water	oil	8B	Hydrophobic	>50	⌢	Yes
9-Aug	water	oil	8B	Hydrophobic	3	⌢	yes, seems to stay on the water side
9-Aug	water	oil	8B	Hydrophobic	6	⌢	yes, seems to stay on the water side, very stable
9-Aug	water	oil	8B	Hydrophobic	4	⌢	yes, seems to stay on the water side
9-Aug	water	oil	8B	Hydrophobic	10	⌢	yes, seems to stay on the water side
9-Aug	water	oil	8B	Hydrophobic	>10	⌢	yes,seems to stay on the water side
9-Aug	water	oil	08Z	Hydrophobic	>10	⌢	Yes, which side is unclear. air bubble was brought in by beads.
9-Aug	water	oil	08Z	Hydrophobic	2	⌢	Yes, seems to stay on the water side.
24-Aug	oil	water	08R	Hydrophilic	>30	⌣	Yes, which side is unclear.
24-Aug	oil	water	08R	Hydrophilic	5	⌣	Yes, seems to be on the water side.
24-Aug	oil	water	08R	Hydrophilic	16	⌣	Yes, difficult to say which side
24-Aug	oil	water	08R	Hydrophilic	18	⌣	Yes, water side
24-Aug	oil	water	8B	Hydrophobic	>40	⌣	yes, 5 or 6 beads on the interface. Difficult to say which side.
24-Aug	oil	water	8B	Hydrophobic	>10	⌣	Nothing on the interface. Couple beads stuck on the wall. It is some distance away from the interface but not on the interface.
24-Aug	oil	water	8B	Hydrophobic	>20	⌣	no beads but an airbubble rise to the interface.
25-Aug	oil	water	8B	Hydrophobic	~10	⌣	Clean interface. Nothing stayed.
25-Aug	oil	water	8B	Hydrophobic	2	⌣	Clean interface. Can see the two beads falling.
25-Aug	oil	water	8B	Hydrophobic	~15	⌣	Clean interface. 2 beads can be seen stuck on the wall. Approximately 1.5 to 2 bead diameter away from the interface
9-Aug	oil drop in water		08Z	hydrophobic	>100		Beads stays in silicone oil, one on the water side
9-Aug	oil drop in water		08R	hydrophilic	>100		Beads pop out to water side

5.0 DISCUSSION

The objectives of first set of ground-based experiments were to test two important aspects of the macroscopic model. First, the coalescence experiments showed that the enlarged model had the same coalescence behaviour as the known solids-stabilized emulsion systems. Second, in the ground-based retraction experiments the model showed that the droplets coated with hydrophobic and hydrophilic particles behave differently.

Based on the traditional understanding of colloidal particles, the location of these particles on the interface only depends on the hydrophobicity of the particles' surface. Therefore, hydrophilic particles should be mostly wetted by the water phase and hydrophobic particles should be mostly wetted by the oil phase. Hence the phase which the particles started in should not effect their position on the interface.

In the microgravity experiments, the hydrophobic glass beads exhibited behaviour that was not expected. The hydrophobic glass beads were first released into the water phase and when they reached the interface they remained mostly wetted by water. Energy-adding events, such as the introduction of fluid flow or coalescence of droplets were needed to push the hydrophobic glass beads to the oil side of the interface. Without the energy-adding events, the hydrophobic glass beads that started in the water phase behaved similar to the hydrophilic beads. Although the result was surprising, past nano-particle emulsion experiments have shown that hydrophobic particles stabilized oil-in-water emulsions, which is normally associated with hydrophilic particles. In a recent emulsion study (Yan, Gray and Masliyah, 2001) the researchers mixed oil with an aqueous solution that contained treated silica (hydrophobic) particles to produce emulsions. Upon examination, they found only oil-in-water emulsions. The experiment

was repeated with latex particles and again, they found oil-in-water emulsions. They speculated that the hydrophobic particles could not cross the interface and this is what was observed with the macroscopic model. To understand this further, ground-based experiments conducted inside capillary tubes were used.

From the ground-based capillary experiments, it was observed that hydrophilic glass beads got on the interface and obtained their thermodynamically favourable position regardless of the phase that the beads started in. If the hydrophilic beads started in the water phase, the beads appeared to move directly on to the interface. When the hydrophilic beads started in the oil phase, the beads appeared to pause on the interface momentarily before moving rapidly across the interface and stopping at their thermodynamically favourable position. The capillary tubes were turned over to confirm that these beads were attached to the interface.

The same experiments were repeated with hydrophobic glass beads. If the hydrophobic beads started in the water phase, the beads got on the interface but remained mostly wetted by water. Turning over the capillary tubes revealed that the hydrophobic beads remained attached to the water-side of the interface. When the hydrophobic beads started in the oil phase, the beads appeared to have got on the interface. However, after turning the capillary tube upside down, the beads left the interface. Since interfacial tension is strong enough to hold the glass beads on the interface, this result suggests that the beads did not get on the interface.

Beads with intermediate hydrophobicity were also used in a few capillary experiments and they were observed to 'pop' on to the interface from the aqueous phase.

These capillary tubes were not turned upside down because the beads were observed to have 'popped' on to the interface.

Four mechanisms that could explain the behaviour of the glass beads near and on the interface were examined and their effects are discussed in the following sections. The following analysis first investigates the behaviour of the beads as they approach the interface. At this stage fluid mechanics and electrostatic forces were investigated. Once the glass beads came in to contact with the interface or when they became very close to the interface (within angstroms), interfacial forces and van der Waals forces were examined. Finally an alternate explanation was also examined.

5.1 Thin Film Drainage

When hydrophilic glass beads were released through the oil phase, the beads paused on the interface momentarily before crossing the interface. This could have been caused by the flow of the silicone oil. As discussed in Chapter 1, before the glass bead reaches the interface, a thin film of fluid will be trapped in between the bead and the interface. This thin layer of liquid must be drained before the particle can reach the interface. As a first approximation, the Stefan-Reynolds Equation, equation (1-1), which is a mathematical model of liquid drainage from a thin disc, is used.

Assuming that the starting film thickness is large enough that the second term on the left hand side of equation (1-1) is small compared to the first term, and setting the final thickness to an arbitrary amount of 10 *nm*, the fluid drainage time can be estimated. Using the force balance method discussed in Chapter 1, the size of the thin film disc can be calculated. For a 130 μm diameter bead, the thin film disc radius is approximately 2μm and it is estimated that 4 seconds are required if the bead is in silicone oil and 0.007

seconds if it is in an aqueous solution. In the capillary experiments in which the beads began in the silicone oil phase, the beads were observed to slow down or stop near the interface and took between 0.5 to 60 seconds before popping onto the interface. When the beads began in the aqueous phase, the beads took anywhere from less than 0.03 seconds to 0.2 seconds before popping to their final position. Due to the camera speed (30 frames per second), the time taken by beads that cross the interface in less then 0.033 seconds cannot be obtained. Understanding that the above equation is a simplified model of the actual problem, it is certainly plausible to use the thin film drainage to explain the pause before the beads popped onto their thermodynamically stable position. However, it does not explain why the hydrophobic beads that started in the aqueous solution remained in the aqueous solution indefinitely.

5.2 Electrical Double Layer Force

In Chapter 1, a force that is present for charged particles in the aqueous phase was discussed. If this force is strong enough it could potentially prevent the glass beads from reaching the interface. According to the theory, this force could be reduced by the addition of salt.

A sodium chloride solution was first used in the experiment (0.42 *mol/L*) resulting in a calculated double layer thickness of 0.47 *nm*. Hydrophobic glass beads were released into the aqueous solution and the beads did not pop on to the interface. Calcium chloride solutions of various concentrations were used in later experiments resulting in a calculated double layer thickness in the range of 0.2 to 0.25 *nm*. Hydrophobic glass beads were again used and their behaviour was noted to be similar to the previous experiments.

The results of these experiments show that the behaviour of the beads at the interface did not change with the addition of salt. This suggests that electrostatic phenomena do not play a role in the observable behaviour of the system.

5.3 Line Tension

In a recent study (Yan, Gray, and Masliyah, 2001), hydrophilic and hydrophobic nano-spheres were used to generate emulsions. First hydrophobic silica particles were mixed into the aqueous phase. This suspension was then mixed with decane and an emulsion was generated via sonication. Only an oil-in-water emulsion was observed. Next another emulsion was created with hydrophobic latex particles in an aqueous phase that was then mixed with Bayol oil. Again, only an oil-in-water emulsion was observed. Since only oil-in-water emulsions were observed with hydrophobic particles that should have stabilized water-in-oil emulsions, the researchers believed that the hydrophobic particles could not cross the oil-water interface.

In the ground-based experiments, hydrophobic glass beads were released into the water phase and they did not cross the interface. When these beads were released in the oil phase, they appeared to have reached the interface. however, when the capillary tubes were turned upside down, these beads left the interface under the effect of gravity. These observations suggest that the hydrophobic glass beads never did obtain the stable position. The ground-based experiments showed that the hydrophobic glass beads have difficulties entering the interface and in the microgravity experiments energy-adding events were observed before hydrophobic glass beads reached their equilibrium state. These observed behaviours of the hydrophobic glass beads are consistent with energy barriers preventing hydrophobic beads from attaining their thermodynamically favourable

position. The experiment conducted with hydrophilic glass beads showed that the beads will reach the thermodynamically stable position without an energy-adding event. This is consistent with energy barriers being small for those beads.

When a spherical particle breaks through the interface, a three-phase contact line would form and this require a finite amount of energy. The effect of line tension was discussed in Chapter 2 and the energy required to create this line is given by the free energy equation, Equation 2-4. Plots of Equation 2-4 for various values of the dimensionless line tension (Figures 5-1 and 5-2) show that for a particle originating in either phase, if line tension is insignificant then there are no energy barriers (local maximums) that would restrict the particle from reaching its minimum free energy location. Therefore, the particles should spontaneously reach their thermodynamically favorable position once they reach the interface regardless of the phase in which the solid particle started. However, if line tension is significant, energy barriers exist that could prevent the beads from arriving at the minimum free energy location.

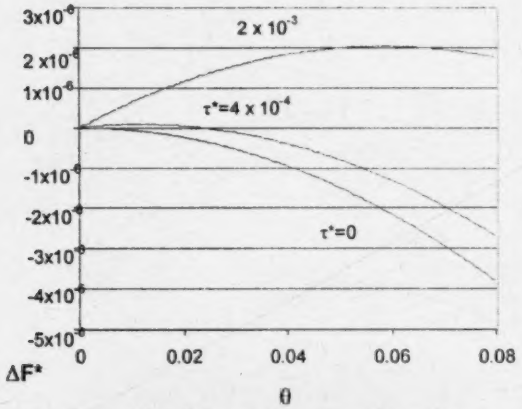

Figure 5-2 Free energy curve for beads entering the interface from the water phase. Various line tension values are used, which affect the energy barrier size. θ_∞=165°. When θ=0° the particle is completely submerged in the water phase.

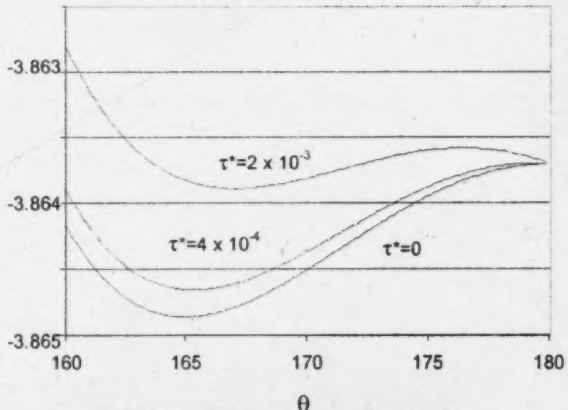

Figure 5-1 Free energy curve for beads entering the interface from the oil phase. Various line tension values are used, which affect the energy barrier and well sizes. θ_∞=165°. When θ = 180° the particle is completely in the oil phase.

In the macroscopic model, when hydrophobic glass beads started in the water phase, they stayed on the water side of the interface. When hydrophobic glass beads did cross the interface and moved to the oil side, one of the following energy-adding events would have to have occurred first: either fluid motion was generated using the syringe or two droplets coalesced. If not enough energy was supplied to these beads they could remain in the water phase. In a colloidal emulsion system, if the hydrophobic particles remained on the water side of the interface, then the emulsion would behave as if the particles were hydrophilic. In other words, if hydrophobic particles begin from the water phase, an oil-in-water emulsion may be formed rather then the water-in-oil emulsion that is expected from hydrophobic particles.

Although the macroscopic experimental results along with the presented free energy arguments may appear to contradict the current understanding of what type of particles stabilize what type of emulsions, it is consistent with the colloidal experimental results in the study done by Yan, Gray, and Masliyah.

5.4 van der Waals Forces

The above arguments suggests that line tension would prevent the hydrophobic particles from entering the interface. However, the ground-based experiments had shown that hydrophobic glass beads remained on the water-side of the interface even after the capillary tubes were turned upside down. van der Waals forces, which were discussed earlier, could also play a significant role when the glass beads were near the interface. Although the exact value of the Hamaker constant for a TMCS treated glass surface is not known, a typical value of this type of system is on the order of 10^{-20} *J*. The radius of the glass beads used in the experiment was approximately 65 x 10^{-6} *m*. The bead and the oil

phase are assumed to be separated by a water molecule, which is about 3×10^{-10} *m* in diameter. The density difference between glass and water is on the order of 10^3 kg/m^3 and the gravitational force is on the order of 10 *N/kg*. With the above values, the van der Waals forces are two orders of magnitude greater then the gravitational force. This shows that van der Waals forces could effect the behaviour of the glass beads at the interface.

If there is a net attraction between the TMCS treated particle and the oil phase (which is probable given the particle's hydrophobic property) then van der Waals forces could hold the hydrophobic beads on the interface even if they had not attained their thermodynamically favourable position. The combination of line tension, which would prevent the particles from reaching their the thermodynamically favourable position, and van der Waals forces could explain why the hydrophobic nano-particles in Yan, Gray and Masliyah's experiment can remain attached to the water side of the interface and stabilize an oil-in-water emulsion.

5.5 Surface Heterogeneities

As discussed earlier, the glass surface is naturally hydrophilic and the glass beads were treated with TMCS to create hydrophobic surfaces. Although the glass beads were fully submerged in the solution, there is no guarantee that surface is homogeneous. In the recent past, atomic force microscopy was used to examine the treated glass surfaces (Biggs and Grieser, 1994). It was observed that chemically treated glass surfaces could be unevenly treated. If the glass beads were unevenly treated, their behaviour could be unpredictable. Assuming that a relatively large hydrophilic patch exists on the hydrophobic glass bead and if this patch came in contact with the interface, then the

beads might behave similar to hydrophilic glass beads. If this theory, however, is not probable because it is unlikely that all the observed glass beads have large patches of untreated surface and all of them came in contact with the interface.

The second possible explanation using the uneven treatment argument is that the treated surface consisted of numerous tiny hydrophilic and hydrophobic patches. This situation could cause the glass beads to have a significantly different advancing and receding contact angle. This could explain the hydrophobic beads' contact angle; however, it could not explain why the hydrophobic beads could not stay on the interface when entering from the oil phase. Furthermore, this theory could not explain the results in the paper published by Yan, Gray, and Masliyah, where hydrophobic latex particles were used because latex is naturally hydrophobic and the hydrophilic patches would not exist.

5.6 Summary

In summary, it was observed that when hydrophilic glass beads were first released into the oil phase the beads paused momentarily before 'popping' onto their position on the interface. This was also observed with glass beads with intermediate hydrophobicity. This momentary pause can be accounted for by the time that is required for a thin film between the glass beads and the interface to drain and rupture.

Line tension and van der Waals forces can be used to explain the behaviour of the hydrophobic glass beads. The presence of line tension could prevent the glass beads from entering the interface. The hydrophobic glass beads have been observed not to enter the interface from the water phase unless an energy-adding event occurred. When

the glass beads are on the water-side of the interface, van der Waals attraction forces could hold the beads against the interface.

Since the hydrophobic glass beads could stay on the water-side of the interface and remain close to the interface, they could appear and act similar to hydrophilic glass beads. This could be used to explain the behaviour observed in a previous study where submicron colloidal particles were used. In that study, hydrophobic treated silica and latex particles were used in emulsion experiments. It was found that the when the particles started in the aqueous phase, hydrophobic particles were capable of stabilizing oil-in-water emulsion which is usually often associated with hydrophilic particles.

6.0 CONCLUSIONS AND RECOMMENDATIONS

6.1 Experimental Conclusions

The goal of this project was to produce an enlarged model of a solids-stabilized emulsion droplet. The first set of experiments was used to test the coalescence behaviour of the model system. The results showed that the enlarged system exhibited similar characteristics to the submicron system. Hydrophobic beads prevented water droplets from coalescing and hydrophilic beads allowed water droplets to coalesce. This behaviour is attributed mostly to the location of the beads on the interface. On a water drop the hydrophobic beads would be mostly outside of drop and form a barrier between the water drops. This is consistent with current understanding but the droplets used in the ground-based experiments were fully covered by the glass beads. Droplets partially coated by glass beads can not be obtained because of the effect of gravity.

In the microgravity experiments, if the hydrophobic particles started in the water phase, they would behave similarly to hydrophilic particles in that they did not cross the interface yet remained attached to the interface. Although this is not consistent with the traditional understanding, it is consistent with a recent published study where nano-scaled hydrophobic particles were used in the experiments. Area contraction experiments were conducted with hydrophilic beads starting in the water phase and hydrophobic glass beads starting in the oil phase. For the experiments conducted with hydrophilic glass beads, it was found that the number of beads on the interface may have an effect on the contraction experiment and better control of this variable is needed to draw any firm conclusions. In experiments where hydrophobic glass beads started in the oil phase, the glass beads appeared to leave the interface during the contraction.

Further ground-based experiments in capillary tubes were used to study the behaviour of the glass beads near and on the interfaces. Fluid drainage between the glass beads and the interface could explain the momentary pause between the time when the glass beads first arrived at the interface and when the glass beads reached their equilibrium position. Line tension and van der Waals forces could be used to explain the observed hydrophobic glass beads' behaviour. Line tension would prevent the glass beads from entering the interface and van der Waals attraction forces between treated glass surfaces and oil could hold the glass beads against the interface while the beads remain mostly wetted by water. Surface heterogeneity could explain some of the behaviour exhibited by the hydrophobic beads. Small patches of hydrophilic surfaces may exist and thus causes a different advancing and receding contact angle. Thus it is possible that hydrophobic glass beads could act similar to hydrophilic glass beads. Surface heterogeneity, however could not explain the result of experiments where hydrophobic glass beads that entered through the oil phase appeared to land on the interface but were not able to remain on the interface after the capillary tube was turned upside down.

6.2 Recommendations

During the first round of microgravity flights, the apparatus was capable of performing the experiment but a number of modifications should be done to improve the apparatus. Some of the suggestions will improve safety and some are to improve the controllability of the experiments.

1. The modified Fisher jack uses scissors jacks to raise and lower the stage. On a few preflight inspections, the pin that provides the pivot point and the pin that slides along

the bottom rail were found to be out of position. It is suspected that the vibration of the aircraft shook the pin loose. This can be eliminated by using screws to lock washers to either side of the pins.

2. The Fisher jack currently uses two diagonal springs (mounted from the top right corner to the bottom left corner) to reduce the slack in the jacking mechanism. This can be further improved by moving one of the springs such that it will be crossing through the opposite diagonal (i.e. from the top left corner to the bottom right corner).
3. During all the experiments, it was found that the syringe used does not offer enough control of the flow. Multiple small syringes (perhaps 5 or 10 *mL*) and one syringe with a threaded plunger connected in parallel may offer better control of the flow.
4. As the previous experiments have shown, glass beads may not get on the interface spontaneously. Physical forces may be required to insure glass beads get on the interface. Since adjusting the camera to capture the droplet may waste valuable time during the microgravity experiments, it is necessary to fix the position of the droplet. A movable container (cone or cup shaped) which would hold the glass beads could be moved to the droplet(s) and the glass beads rubbed against the interface. This container can then be moved away from the droplet(s).
5. Future theoretical analysis may include the effect of gravity on line tension value and thus the free energy curve.
6. Immediate development of the model should examine the use of solids with varied intermediate hydrophobicities. Future development of the macroscopic emulsion model may use small rods to simulate surfactants.

REFERENCES

Alexandrov, A. D., B. V. Toshev, and A. D. Scheludko, "Nucleation from Supersaturated Water Vapour on Immiscible Liquid Substrates: Effect of the Macroscopic Geometry of the Three-Phase System on the Critical Supersaturation and the Line Tension", Colloids Surfaces A, 79, 43-50, 1993.

Scheludko, A., B. V. Toshev and D. T. Bojadjiev, "Attachment of Particles to a Liquid Surface (Capillary Theory of Floatation)", J. Chem. Soc. Faraday Trans, 72, 2815-2828, 1976.

Aveyard, R., and J. H. Clint, "Liquid Droplets and Solid Particles at Surfactant Solution Interfaces", J. Chem. Soc., Faraday Trans., 91(17) 2681-2697, 1995.

Aveyard, R., and J. H. Clint, "Liquid Lenses at Fluid-Fluid Interfaces", J. Chem. Soc., Faraday Trans., 93(7) 1397-1403, 1997.

Aveyard, R., and J. H. Clint, "New Method for the Measurement of Line Tensions at the Solid/Liquid/Air Three-Phase Contact Line", J. Chem. Soc. Faraday Trans. 91(1), 175-176, 1995.

Aveyard, R., and J. H. Clint, "Particle Wettability and Line Tension", J. Chem. Soc. Faraday Trans, 92(1) 85-89, 1996.

Aveyard, R., B. D. Beake, and J. H. Clint, "Wettability of Spherical Particles at Liquid Surfaces", J. Chem. Soc., Faraday Trans., 92(21), 4271-4277, 1996.

Aveyard, R., B. P. Binks, P. D. I. Fletcher and C. E. Rutherford, "Contact Angles in Relation to the Effects of Solids on Film and Foam Stability", J. Dispersion Sci. Tech. 15(3), 251-271, 1994.

Aveyard, R., B. P. Binks, P. D. I. Fletcher, and T. G. Peck, "Entry and Spreading of Alkane Drops at the Air/Surfactant Solution Interface in Relation to Foam and Soap Film Stability", J. Chem. Soc. Faraday Trans, 89(24), 4313-4321, 1993.

Aveyard, R., J. H. Clint, and D. Nees, "Small Solid Particles and Liquid Lenses at Fluid/Fluid Interfaces", Colloid Polym Sci, 278, 155-163, 2000.

Bearchell, C. A., D. M. Heyes, D. J. Moreton, and S. E. Taylor, "Overbased Detergent Particles: Experimental and Molecular Modelling Studies", Phys. Chem. Chem. Phys., 3, 4774-4783, 2001.

Bergeron, V., M. E. Fagan, and C. J. Radke, "Generalized Entering Coefficients: A Criterion for Foam Stability Against Oil in Porous Media", Langmuir, 9, 1704-1713, 1993.

Biggs, S., and F. Grieser, "Atomic Force Microscopy Imaging of Thin Films Formed by Hydrophobing Reagents", J. Colloid Interface Sci 165, pp. 425-430, (1994).Blake, P., and

J. Ralston, "Controlled Methylation of Quartz Particles", Colloids Surfaces, 15, 101-118, 1985.

Boruvka, L., and A. W. Neumann, "Generalization of the Classical Theory of Capillarity", J. Chem. Phys., 66(12), 5464-5476, 1977.

Bresme, F., and N. Quirke, "Computer Simulation of Wetting and Drying of Spherical Particulates at a Liquid-Vapor Interface", J. Chem. Phys., 110(7), 3536-3547, 1999.

Bresme, F., and N. Quirke, "Computer Simulation Study of the Wetting Behavior and Line Tensions of Nanometer Size Particulates at a Liquid-Vapor Interface", Phys. Rev. Letter, 80(17), 3791-3794, 1998.

Bresme, F., and N. Quirke, "Nanoparticulates at Liquid/Liquid Interfaces", Phys. Chem. Chem. Phys, 1(9), 2149-2155, 1999.

Chan, C. C. V., "Investigation of Anomalous Surface Properties of Polyethylene Melt Using the Spinning Drop Method, and the Error Analysis of the Spinning Drop Tensiometer", pp. 96-97 Master's Thesis, University of Alberta, Department of Chimical and Materials Engineering, Fall, 2001.

Chen, P., S. S. Susnar, A. Amirfazli, C. Mak, and A.W. Neumann, "Line Tension Measurements: An Application of the Quadrilateral Relation to a Liquid Lens System", Langmuir, 13, 3035-3042, 1997.

Clint, J. H., and Nick Quirke, "Contact Angles on Particles from Langmuir Trough Studies", Colloids Surfaces A, 78, 277-278, 1993.

Clint, J. H., and S. E. Taylor, "Particle Size and Interparticle Forces of Overbased Detergents: A Langmuir Trough study", Colloids and Surfaces, 65, 61-67, 1992.

Cooper, K., N. Ohler, A. Gupta, and S. Beaudoin, "Analysis of Contact Interactions between a Rough Deformable Colloid and a Smooth Substrate", J. Colloid Interface Sci., 222, 63-74, 2000.

Dabros, T., A. Yeung, J. Masliyah, and J. Czarnecki, "Emulsification Through Area Contraction", J. Colloid Interface Sci. 210, 222-224, 1999.

Drelich, J., and J. D. Miller, "The effect of Solid Surface Heterogeneity and Roughness on the Contact Angle/Drop (Bubble) Size Relationship", J. Colloid Interface Sci., 164, 252-259 (1994).

Drelich, J., J. D. Miller, and J. Hupka, "The Effect of Drop Size on Contact Angle Over a Wide Range of Drop Volumes", J. Colloid Interface Sci. 155, 379-385, 1993.

Duncan, D., D. Li, J. Gaydos, and A. W. Neumann, "Correlation of Line Tension and Solid-Liquid Interfacial Tension from the Measurement of Drop Size Dependence of Contact Angles", J. Colloid Interface Sci. 169, 256-261, 1995.

Dussaud, A., and M. Vignes-Adler, "Wetting Transition of n-Alkanes on Concentated Aqueous Salt Solutions. Line Tension Effect", Langmuir, 13, 581-589, 1997.

Finkle, P., H. D. Draper and J. H. Hildebrand, "The Theory of Emulsification", J. Am. Chem. Soc, 45, 2780-2788, 1923.

Fuji, M., H. Fujimori, T. Takei, T. Watanabe, and M. Chikazawa, "Wettability of Glass-Bead Surface Modified by Trimethylcholorosilane", J. Phys. Chem. B, 102, 10498-10504, 1998.

Gaydos, J., and A. W. Neumann, "The Dependence of Contact Angles on Drop Size and Line Tension", J. Colloid Interface Sci. 120(1), 76-86, 1987.

Gibbs, J., The scientific Papers of J.Willard Gibbs, Volume One Thermodynamics, pp. 288, Ox Bow Press, Connecticut, 1993, Originally published: London, Longmans, Green, 1906.

Gu, Y. , "Experimental Determination of the Hamaker Constants for Solid-Water-Oil Systems", J. Adhesion Sci. 15(11), 1263-1283, 2001.

Ha, J. W., and S. M. Yang, " Breakup of a Multiple Emulsion Drop in a Univform Electric Field", J. Colloid Interface Sci. 213, 92-100 (1999).

Ha, J. W., and S. M. Yang, "Effect of Nonionic Surfactant on the Deformation and Breakup of a Drop in an Electric Field", J. Colloid Interface Sci. 206, 195-204 (1999).

Hadjiiski, A., R. Dimova, N. D. Denkov, I. B. Ivanov, and R. Borwankar, "Film Trapping Technique: Precise Method for Three-Phase Contact Angle Determination of Solid and Fluid Particles of Micrometer Size", Langmuir, 12, 6665-6675, 1996.

Hiemenz, P.C. and R. Rajagopalan, *Principles of Colloid and Surface Chemistry*, 3rd ed, pp. 499-530, Mercel Dekker, New York, 1997

Horvolgyi, Z. , S. Nemeth, and J. H. Fendler, "Monoparticulate Layers of Silanized Glass Spheres at the Water-Air Interface: Particle-Particle and Particle-Subphase Interactions", Langumir, 12, 997-1004, 1996.

Jensen, W. C., and D. Li, "Determination of Line Tensions From the Capillary Rise in a Conical Tube", 156, 519-524, 1999.

Johans, C., P. Liljeroth and K. Kontturi, "Electrodeposition at Polarisable Liquid/Liquid Interfaces: The Role of Interfacial Tension on Nucleation Kinetics, Phys. Chem. Chem. Phys., 4, 1067-1071, 2002.

Levine, S., and B. D. Bowen, "Capillary Interaction of Spherical Particles Adsorbed on the Surface of an Oil/Water Droplet Stabilized by the Particles. Part I", Colloids Surfaces, 59, 377-386, 1991.

Levine, S., B. D. Bowen, and S. J. Partridge, "Stabilization of Emulsions by Fine Particles I. Partitioning of Particles Between Continous Phase and Oil/Water Interface", 38, 235-343, 1999.

Levine, S., B. D. Bowen, and S. J. Partridge, "Stabilization of Emulsions by Fine Particles II. Capillary and van der Waals Forces Between Particles", 38, 345-364, 1999.

Li D., and A. W. Neumann, "Determination of Line Tension from the Drop Size Dependence of Contact Angles", Colloids and Surfaces, 43, 195-206, 1990.

Lobo, L., and D. T. Wasan, "Mechanisms of Aqueous Foam Stability in the Presence of Emulsified Non-Aqueous-Phase Liquids: Structure and Stability of the Pseudoemulsion Film", Langmuir, 9 1668-1677, 1993.

Marmur, A., "Line Tension and the Intrinsic Contact Angle in Solid-Liquid-Fluid Systems", J. Colloid Interfaace Sci., 186, 462-466, (1997).

Marmur, A., "Wetting on Real Surfaces", J. Imaging Sci. Tech., 44(5), 406-409, 2000.

Masliyah, J. H., Electrokinetic Transport Phenomena, AOSTRA Technical Publication Series #12 1999.

Menon, V. B., and D. T. Wasan, "A Review of The Factors Affecting the Stability of Solids-Stabilised Emulsions", Separation Sci. Tech., 23 (12 and 13), 2131-2142, 1988.

Mingins, J. and Alexei Scheludko, " Attachment of Spherical Particle to the Surface of a Pendant Drop and the Tension of the Wetting Perimeter", J. Chem. Soc. Faraday Trans, 1(75), 1-6, 1979.

National Research Council of Canada, *Falcon 20 User's Guide*, 2000.

Neuhausler, U., S. Abend, C. Jacobsen, and G. Lagaly, "Soft X-ray Spectromicroscopy on Solid-Stabilized Emulsions", Colloid Polym. Sci. 277, 719-726, 1999.

Pethica, B. A., "Two-dimensional Colloids. The Linear Thermodynamics of Monolayers", Colloids and Surfaces A, 88, 147-155, 1994.

Pickering, S. U., "Emulsions", J. Chem. Soc. 91, 2001-2021, 1907.

Pompe, T., "Line Tension Behavior of a First-Order Wetting System", Phys. Rev. Letters, 89(7), 0761021-0761024, 2002.

Preuss, M., and H.J. Butt, "Measuring the Contact Angle of Individual Colloidal Particles", J. Colloid Interface Sci, 208, 468-477, 1998.

Quesada-Perez, M., A. Moncho-Jorda, F. Martinez-Lopez, and R. Hidalgo-Alvarez, "Probing Interaction Forces in Colloidal Monolayers: Inversion of Structural Data", J. Chem. Phys., 115(23), 10897-10902, 2001.

Sasges, M. R., and C. A. Ward, "Effect of Gravity on Contact Angle: an Experimental Investigation", J. Chem. Phys., 109(9), 3661-3670, 1998.

Schwartz, H., Y. Harel, and S. Efrima, "Surface Behavior and Buckling of Silver interfacial Colloid Films", Langmuir, 17, 3884-3892, 2001.

Sun, J., and T. Stirner, "Molecular Dynamics Simulation of the Surface Pressure of Colloidal Monolayers", Langmuir, 17, 3103-3108, 2001.

Suslick, K. S., E. B. Flint, M. W. Grinstaff, and K. A. Kemper, "Sonoluminescence from Metal Carbonyls", J. Phys. Chem., 97, 3098-3099, 1993.

Tambe, D. E., and Mukul M. Sharma, "Factors Controlling the Stability of Colloid-Stabilized Emulsions I An Experimental Investigation", J. Colloid Interface Sci, 157, 244-253, 1993.

Tambe, D. E., and Mukul M. Sharma, "Factors Controlling the Stability of Colloid-Stabilized Emulsions, II A Model for the Rheological Properties of Colloid-Laden Interface", J. Colloid Interface Sci, 162, pp.1-10, 1994.

Taylor, S., "Colloidal Interactions in Water/Oil Emulsions", Ph.D. Thesis, University of Alberta, 2002.Toshev, B. V., D. Platikanov, and A. Scheludko, "Line Tension in Three-Phase Equilibrium Systems", Langmuir, 4(3), 489-499, 1988.

Torquato, S., T. M. Truskett and P. G. Debenedetti, "Is Random Close Packing of Spheres Well Defined?", Phys. Rev. Letters, 84(10), 2064-2067, 2000

Menon, V. B., and D. T. Wasan, "A Review of the Factors Affecting the Stability of Solids-Stabilized Emulsions", Separation Sci. Tech. 23(12&13), 2131-2142, 1988.

Vera, P., V. Gallardo, J. Salcedo, and A. V. Delgado, "Colloidal Stability of a Pharmaceutical Latex: Experimental Determinations and Theoretical Predictions", J. Colloid Interface Sci. 177, 553-560, 1996.

Ward, C. A., and M. R. Sasges, "Effect of Gravity on Contact Angle: A Theoretical Investigation", J. Chem. Phys., 109(9), 3651-3660, 1998.

Ward, C. A., and M. R. Sasges, "Response to Comment on 'Effect of Gravity on Contact Angle: A Theoretical Investigation' ", J. Chem. Phys., 112(12), 5513-5514, 2000.

Ward, C. A., D. Yee, M. R. Sasges, L. Pataki, and D. Stanga, "Configurational Stability of Fluid Systems in Near Weightlessness", Fluid Mechanics Phenomena in Microgravity, AMD 154, 111-123, 1992.

Ward, C. A., P. Rahimi, M. R. Sasges, and D. Stanga, "Contact Angle Hysteresis Generated by the Residual Gravitational Field of the Space Shuttle", J. Chem. Phys., 112(16), 7195-7202, 2000.

Wu, X., and T. G. M. van de Ven, "Characterization of Hairy Latex Particles with Colloidal Particle Scattering", Langmuir, 12, 3859-3865, 1996.

Wu, X., and T. G. M. van de Ven, "Retarded van der Waals Forces Between Triblock-Coated Latex Spheres", Langmuir, 12, 6291-6294, 1996.

Wu, X., T. Dabros, and J. Czarnecki, "Determining the Colloidal Forces between Bitumen Droplets in Water Using the Hydrodynamic Force Balance Technique", Langmuir, 15, 8706-8713, 1999.

Yan, N., and J. H. Masliyah, "Adsorption and Desorption of Clay Particles at the Oil-Water Interface", J. Colloid Interface Sci. 168, 386-392, 1994.

Yan, N., and J. H. Masliyah, "Characterization and Demulsification of Solids-Stabilized Oil-in-Water Emulsions, Part 2. Demulsification by the Addition of Fresh Oil, "Colloids Surfaces A, 96, 243-252, 1995.

Yan, N., and J. H. Masliyah, "Creaming Behavior of Solids-Stabilized Oil-in-Water Emulsions", Ind. Eng. Chem. Res., 36, 1122-1129, 1997.

Yan, N., and J. H. Masliyah, "Effect of pH on Adsorption and Desorption of Clay Particles at Oil-Water Interface", J. Colloid Interface Sci. 181, 20-27, 1996.

Yan, N., and J. H. Masliyah, "Solids-stabilized Oil-in-water Emulsions: Scavenging of Emulsion Droplets by Fresh Oil Addition", Colloids Surfaces A, 75, 123-132, 1993.

Yan, N., C. Kurbis, and J. H. Masliyah, "Continuous Demulsification of Solids-Stabilized Oil-in-Water Emulsions by the Addition of Fresh Oil", Ind. Eng. Chem. Res. 36, 2634-2640.

Yan, N., M. R. Gray, and J. H. Masliyah, "On Water-in-Oil Emulsions Stabilized by Fine Solids", Colloids Surfaces A, 193, 97-107, 2001.

Yan, N., Y. Maham, J. H. Masliyah, M. R. Gray and Alan E. Mather, "Measurement of Contact Angles for Fumed Silica Nanospheres Using Enthalpy of Immersion Data",J. Colloid Interface Sci. 228, 1-6, 2000.

Zahn, K., J. M. Mendez-Alcaraz and G. Maret, "Hydrodynamic Interactions May Enhance the Self-Diffusion of Colloidal Particles", Phys. Rev. Letters, 79(1), 175-178, 1997.

APPENDIX 1

Test Equipment Data Package for Falcon 20 Flights January 28 – February 1, 2002 Connected with contract entitled "Interface Effects in Multiphase Fluid Systems"

Contract No. 9F007-00605/001/SR
Performed for the Canadian Space Agency

Submitted December 7, 2001

Raymond Chiang
Graduate Student

Janet A.W. Elliott
Associate Professor and
Canada Research Chair in Interfacial Thermodynamics

Department of Chemical and Materials Engineering
University of Alberta, Edmonton, AB T6R 2J5

Contact Information

Raymond Chiang	**rchiang@ualberta.ca**
Janet A.W. Elliott	**janet.Elliott@ualberta.ca**

A. Synopsis

A macroscopic model of a solids-stabilized emulsion drop has been developed using water, silicone oil and glass beads. In past ground-based experiments, water was used as the continuous phase. Oil drops with diameters of approximately 3 mm were used to simulate emulsion drops. Glass beads with different surface properties were used to simulate the solid particles at the oil-water interface. The ground-based experiments showed the model behaved similarly to industrially relevant solids-stabilized emulsion systems in several ways. Hydrophilic glass beads prevented the coalescence of oil drops in water and hydrophobic glass beads allowed the oil drops to coalesce. Under the effect of gravity, the enlarged emulsion model has several weaknesses. First, the beads on the interface accumulate at the bottom of the drop. Second, it was observed that the three-phase contact angle varies with the vertical position of the beads on the droplets. For these reasons, it is desirable to carry out similar experiments under the reduced gravity conditions that the Falcon 20 could provide. An apparatus has been designed to carry out similar experiments under reduced gravity conditions.

The apparatus is composed of a test cell, a digital camcorder, a light, and a frame. All the components will either be secured to the frame or secured to each other. The total weight of the equipment is approximately 66 pounds (including all test-cells). The normal electrical power consumption from the Falcon on board 60 Hz power source will be less then 30W and the maximum power usage from the 60 Hz power source will be 53 W.

In order to synchronize the video recording with the accelerometer data recorded by the on board data acquisition system, it is requested that the operator will be allowed access to take video of the data acquisitions' system clock before and after each flight.

B. Test Objective

The overall objective of this study is to better understand the geometry and behaviour of the three-phase systems involved in solids-stabilized emulsions. For the January flights, two sets of experiments will be conducted. The first set of experiments is to study the effect of pressure on contact angle formed by silicone oil and water in contact with the surfaces of the beads. The second set of experiments will study the effect of particle properties on the behaviour of shrinking oil droplets.

C. Test Description

Distilled water, silicone oil droplets and glass beads will be used to model solids-stabilized emulsions. Distilled water will be used as the continuous phase and glass beads, which (in 1g) rest at the bottom of the container, will model the solid particles that may affect the behaviour of emulsion droplets. A silicone-oil-filled syringe will inject a small amount of oil into the continuous phase via a stainless steel tube. A small oil drop will thus form at the tip of the tube (Figure 1). In the first set of experiments, the tube will be lowered to collect a few beads on to the oil-water interface. The drop will be raised up and the contact angle can then be observed and recorded. For the second set of experiments, the drop will be lowered into the beads to collect various amounts of beads on to the oil-water interface. Then the oil drop will be raised and by using the syringe, the oil will be retracted back into the tube. During this process, the behaviour of the glass beads and the oil drop will be observed and recorded.

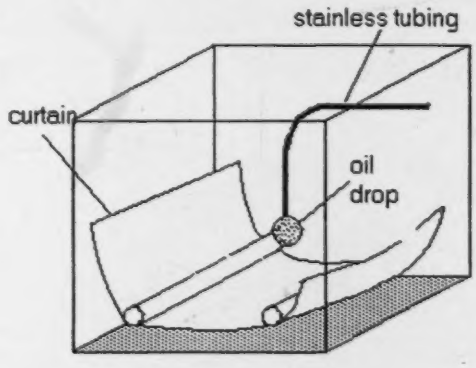

Figure 1 Schematic of the test-cell.

D. Equipment Description

The test equipment is composed of the following components: frame, test cell, camcorder, light and stage. Figure 2 shows the major components of the apparatus and Figure 3 is a summary of the major equipment. The detailed descriptions of each component follow below.

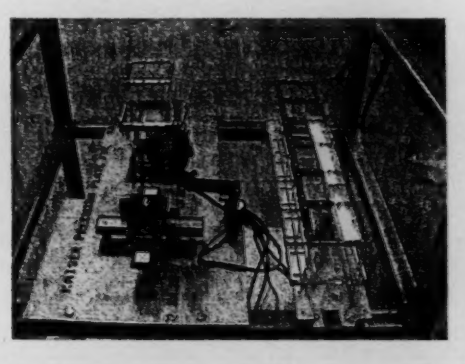

Figure 2 The apparatus without the camcorder.

	Frame	Test Cell	Camcorder	Light	Stage
Approx. Weight (lb)	25	1 (per cell)	2	0.3	1
Approx. dimension W x D x H (in)	25 x 21 x 25	3 x 3 x 3	3 3/8 x 8 1/8 x 4 1/8	4 x 4 x 3.5 when folded	4 x 4 x 2 when folded
Material	1010 Square Steel Tubing 1.25" x 1/16"	Acrylic and Glass Panels	Various	Various	Alumium

Figure 3 Summary of the major components.

D.1 Frame

The frame of the apparatus is constructed from 1010 mild steel square tubing with a width of 1.25" and a wall thickness of 1/16". It is formed into a rectangular frame as shown in Appendix A. All joints are TIG welded. The frame weighs approximately 25 pounds. A stress analysis was completed and the result is shown in Section 'E.'

D.2 Test Cells

Each test cell is made from five ¼" acrylic panels and one 3 mm glass panel. The panels form a cube (see Appendix B) that contains water and glass beads. Two stainless steel tubes enter the container from the sides. The stainless steel tubes are connected to two syringes where silicone oil is stored. A plastic curtain will be used to prevent the glass beads from floating up and blocking the view of the camera during low gravity conditions. Rubber gasket and boots will be used to seal the test cell. The estimated weight of one cell containing water and glass beads is one pound.

D.3 Camcorder

A digital video camcorder (Sony DCR-TRV530) will be used to record the experiment. The camcorder accepts both DC (battery) and AC power sources. For the experiment, the battery will be used as the primary power source. A spare battery will also be brought on board the aircraft. In the case where both batteries fail to provide the power required, an AC adaptor would be used to power the camera. The maximum power consumption for the camera while using the AC adaptor is 23 W.

In addition to the Sony camcorder, an add-on lens and a focusing rail will be used with the camcorder. The screw-on macroscopic lens (Raynox VM3000) will provide the necessary magnification to capture the details of the experiment. The camcorder will be bolted to a Rokunar focusing rail (Figure 4). This rail allows the camera to move in two axes independently.

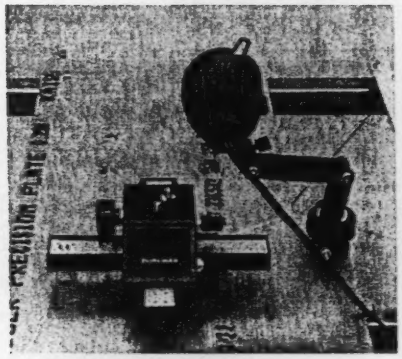

Figure 4 Rokunar focusing rail (left) and Leica halogen lamp (right).

D.4 Lighting

A halogen lamp (Leica Model 13410311) will provide the lighting for the camera (Figure 4). The light requires a 120 V 60Hz power source and the maximum power consumption is 30 W.

D.5 Stage

The stage is a modified Fisher lab jack (Figure 5). The test cell will latch on to the stage and a pin will secure the cell in to position. The stage can then move the test cell vertically into camera's view.

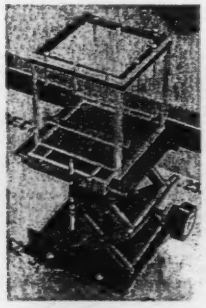

Figure 5 A test-cell on the Fisher lab jack.

E. Structure load analysis

Stress calculations for the frame under various conditions described in Appendix 6 of Falcon-20 User Guide were made in an Excel spreadsheet. Figure 6 shows the estimated loading on the frame. Figure 7 below shows the result of the stress calculation for the frame shown in Appendix A. The formulae and the procedures used can be found in Appendix C.

Load	kg	lb
camcorder	1.1	2.42
rail	0.67	1.474
stage	0.45	0.99
cell	0.5	1.1
support	2.0	4.4
Total	4.72	10.384

Figure 6 Estimated load.

Assume square tubing with width of 1.25" and thickness of 0.0625".

Assume total loading of 12 lb (5.4 kg).

Assume the combined center of gravity is 2" above the table-top.

Case 1 Forward 9g		Case 2 Lateral 3g		Case 3 down 6g	
9 g load	533.9661	3 g load	160.1898	6 g load	320.3797
Mz	52.55562 Nm	Mz	15.76669 Nm	Mx	23.39573
My	35.60219 Nm	My	11.69786 Nm	Mz	21.36132
Fx	133.4915 N	Fx	40.04746 N	Fy	80.09492
Normal Stress due to Mz		Normal Stress due to Mz		Normal Stress due to Mx	
	48.63578 M Pa		14.59073 M Pa		21.65077 M Pa
Shear Stress due to My use thin wall approximation		Shear Stress due to My use thin wall approximation		Normal Stress due to Mz	
	74.54218 M Pa		24.49243 M Pa		19.76809 M Pa
Shear Stress due to Fx		Shear Stress due to Fx		Combine normal stress	
					41.41886 M Pa

1.863064 M Pa	0.558919 M Pa	
		Shear Stress due to Fy
Max Shear Stress	Max Shear Stress	
		1.117839 M Pa
76.40524 M Pa	25.05135 M Pa	
Mohr's Circle	**Mohr's Circle**	**Mohr's Circle**
Max Stress	**Max Stress**	**Max Stress**
104.5 M Pa	**33.4** M Pa	**41.4** M Pa

Figure 7 Result from the tress calculation.

Where the tensile yield strength of 1010 steel is 305 M Pa.

Stress calculations for the support plate, lock pin and bolt for various components are also shown in Appendix C.

F. Electrical Load Analysis

During normal operation, only the light will need the on board power source. The Leica illuminator will draw no more than 30W from the 60 Hz source.

In the unlikely event that both batteries for the camera fails, the AC adaptor will be used and it will draw no more than 23W from the 60 Hz source.

G. Pressure vessel certification

Not applicable because the test cells used during the experiment will not be under any pressure. In case of minor temperature variations, rubber boots used to seal the test cells will allow the expansion of water.

H. In-flight Test Procedures

The following gives the in-flight test procedures in checklist format.

After installing the equipment
1. All nuts and pins (tighten and secured)
2. Stage (lowered)
3. Camcorder (on camera)
4. Thermometer (on)
5. Light (on)
6. All electronics (off)

Pre-flight
1. Test-cells (available and secured)
2. Stage (lowered)
3. Camcorder (New Tape, on-camera and free from apparatus)
4. Stopwatch (start)
5. Video tape on board system clock
6. Video tape the stopwatch
7. Camcorder (back on the focusing rail)
8. Camcorder (secured and off)

Level off after initial climb
1. Lights (on)
2. Thermometer (on)
3. Camcorder (on-camera and record)

During level flight
1. Temperature (read out loud)
2. Install new test-cell if required (pins secure)
3. Inject oil (as required)
4. Setscrews (loosen)
5. Plastic curtain (open)
6. Tube (lowered and collect beads as required)
7. Tube (raise back up just above the curtain)
8. Setscrews (tighten)
9. Plastic curtain (closed)

During reduced gravity
1. Setscrews (loosen)
2. Tube (raise back up)
3. Setscrews (tighten)
4. Adjust focusing rail to film the drop (if required)
5. Adjust syringe (if required)
6. Temperature (read out loud)

Pre-landing check
1. Stage (lowered)
2. All test cells secured
3. Video tape the stop watch
4. Temperature (read out loud)

5. Light (off)
6. Camcorder (off)
7. Thermometer (off)

After Landing

1. Camcorder (free and on-camera)
2. Video tape the stop watch
3. Video tape the on board clock
4. Camcorder (off and insert new tape)
5. Remove unnecessary test-cells
6. Get the test cells for the next flight
7. Stop watch (stop and reset)

I. Parabola Requirements

The proposed experiments for each flight and parabola are listed in Appendix D. Twenty-four (24) twenty-second-parabolas are requested to complete all the experiments.

J. Test Support Requirement

In order to synchronize the video recording with the accelerometer data recorded by the on board data acquisition system, it is requested that the operator will be allowed access to take video of the data acquisitions' system clock before and after each flight.

Only one or two test-cells will be needed for each flight; therefore, a storage space on the ground for the other test-cells is requested.

K. Data Acquisition system

A copy of the acceleration data in either text or Excel spreadsheet format is requested for each flight.

L. Test Operating Limits or Restrictions

The test cells and the camcorder must be stored at a temperature above 0°C.
Vibration may have an effect on the experiment. For the January flight, the experiments will be completed with out any vibration isolation. However, a vibration isolation mount might be requested for the future flights.

M. Proposed Manifest for Each Flight

One operator is needed for the experiments. The proposed operator for this experiment is Raymond Chiang. A photocopy of his medical certificate is in Appendix E of this report. It is also requested that Eric Vachon of Canadian Space Agency be on board the aircraft.

N. Photographic Requirements

The experimental apparatus includes a Sony digital camcorder and the necessary lighting system (Section D). Therefore additional photographic support is not required.

O. Hazard Analysis

All the components of the experiment will be bolted, or strapped down so there will be no free floating objects during the parabolic flight.

The fluids involved in the experiments are water and silicone oil at room temperature. They are not considered to be hazardous and are contained in sealed containers.

All electrical equipment, except for a stopwatch, will be shut-off during take-off and landing to avoid electrical interference with aircraft instruments.

APPENDIX A
3-VIEW DRAWINGS OF THE FRAME

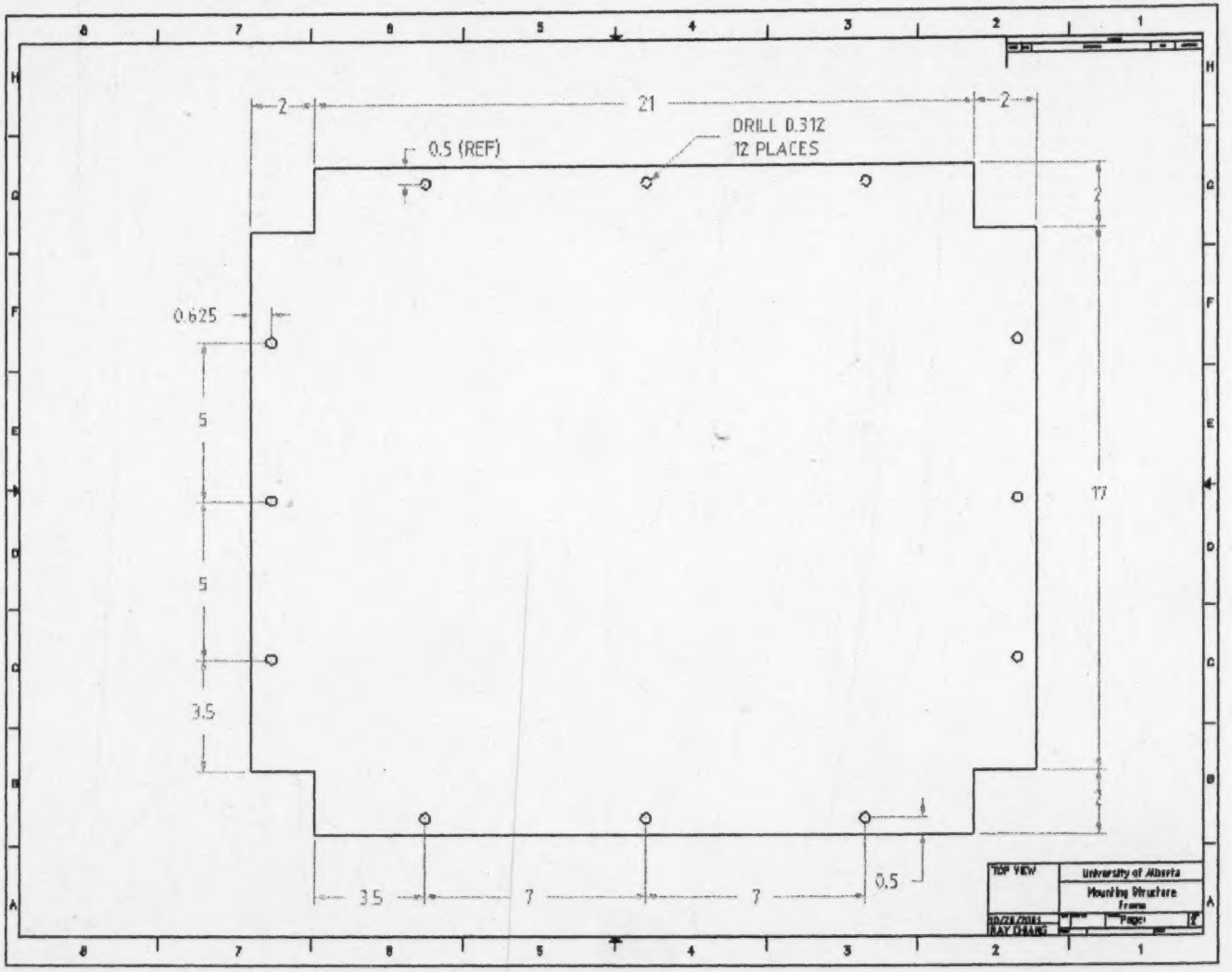
2
21
2
DRILL 0.312
12 PLACES
0.5 (REF)
2
0.625
5
5
3.5
17
2
3.5
7
7
0.5
TOP VIEW
University of Alberta
Mounting Structure
Frame

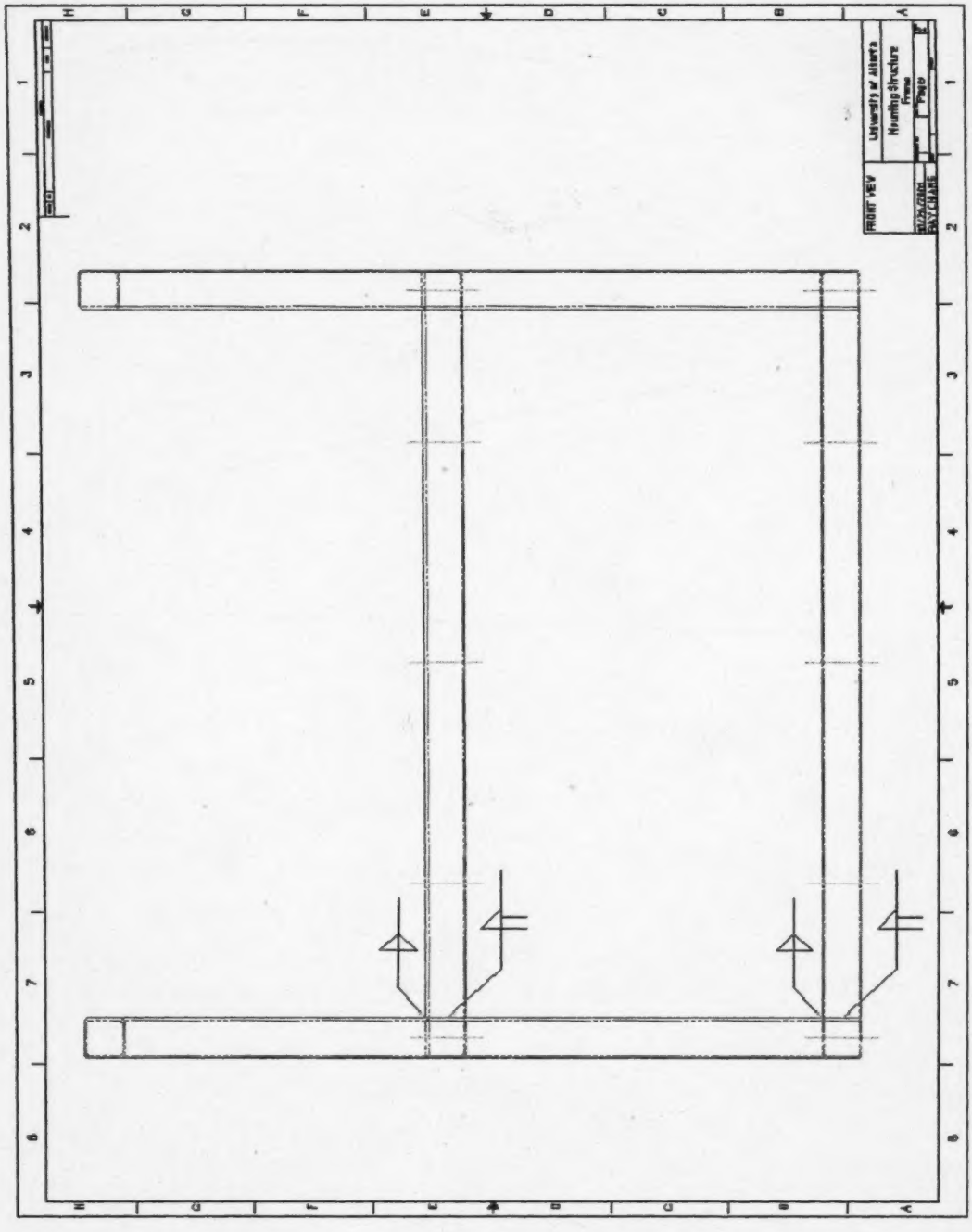
University of Alberta
Mechanical Engineering
FRONT VIEW

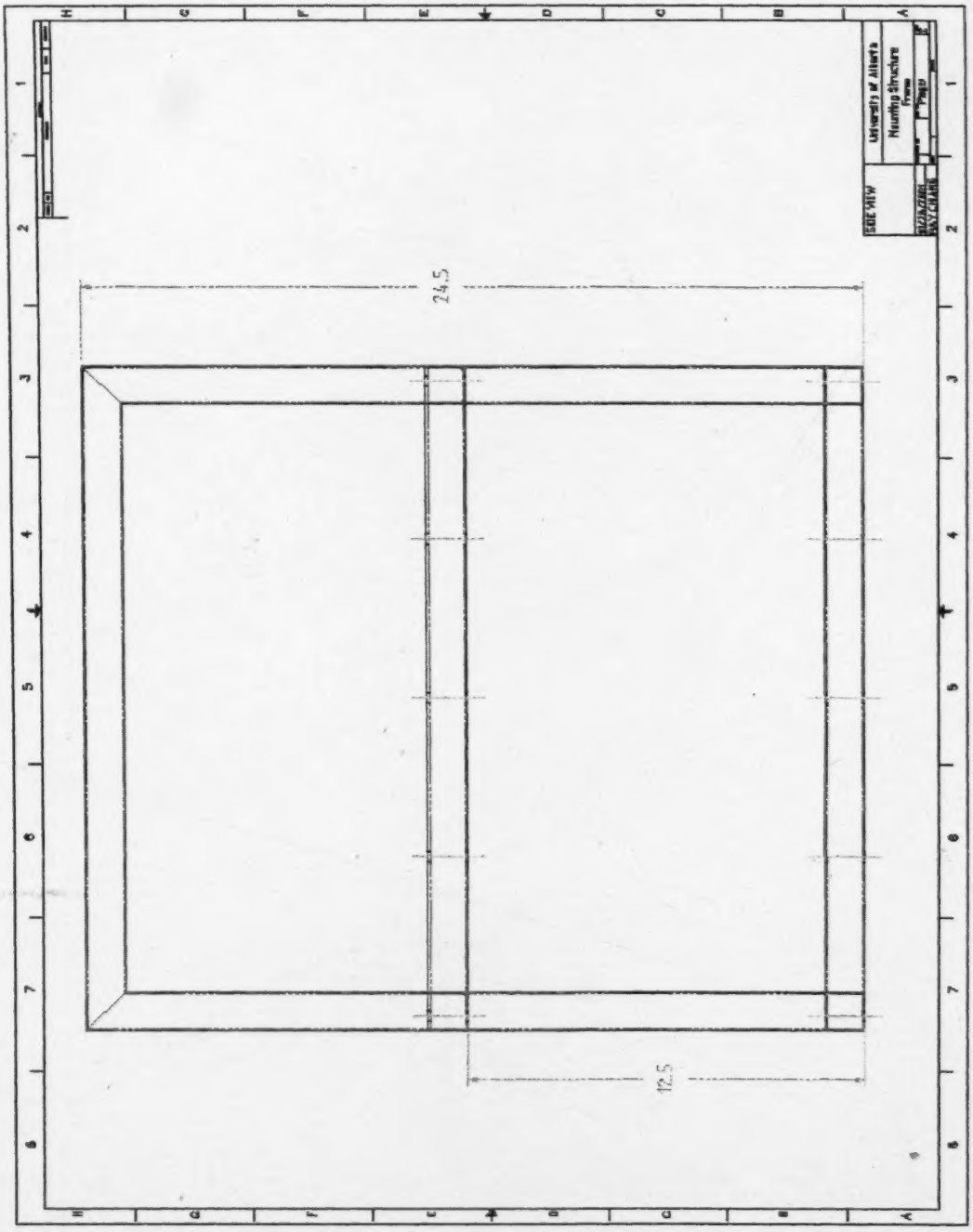
24.5
12.5
University of Alberta
Mounting Structure
Frame
Page

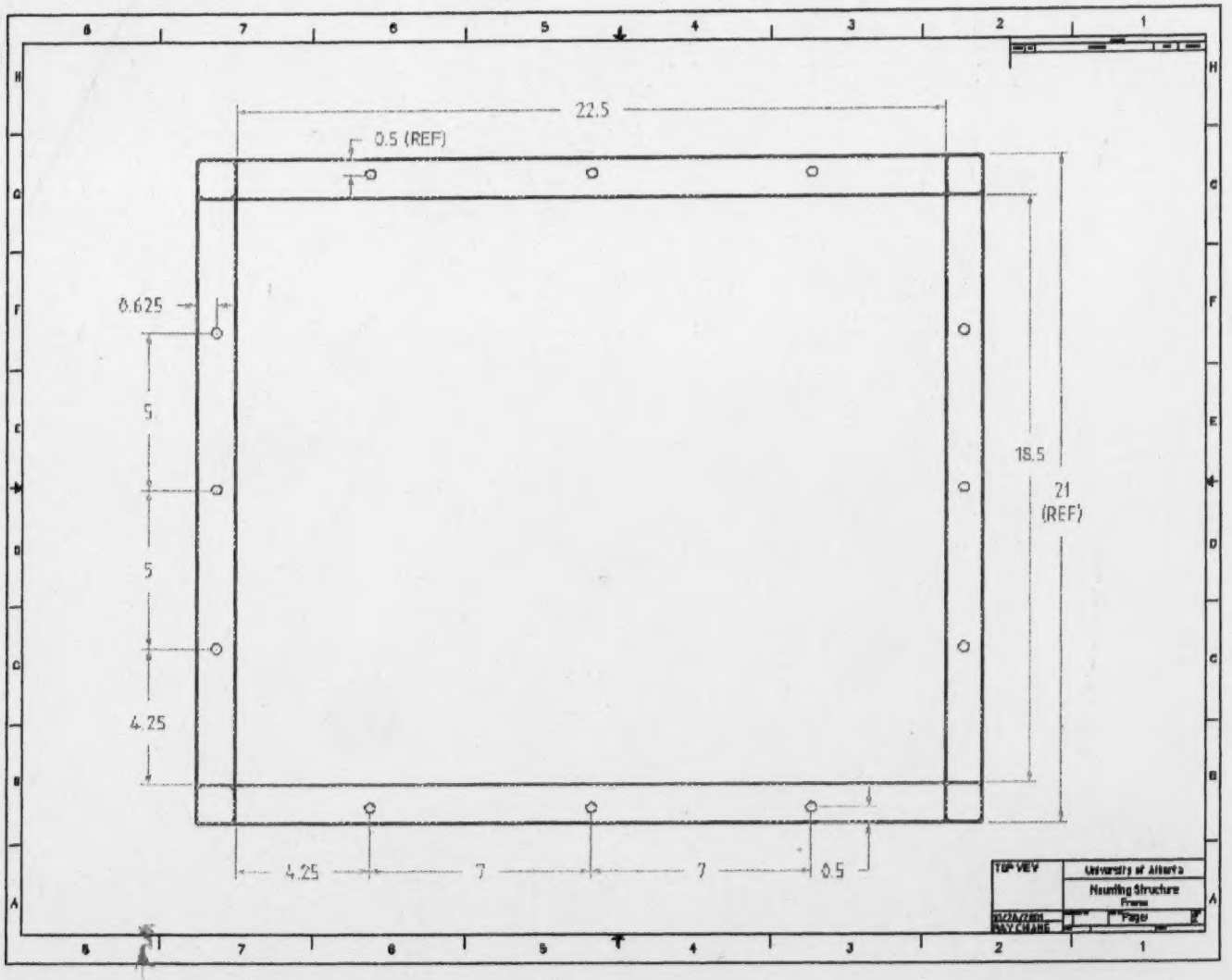
22.5
0.5 (REF)
0.625
5
5
4.25
18.5
21
(REF)
4.25
7
7
0.5
TOP VIEW
University of Alberta
Mounting Structure
Frame

APPENDIX B

3-VIEW DRAWINGS OF THE TEST CELL

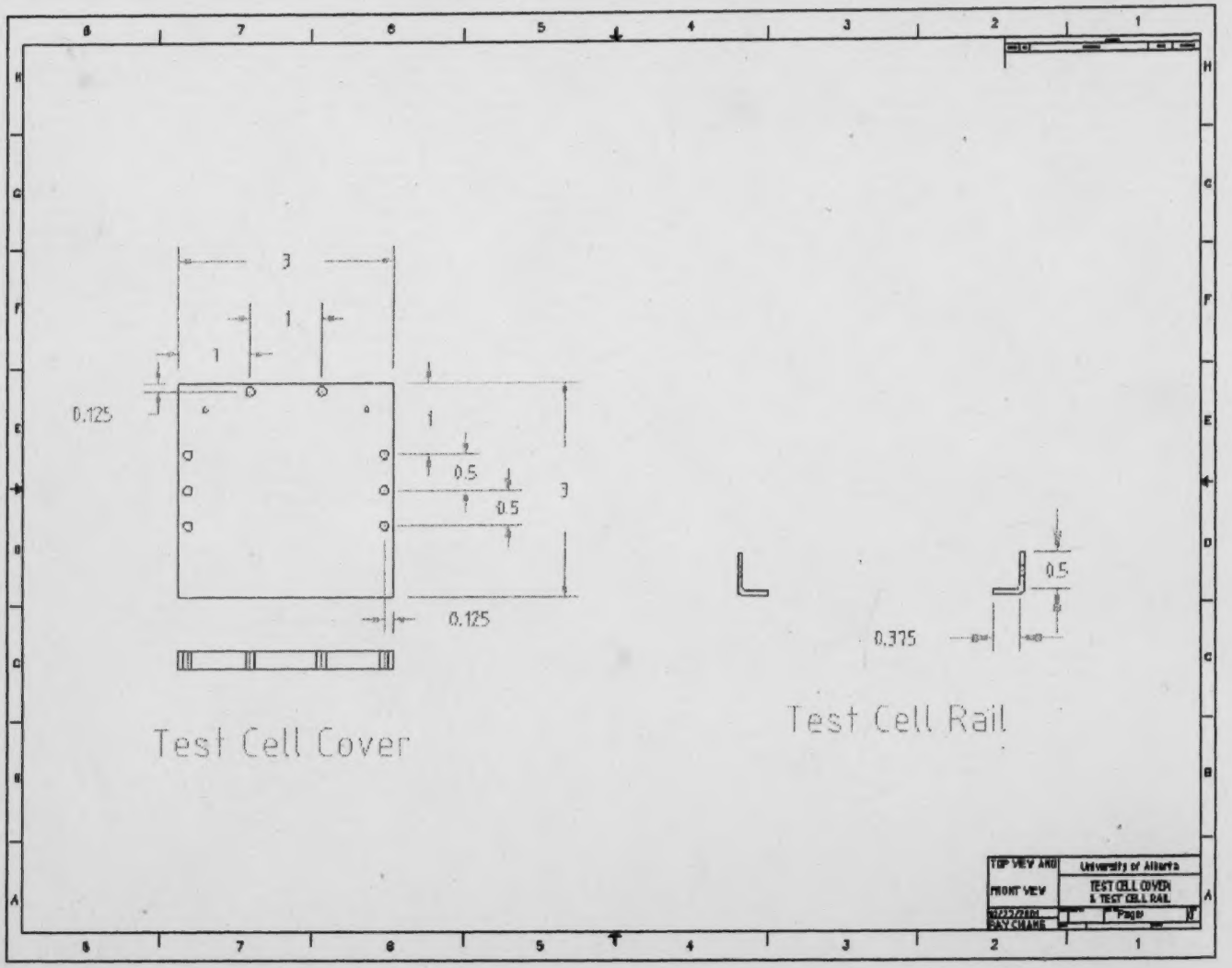
3
1
1
0.125
1
0.5
0.5
3
0.125
Test Cell Cover
0.5
0.375
Test Cell Rail
TOP VIEW AND FRONT VIEW
University of Alberta
TEST CELL COVER & TEST CELL RAIL

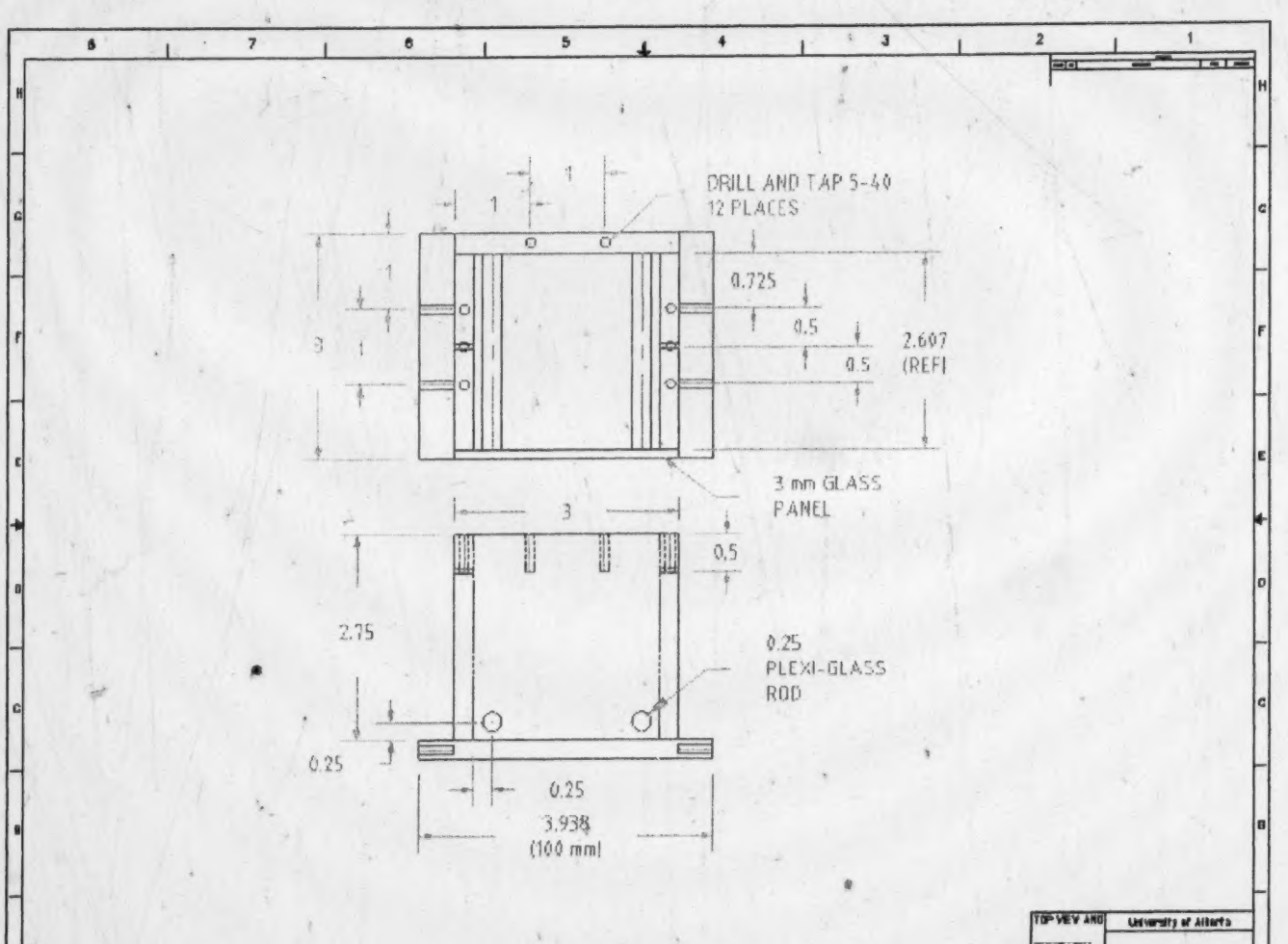
DRILL AND TAP 5-40
12 PLACES
1
1
1
1
3
0.725
0.5
0.5
2.607
(REF)
3 mm GLASS
PANEL
3
0.5
2.75
0.25
PLEXI-GLASS
ROD
0.25
0.25
3.938
(100 mm)
TOP VIEW AND
FRONT VIEW
University of Alberta
TEST CELL

APPENDIX C
STRESS CALCULATIONS

Formulae and method for stress calculation

For forward loading case.
Assuming a box shaped frame
Load on the frame

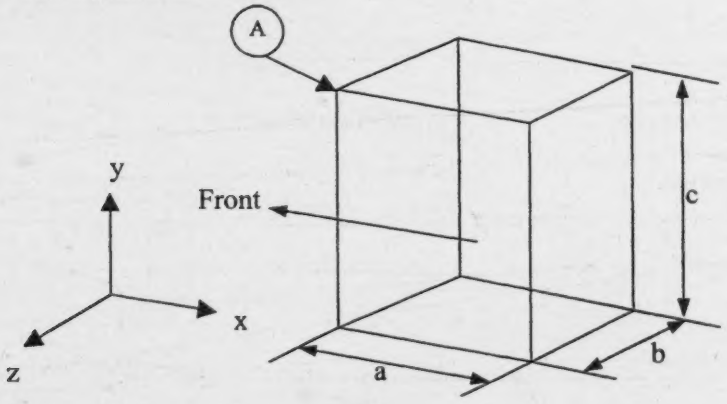

Assume the load, 'w' is at the centre of the frame and located at a height of 'c+d'.
The stress at point A is given by:

$$M_Z = -\frac{1}{4} W * d$$

$$M_y = -\frac{1}{4} W * \frac{b}{2}$$

$$F_x = \frac{W}{4}$$

Stress on the vertical members is shown by the shear and moment diagram below:

Maximum stress occur at the bottom corners.

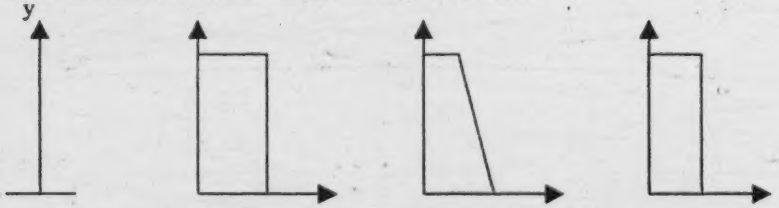

Max shear
V = 450/2

Max moment
Mz = 450 (e+d)/2

Max moment
My=-450 b / 8

Moment of inertia, I, (for thin wall tubing)

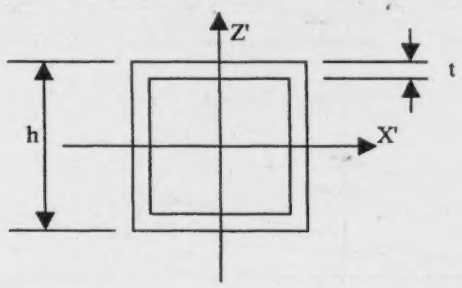

$$I_{x'} = \frac{1}{12}h^4 - \frac{1}{12}(h-2t)^4$$

Cross section area:

$$A = 4ht - 4t^2$$

Normal stress due to M_z:

$$\sigma_x = \frac{M_z 0.5h}{I_{x'}}$$

Shear stress due to M_y:

$$\tau = \frac{M_y}{2At}$$

Maximum and minimum stress as given by Mohr's circle for plane stress:

$$\sigma_{max,min} = \frac{\sigma_x + \sigma_y}{2} \pm \sqrt{\left(\frac{\sigma_x + \sigma_y}{2}\right)^2 + \tau^2}$$

APPENDIX D
PROPOSED EXPERIMENTS

Flight 1

Test-cell #1. Size 7 **hydrophilic** beads.

Parabola 1: Two 3mm drops. One with few beads and the other with lots of beads.
Parabola 2: Same as 1.
Parabola 3: Similar to previous but with larger drops (6 mm)
Parabola 4: Same as 3.

Flight 2

Test-cell #2
With **hydrophobic** beads

Parabola 1, 2: Two 3mm drops. One with few beads and the other with lots of beads.
Parabola 3, 4: Similar to previous but with larger drops (6 mm)

Flight 3

Parabola 1 and 2
Test-cell #3. Size 7 **hydrophilic** beads.
With 3 mm oil drops. Beads **FULLY** cover the oil drops.
Reduce the size through suction.

Parabola 3, and 4
Similar to 1 and 2 but with 6 mm oil drops.

Flight 4

Parabola 1 and 2
Test-cell #4. Size 7 **hydrophilic** beads.
With 3 mm oil drops. Beads **PARTIALLY** cover the oil drops.
Reduce the size through suction.

Parabola 3, and 4
Similar to 1 and 2 but with 6 mm oil drops.

Flight 5

Test-cell # 5. Same as flight 3 but with **hydrophobic** beads.

Flight 6

Test-cell #6. Same as flight 4 but with **hydrophobic** beads.

APPENDIX E

OPERATOR MEDICAL CERTIFICATE

(Omitted for Raymond Chiang's Thesis)

APPENDIX 2

The section below recounts the microgravity experiments that failed to produce any tangible results.

Flight 1 Parabola 4

A small droplet, approximately 4 *mm*, was formed during level flight. It had approximately half of its volume occupied by the glass beads. The droplet fell off the needle tip during the 2-*g* pull up portion of the flight. Several droplets were squeezed out in an attempt to form another droplet before the reduced gravity portion of the flight ended. A 6 *mm* droplet with a number of glass beads on the oil-side of the interface was formed during reduced gravity. The droplet stabilized just prior to the 2-*g* pull out and no manipulation was made to this droplet.

Flight 2 Parabola 1

Once the aircraft went into the reduced gravity portion of the parabola, water and beads were injected into the cell. In order to create fluid motion, the second needle was used to inject more water into the droplet. Unfortunately, the second needle had been previously used to suck in another droplet and was contaminated with oil. A water droplet was formed but with oil droplets within the droplet and no glass beads were observed to be on the oil-side of the interface.

Flight 2 Parabola 2

Although the attempt to form a droplet during the reduced gravity portion in parabola 1 was not successful, another attempt was made to repeat that procedure. A small droplet was made during level flight, and once the reduced gravity portion started, the 'pumping' motion began. Although fluid motion and the number of beads were significant, no beads were observed to be on the oil-side of the interface.

Flight 3 Parabola 2

A droplet of approximately 8 *mm* diameter was formed in reduced gravity with an unknown number of beads inside. The droplet was fully retracted within three seconds and in the last 0.33 seconds, the droplet went from 5 *mm* down to 1.75 *mm* (Figures 1 through 3). During the last part of the retraction, the droplet broke into several smaller droplets (Figure 4).

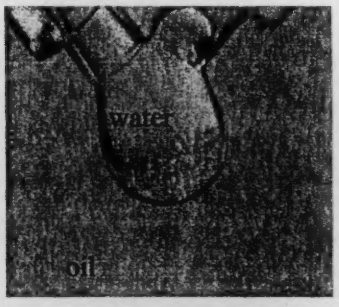

Figure 1 A water droplet filled with hydrophilic beads during retraction.

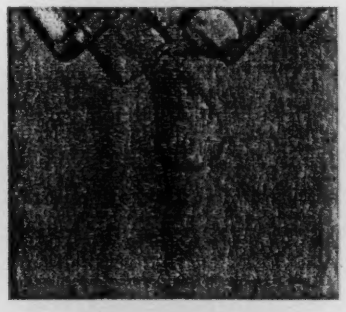

Figure 2 The same water droplet few frames later.

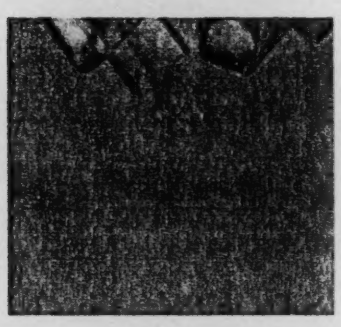

Figure 3 The water droplet just before breaking off.

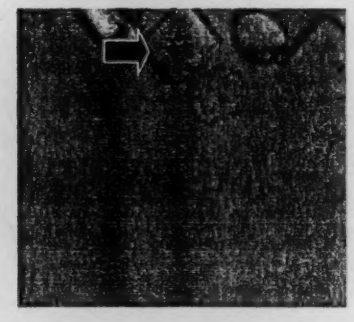

Figure 4 The water droplet broke into several smaller droplets.

These small droplets then coalesced when they came into contact with each other. The coalescence between the droplets was captured by the video camera and an example of this is shown in figures 5 through 8. The coalescence of these two droplets took about four frames or approximately 0.13 seconds.

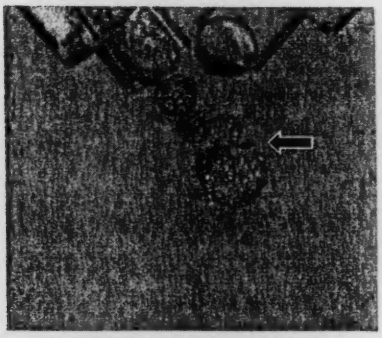

Figure 5 An arrow showing the two water droplets that were about to coalesce.

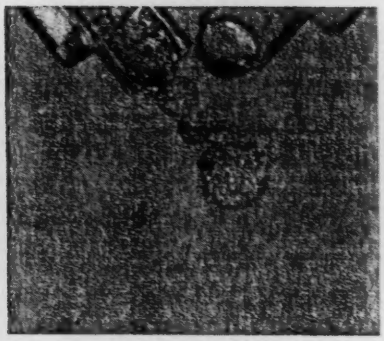

Figure 6 One frame later, the two water droplets began to join.

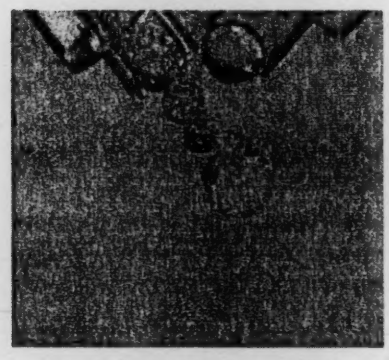

Figure 7 The two water droplets became a single, non-spherical droplet.

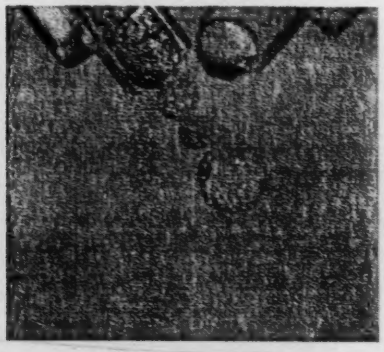

Figure 8 The water droplet began to reshape itself.

Flight 4 Parabola 1

A droplet of approximately 6.5 *mm* was formed during the parabola (Figure 9). Approximately one quarter of the droplet was covered by beads just before the droplet was retracted. The droplet was hanging onto the side of the right needle and thus when the droplet retracted it was asymmetric. It took approximately 2 seconds to retract most of the droplet into the needle. A smaller droplet, which contained most of the beads,

remained stuck to the side of the needle (Figure 10). Before the reduced gravity portion ended, water was injected to form another droplet. This new droplet coalesced with the small droplet that was on the side of the needle and formed a droplet of approximately 6.5 *mm* (Figure 11). This was again retracted into the needle in less then 2 seconds. Similar to the previous retraction, a small droplet was left behind on the side of the needle (Figure 12).

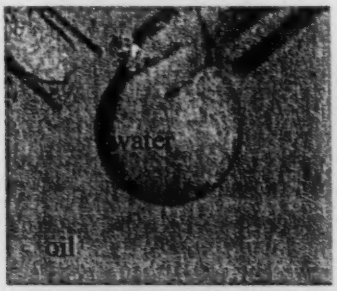

Figure 9 The water droplet became attached to the side of the glass needle.

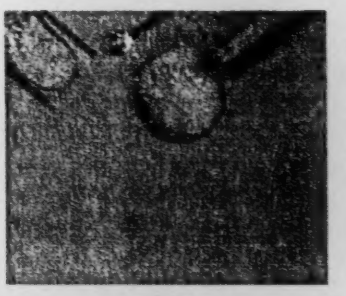

Figure 10 A small water droplet left behind on the side of the needle.

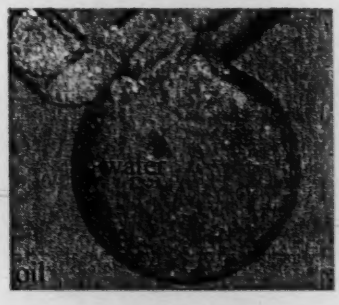

Figure 11 A second attempt to form a water droplet.

Figure 12 A small water droplet was again left behind.